Summer 2011

Aerogels and films through free radical polymerization

Anand G. Sadekar

Department: Chemistry

Recommended Citation

Sadekar, Anand G., "Aerogels and films through free radical polymerization" (2011). *Doctoral Dissertations*. 2125.
https://scholarsmine.mst.edu/doctoral_dissertations/2125

primary particles with a diameter of <1 nm. Generation and aggregation of the particles is controlled by chemical processes, usually the sol-gel process.[9]

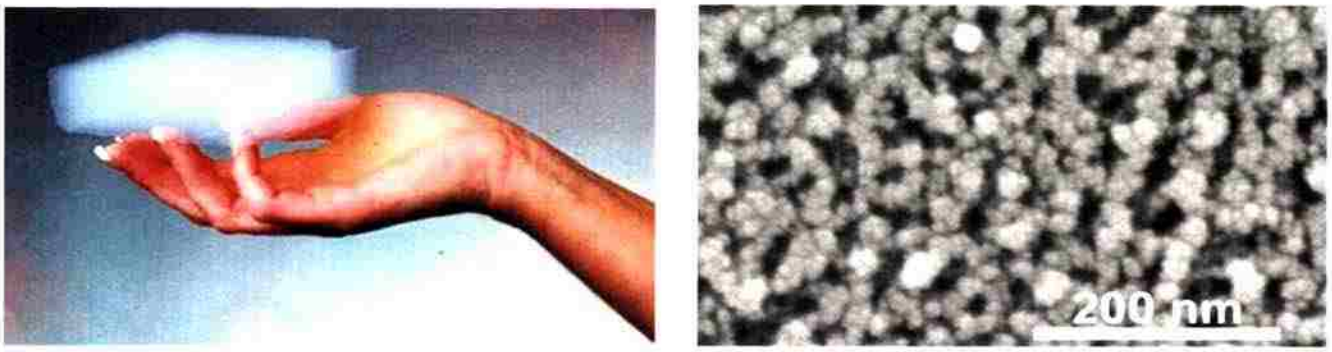

Figure 1.1 A typical picture of silica aerogel in left and its microscopic structure on right.

Aeogels were invented by Kistler[10,11] in 1930s for studying the nature of the gels. He eventually ended up commercializing the first aerogels with Monsanto. Kistler showed impressively that the liquid of the gels can be removed without destroying the gel structure. One of the reasons why it took 30 years for the aerogels to become interesting for industrial applications was certainly the time-consuming preparation, which took more than a week. Nicolaon and Teichner[12] improved the process of making silica aerogels by employing sol-gel chemistry with tetramethylorthosilicate (TMOS) as the metal alkoxide. The key to the improvement was the use of methanol as the solvent, which was then removed under supercritical conditions.

1.2 NETWORK FORMATION AND STRUCTURE

Formation of highly porous three-dimensional network is one of the key steps in the preparation of aerogels. Network formation is an excellent example of the influence of chemical parameters, in particular the kind of precursors and the reaction conditions, on the resulting microstructure.

Figure 1.2 shows the preparation of a silica aerogel via the sol-gel process.

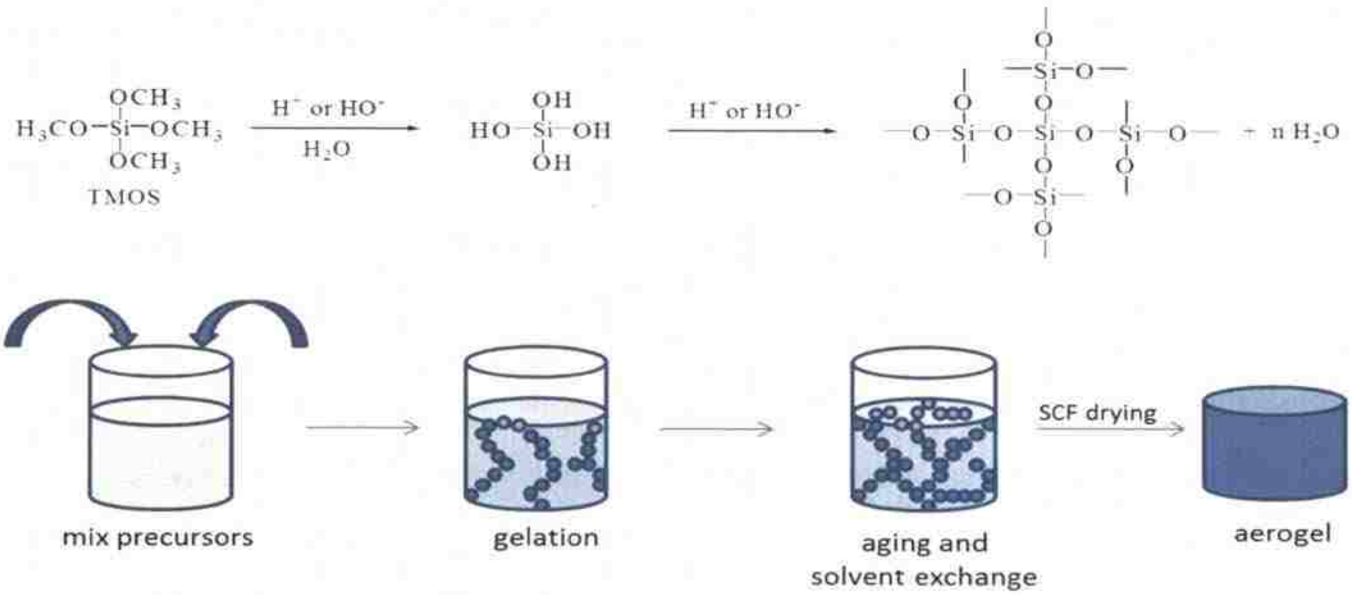

Figure 1.2 Preparation of a silica aerogel using the sol-gel process.

As discussed by Livage and Sanchez,[13] the first step in the preparation of a silica aerogel, is the hydrolysis of a silicon organic precursor, followed by condensation of the hydroxyl groups to produce –Si-O-Si- linkages. Nucleophilic substitution reactions are the backbone of the hydrolysis step which occurs through SN_2 mechanism. Typically, tetraethoxysilane (TEOS) of formula $Si(OC_2H_5)_4$ or tetramethoxysilane (TMOS) of formula $Si(OCH_3)_4$ are used as precursors. These silicon alkoxides are dissolved in their respective alcohol, which also serves as a solvent for water in the hydrolysis step in the presence of either an acidic or basic catalyst. The gels thus formed by this process are exchanged with alcohol several times to remove water from the network before drying them.

been used *only* in certain specialized environments, like the production and detection of Cherenkov radiation aboard spacecraft, as collectors for cosmic particles,[25] and for thermal insulation in planetary vehicles.[19] Main issues in the commercialization of aerogels are their fragility and their extremely weak mechanical properties. In our past work, we have solved these problems by crosslinking aerogels with organic polymers.[29-32] Aerogels have well defined weak points on the skeletal framework which are the interparticle necks so by using the surface functional groups as anchors, the entire framework is coated conformally with a polymer that bridges chemically (crosslinks) the nanoparticles and reinforces the interparticle necks, while the pores remain open (Figure 1.3). The resulting polymer-crosslinked (X-aerogels) are exceptionally strong materials in comparison not only with native aerogels, but also with materials that are usually considered strong such as steel, Kevlar and silicon carbide.[33-35]

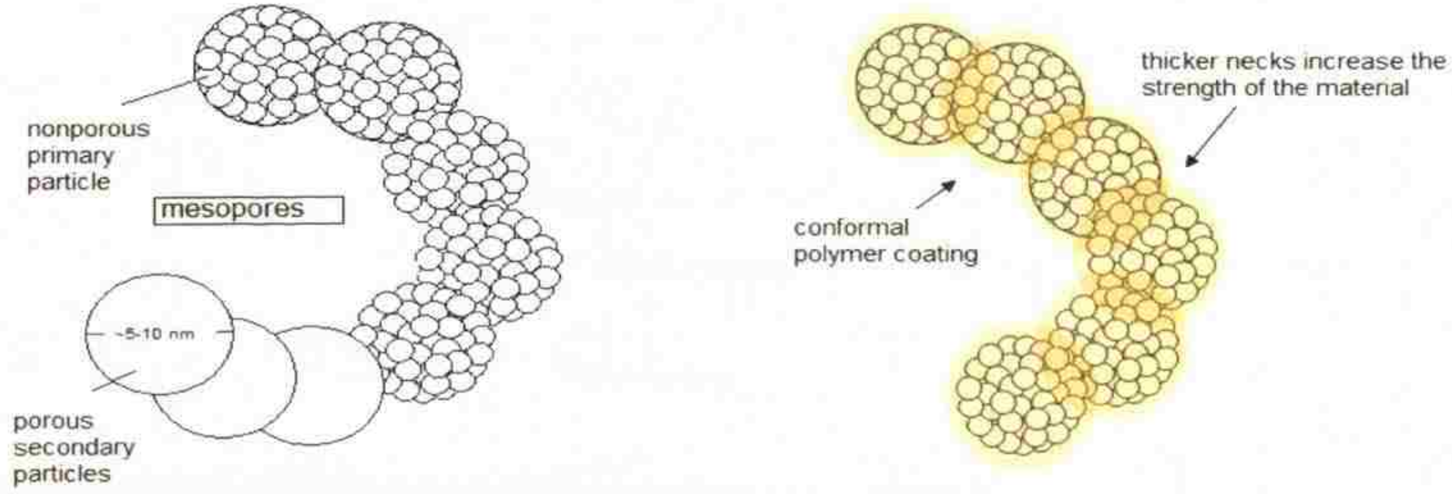

Figure 1.3 A thin polymer layer coats conformally the skeletal silica nanoparticles.

There are three degrees of freedom in the design of polymer crosslinked aerogels: the chemical identity of the framework, the chemical identity of the polymer and the surface functionality of the nanoparticles. The latter was determined to be a versatile parameter by careful choice of the reactive groups on the surface of silica. More versatile polymer reinforcement can be easily achieved if reactive functional groups are introduced onto the surface of silica by using trialkoxysilanes as precursors. Figure 1.4 demonstrates functionalization of silica aerogels using 3-aminopropyltriethoxysilane (APTES) to give amine decorated silica aerogels[26] for attachment of epoxy resins,[27-28] polyurea,[29-30] or polystyrene.[31-32]

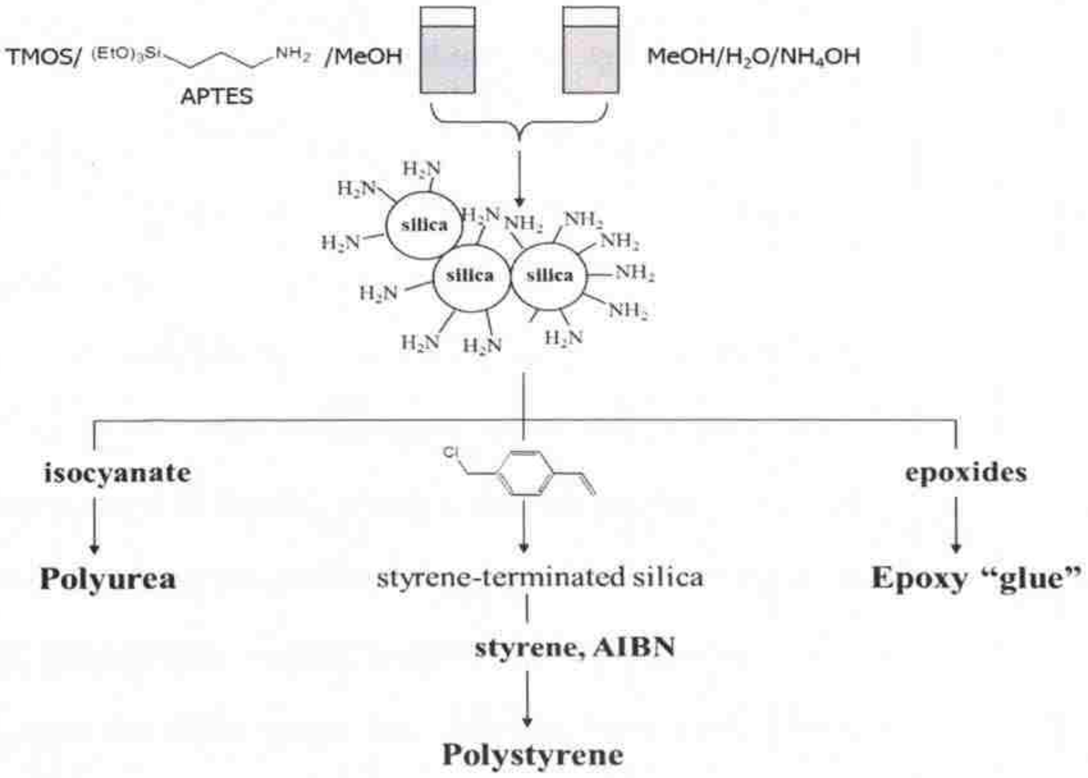

Figure 1.4 Surface modification of silica for polymer crosslinking.

It is noteworthy to mention that the internal void space in a X-aerogel is not compromised significantly, while the flexural strength of a typical monolith is increased by 300 times for a nominal increase in density only by a factor of three. The increase in cleavage they would produce one surface-bound radical, which is the desirable outcome, but they would also release a second radical in the mesopores. The polymer formed in the solution filling the mesopores will have to be removed, and that introduces more solvent exchange steps. For this purpose, we designed a *bidentate* free-radical initiator: ***Si-AIBN*** (Figure 1.5) which possesses $Si(OEt)_3$ groups on both sides and a group capable for free radical initiation (N=N) at the center. With the help of these $Si(OEt)_3$ groups, Si-AIBN anchors onto the surface of silica so that no free radical will ever leave the silica particles.

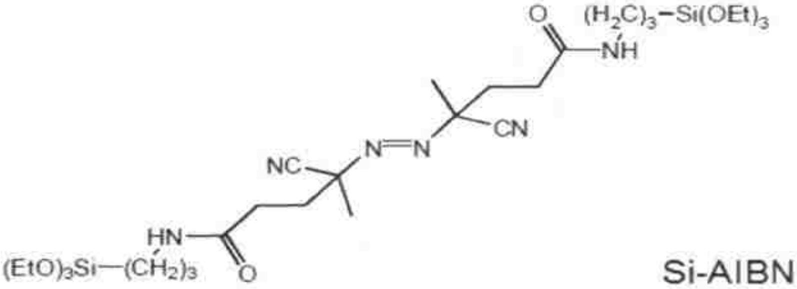

Figure 1.5 Bidentate initiator Si-AIBN.

The simplified crosslinking mechanism with Si-AIBN can be explained via classical free radical chemistry where initiation begins by heating with olefins in proper solvents. Silica wet-gels decorated with radical initiator sites, act like macro initiators. In the propagation step, thermally generated radicals react with the monomers in the reaction mixture from the surface of silica. When radicals at the tips of the growing chains meet, they combine and the radical process is terminated resulting in the formation of polymer tethers which connect the particles to each other (Figure 1.6). Consistent with the previous observations, these aerogels too are mechanically strong and they can take up to 800 MPa of stress at approximately 90% strain. Surface initiated polymerization of olefins like styrene or methyl methacrylate (MMA) can form covalently bound conformal coating on the mesoporous silica surfaces.[32]

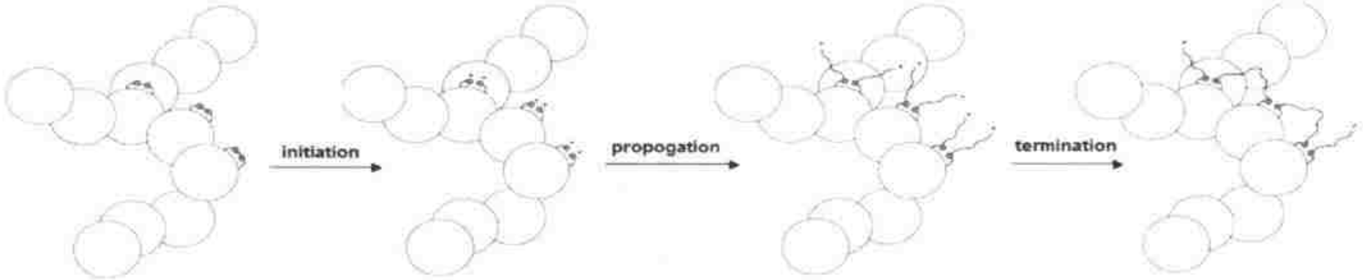

Figure 1.6 Simplified crosslinking mechanism with Si-AIBN.

SIP with Si-AIBN paves the way for more innovative research at the interface of sol-gel materials and films. In this dissertation, we extend the application of this initiator mainly in two different areas. The first application entails covalently bonded thin conducting polymer films, where Si-AIBN can attach itself to the surface of glass and assist in polymer growth from the surface of glass. The judicious use of several chemistries yields polythiophene covalently bonded to glass substrate. The second application involves polymer-crosslinked aerogels based on SIP as starting materials for making new kind of porous materials. Here, we demonstrate synthesis of silicon carbide (SiC) aerogels by carbothermal reduction of silica at temperatures between 1200 °C-1600 °C. For this purpose, silica was conformally coated with polyacrylonitrile, with a similar process as described earlier.

This work with SiC, led to all-organic aerogels based on polyacrylonitrile (PAN), reasoning that since PAN is the major industrial source of carbon fiber, PAN aerogels should be excellent sources of porous carbon. Carbon aerogels can be used as adsorbers,

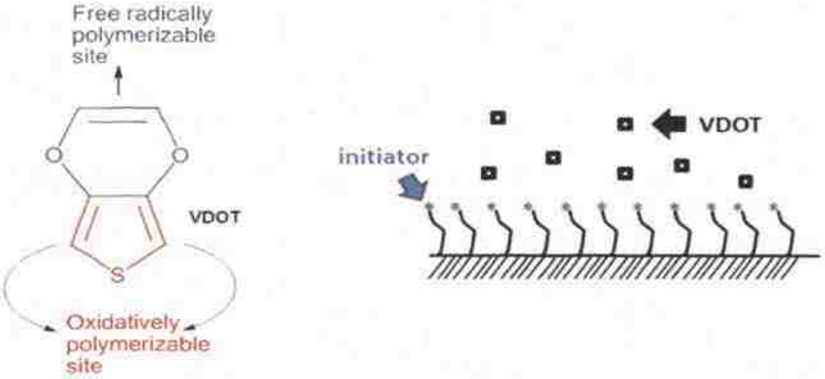

Figure 1.7 Surface binding of VDOT using Si-AIBN on glass.

Si-AIBN is attached to the surface of glass by hydrolysis of the -Si(OEt)$_3$ groups and reaction with the hydroxyl groups on the glass surface. Subsequently, BVOT was polymerized via a free radical mechanism using its vinyl groups and the glass surface-bound Si-AIBN. In turn, dangling thiophene groups were polymerized oxidatively.[50] Since the distance and spatial orientation of the thiophene groups are such that they cannot be polymerized on their own, they were bridged by oxidative co-polymerization with EDOT. This unique film-making method offers the obvious advantage of excellent adhesion as compared to the physically bonded films.

1.6 SILICON CARBIDE AEROGELS

In general, commercial catalysts are composed of a support material and an active catalyst component. Support materials provide a porous framework permitting access to the active phase for the reactants and free exit for the products from the catalyst particles. A good catalyst support should have high mechanical and thermal stability in order to avoid collapse during reaction or oxidative regeneration. All of these must be achieved with the support being chemically resistant, cheap, and abundant. For more than sixty

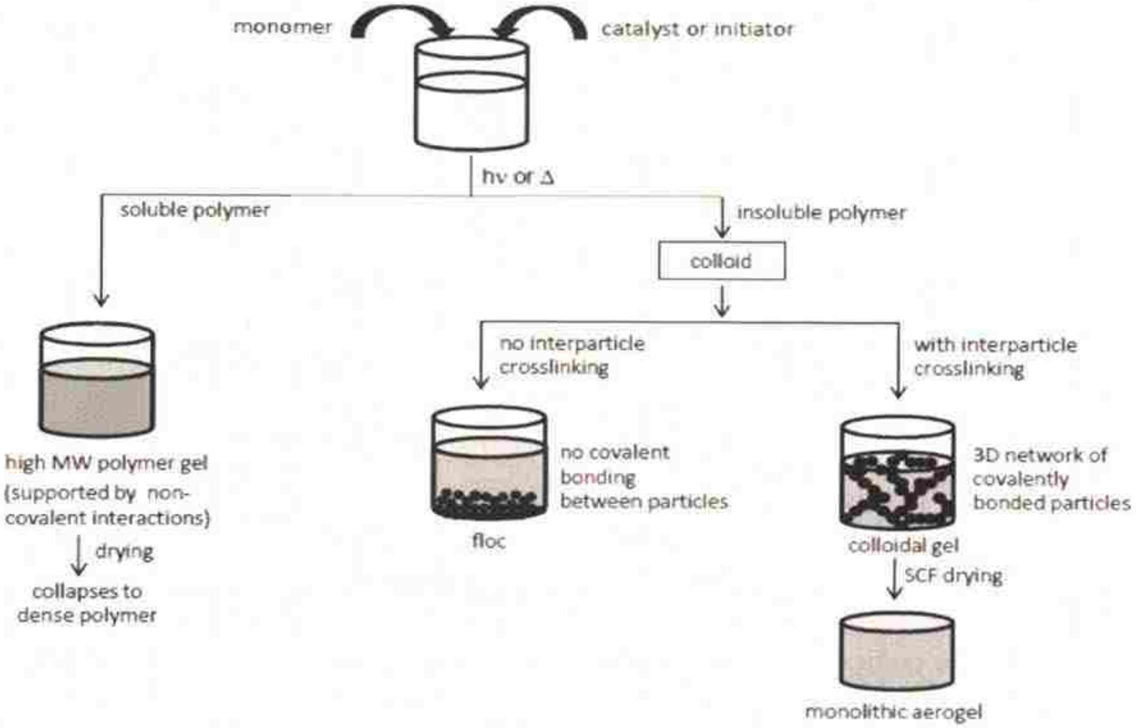

Figure 1.8 Different pathways towards formation of organic gels.

Most of the work in organic aerogels has been concentrated on resorcinol-formaldehyde (RF) aerogels, which upon pyrolysis, yield carbon aerogels. Nevertheless, a few reports have been published on other classes of organic aerogels, including polyimide, polystyrene, polydicyclopentadiene, polyurethane, and polyurea aerogels.[68-72] The targeted practical applications have always been either in the area of thermal insulation or in the conversion to electrically conducting carbon aerogels. In that regard, we became interested in polyacrylonitrile (PAN) aerogels, as PAN aerogels should be an excellent source of porous carbon. Although acrylonitrile can be polymerized via a free radical process, gels of the resulting linear polymer lack the rigidity necessary to be dried into aerogels. For this, 1,6-hexanediol diacrylate (HDDA) and ethylene glycol dimethacrylate (EGDMA) were used as crosslinkers to develop molecular 3D networks that induce phase-separation and provide the structure with the necessary rigidity that allows drying into aerogels. This process was carried out in toluene as an organic solvent to make mechanically strong aerogels based on PAN and then converted to monolithic carbon after controlled pyrolysis.

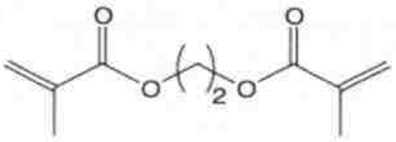

EGDMA

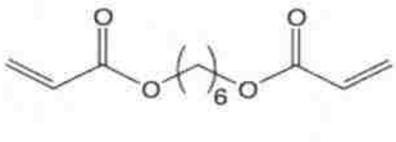

HDDA

Later, the work was extended to water based technology by borrowing chemistry from emulsion polymerization.[73] Upon pyrolysis at 2300 °C, we start observing formation of graphitic ribbons. The significance of this part of my work is related to the growing awareness of the environmental impact of chemical processing and the unavoidable transition from a growth to a sustainable economy. Emulsion polymerization is not typically used for gels, and by and large for aerogels. With relatively high concentration of monomer (AN), crosslinker (EGDMA or HDDA) and surfactants, the process yields relatively large, by aerogel standards, primary particles that form large pores, thus reducing the surface tension forces and wet-gels are dried into aerogels from water under ambient pressure. Acrylontrile (AN) was specifically chosen, because it comprises the main non-phenolic source of carbon. Emulsion-derived PAN aerogels are pretty similar materials to their conventional solution-polymerization derived counterparts prepared for comparison. After aromatization and carbonization at 800 °C, the derived amorphous carbons are identical, irrespective of the process they came from and the only differences (mainly in surface areas and electrical conductivity) are traced to the crosslinker. Shorter, more rigid EGDMA yields 800 °C carbons with higher surface areas but lower electrical conductivity than longer, more flexible HDDA. By 1600 °C, all samples consist of ~97.5% carbon and have developed microporosity, attributed to a self-etching mechanism ($C+CO_2 \rightarrow 2CO$). By 2300 °C, samples are >99.5% carbon and by HRTEM show ribbon-like graphitic structures. By XRD and Raman, carbons from EGDMA-crosslinked PAN show higher order than those from HDDA-crosslinked samples. Remarkably, even though the crosslinker itself has been lost by 800 °C, there seems to be a memory effect whereas its molecular rigidity is transferred all the way to 2300 °C, and is imprinted upon the molecular structure of the graphitized samples.

REFERENCES

1. Gesser, H. D.; Goswami, P. C. *Chem. Rev.* **1989**, *89*, 765–788.
2. Hüsing, N.; Schubert, U. *Angew. Chem. Int. Ed.* **1998**, *37*, 22–45.
3. Rolison, D. R.; Dunn, B. J. *Mater. Chem.* **2001**, *11*, 963–980.
4. Pierre, A. C.; Pajonk, G. M. *Chem. Rev.* **2002**, *102*, 4243–4265.
5. Al-Muhtaseb, S. A.; Ritter, J. A. *Adv. Mater.* **2003**, *15*, 101–114.
6. Tillotson, T. M.; Hrubesh, L. W. *J. Non-Cryst. Solids.* **1992**, *145*, 44–50.
7. Yoldas, B. E.; Annen, M. J.; Bostaph, J. *Chem. Mater.* **2000**, *12*, 2475–2484.
8. Zhang, S. Q.; Wang, J.; Shen, J.; Deng, Z. S.; Lai, Z. Q.; Zhou, B.; Attia, S. M.; Chen, L. Y. *Nanostruct. Mater.* **1999**, *11*, 375-381.
9. Kanamori, K; Nakanishi, K. *Chem. Soc. Rev.* **2011**, *40*, 754-770.
10. Kistler, S. S. *J. Phys. Chem.* **1932**, *36*, 52-64.
11. Kistler, S. S.; Sherlock, S.; Appel, E. G. *Ind. Eng. Chem.* **1934**, *26*, 388-391.
12. http://www.aerogel.org/?p=822
13. Livage J.; Sanchez, C. *J. Non-Cryst Solids* **1992**, *145*,11-19.
14. Laudise, R. A.; Johnson Jr., D.W. *J. Non-Cryst. Solids.* **1986**, *79*, 155-164.
15. Zarzycki, J.; Prassas, M.; Phalippou, J. *J. Mat. Sci.* **1982**, *17*, 3371-3379.
16. Tewari, P. H.; Hunt, A. J.; Lofftus, K. D. *Mater. Lett.* **1985**, *3*, 363-367.
17. Nguyen, M. H.; Dao, L. H. *J. Non-Cryst. Solids* **1998**, *225*, 51-57.
18. Saliger, R.; Bock, V.; Petricevic, R.; Tillotson, T.; Geis, S.; Fricke, J. *J. Non-Cryst. Solids* **1997**, *221*, 144-150.
19. Wittwer, V. *J. Non-Cryst. Solids* **1992**, *145*, 233–236.
20. Fricke, J.; Emmerling, A. *J. Sol-Gel Sci. Technol.* **1998**, *13*, 299–303.
21. Gerlach, R.; Kraus, O.; Fricke, J.; Eccardt, P. C.; Kroemer, N.; Magori, V. *J. Non-Cryst. Solids* **1992**, *145*, 227–232.

(SIP),[20] we use R′=2,2′-azobisisobutyronitrile (AIBN) and introduce an alternative method for coating glass and oxidized metals with polymers. For this, a bidentate free radical initiator, ***Si-AIBN***, is attached covalently to a surface, and upon heating it induces "grafting from" polymerization of monomers in contact with the surface.[21] The method is predicated on the fact that polymers are end-capped with an initiator fragment. Experimental parameters are worked out with poly(methylmethacrylate) (PMMA) and poly(styrene) (PS). Subsequently, the findings are used to improve the adhesion of poly(3,4-ethylenedioxythiophene), PEDOT, arguably the most successful commercially conducting polymer manufactured and marketed by Bayer under the trade name *Baytron*® P as an aqueous solution of the poly(styrenesulfonate), PSS, salt of its oxidized-conducting form for use in antielectrostatic coatings.[22]

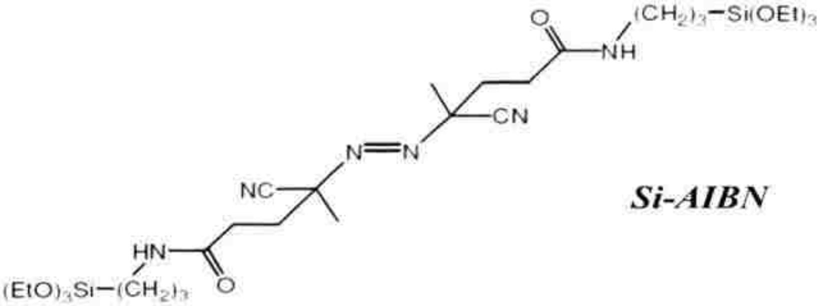

Si-AIBN

Since EDOT is not polymerizable by a free radical process, we use EDOT bifunctional analogues, 3,4-(vinylenedioxy)thiophene (VDOT), or 3,4-bis(vinyloxy)thiophene (BVOT), which have free radical reactive sites and a thiophene moiety that can be co-polymerized oxidatively with EDOT.[23]

Overall, the process of applying VDOT-EDOT films involves simple sol-gel chemistry and chemical oxidation, and can be integrated easily with conventional microfabication methods as demonstrated herewith with robust photolithographic patterning. Being covalently bonded to the substrate, the resulting VDOT-EDOT films are mechanically robust, hard, extremely adhering to the underlying surface, while they show similar electrically conductivity to PEDOT/PSS films obtained from *Baytron*® P.

EDOT:

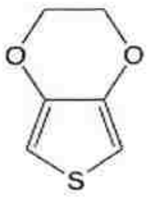

PEDOT:

VDOT:

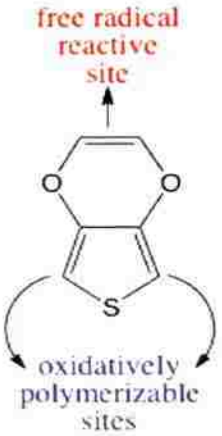

2. Results and Discussion

Covalent attachment of polymers to surfaces can be carried out either by "grafting to" or by "grafting from" methods. In both cases, prior to coating, the surface needs to be modified with an appropriate functionality. In the "grafting to" approach bulk polymerization is carried out in the solution in contact with the surface; then, periodically, randomly growing polymeric chains engage the surface functionality and get attached to the substrate. The bulk of the polymer though is formed in the solution, hence the method is not appropriate for high value added monomers. Thus, here we have opted for a "grafting from" approach using a free radical polymerization method and reasoning that by employing a bidentate free radical initiator all polymer should be confined on the surface, and precious unreacted monomer could be recovered. Clearly, this approach is based on the fact that in free radical polymerization polymeric chains are capped with an initiator fragment. As a suitable initiator for that purpose we use ***Si-AIBN***, which is synthesized in one step from 2,2′-azobiscyanovaleric acid and 3-aminopropyltriethoxysilane (APTES) as described before.[20] ***Si-AIBN*** was stored as a THF stock solution, which was typically applied on glass slides by spin coating (see Experimental). Films were aged in the dark and their thickness was found at around 350 nm (by Dektak profilometry, Figure 1.) For its own merit, but also in order to work out experimental details, the method was first applied successfully on conventional polymers such as polystyrene (PS) and polymethylmethacrylate (PMMA), and only then onto high value added conducting PEDOT films. In all cases, 2′′×2′′ glass slides have been used as substrates, even though PS or PMMA films have been also grown onto oxidized metal surfaces.

2.1 Control case: PMMA and PS films on Si-AIBN modified glass. For this, two methods were followed. The first involves dipping and incubating initiator coated glass slides in solutions of the monomer, while the second one involves spin-coating of a viscous prepolymer solution on top of the initiator layer followed by heating. For control, glass slides with no initiator were spin-coated with the prepolymer solution and heated. In all cases, slides were sonicated in toluene at the end. No polymer layer was visible on the control slides. Initiator bearing slides appear macroscopically uniform, and profilometry shows that the prepolymer route yields thicker films (up to 4000 nm) than incubation in monomer solutions (150 nm, see Figure 1). The chemical identify of the films was confirmed with IR spectroscopy (Figure 2) by scrapping the material accumulated on the glass slides. No features associated with the glass substrate, or the initiator are visible.

pattern are concerned, EDOT and VDOT are equivalent. Indeed, electrochemically (Figure 4) both EDOT and VDOT show an identical oxidation onset in acetonitrile at 1.2 V vs. Ag/AgCl. Unlike EDOT, however, VDOT carries an isolated double bond prone to radical addition.

Scheme 1. Synthesis of VDOT and BVOT

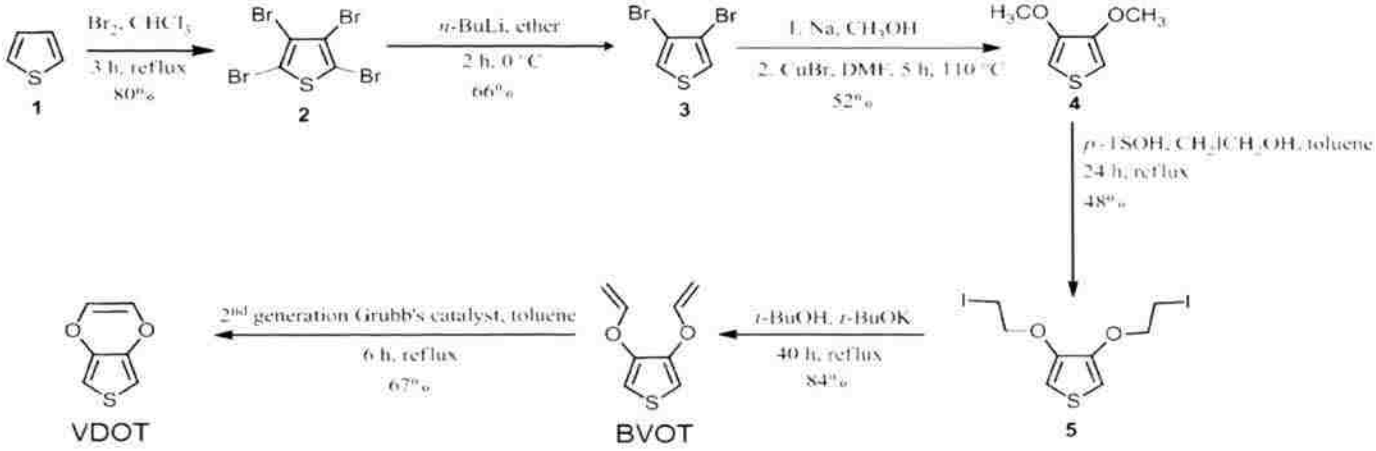

VDOT was synthesized from thiophene in satisfactory yields by modification of literature procedures according to Scheme 1.[31-35] It is noted that traditionally synthesis of EDOT is a five-step process,[36] but more recently a convenient synthesis has been described through a common intermediate with VDOT, namely compound **4** (3,4-dimethoxythiophene),[37] so that the overall synthesis of VDOT is only two more steps longer than the shortest route to EDOT.

Based on the findings with PS and PMMA, neat VDOT (or BVOT) was applied and spread evenly with a brush over glass slides, spin-coated with the initiator (***Si-AIBN***). However, after heating, aging and $FeCl_3$ treatment, VDOT-modified glass slides failed to give the characteristic blue color expected from the oxidized-conducting form of the polymer, and indeed the substrate remained electrically insulating. At that point it was reasoned that the random, but fairly rigid stereochemical arrangement of the thiophene moieties on the glass surface (refer to Scheme 2) was preventing them from reaching and coupling with one another via their 2- and 5- positions. Since, however, VDOT and EDOT have the same onset for oxidation (Figure 4), the gap between surface immobilized VDOT moieties could be bridged by co-polymerization with EDOT in a "grafting-to" approach, by simultaneous $FeCl_3$-oxidation of both moieties. The resulting films would remain covalently bonded to the substrate via VDOT (Scheme 2) and therefore should be extremely robust.

Scheme 2. Co-polymerization of VDOT and EDOT on a surface. (Depicting three EDOT bridging moieties is arbitrary and is used only for illustration.)

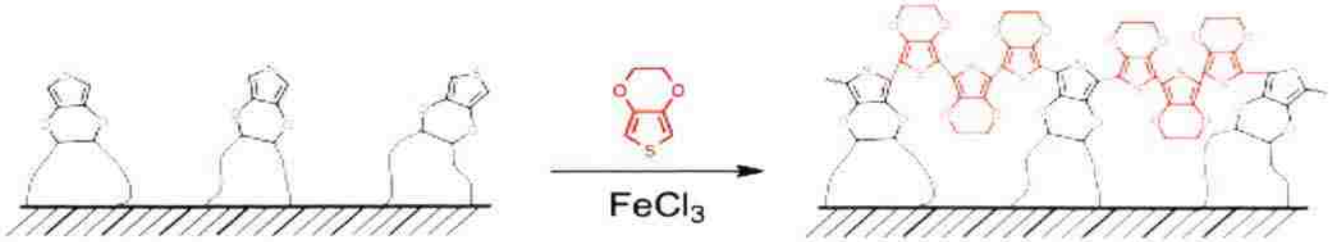

Scheme 3 summarizes the practical implementation of the process outlined above, and includes patterning of the resulting films by classical positive resist photolithography. Thus, dipping a colorless VDOT modified glass slide in a $FeCl_3$ solution in acetonitrile, followed by addition of EDOT produced an opaque-blue solution and left a deep blue coating on the VDOT-modified glass slide. Brief ultrasonication in acetonitrile removed all loosely held polymer from the glass slide, leaving behind a transparent light-blue coating that is not affected by further ultrasonication (even lasting for several hours). The films are both macroscopically (Figure 5) and microscopically (Figure 6) uniform. By profilometry, the film thickness was similar to what was measured for PMMA and PS films obtained by incubation of ***Si-AIBN*** modified glass slides in the monomer solutions (about 150 nm). Patterning is carried out by applying photoresist to protect the areas where the film is intended to survive, followed by etching (with HF) the photoresist unprotected areas (Scheme 3). Remaining photoresist over the blue film is removed with acetone. A photograph of a typical patterned film, made using a photomask from previous studies,[38] is included in Figure 5.

Scheme 3. Process summary for applying covalently bonded, conducting VDOT-EDOT films on glass and photolithographic patterning

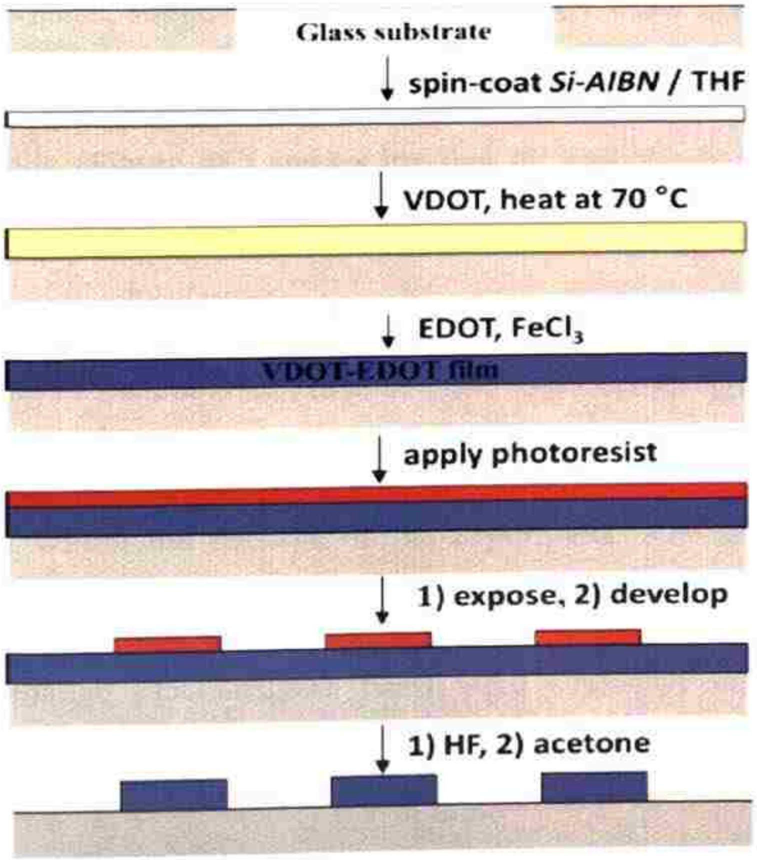

commercial *Baytron*® P on similar 2′′×2′′ glass slides. Table 1 summarizes the results. The conductivity of typical VDOT-EDOT films was measured with a four-point probe and it was found at 52 mho cm^{-1}, comparable to that of PEDOT/PSS films of similar thickness (150 nm). Again, similarly to the results obtained with PMMA and polystyrene films, VDOT-EDOT films show excellent adhesion retaining all 100 squares of the grid after a tape adhesion test, while the entire PEDOT/PSS film was lifted completely. The film hardness, evaluated by a pencil test (ASTM D 3363-00), was found higher than 6H, while that of the PEDOT/PSS films was just at the HB level. For further comparison, the hardness of poly-3-methylthiophene films has been found <6B, while by introducing molecular crosslinking at the monomer level prior to electropolymerization via esterification of 3-(3-thienyl)ethanol and 3-thienylacetic acid the hardness improved only up to the 3H level.[40]

Table 1. Selected properties of the VDOT-EDOT films of this study in comparison to those of PEDOT/PSS films applied from commercial *Baytron*® P under similar conditions (spin-coating)

	Film Type	
Property	**VDOT-EDOT (this study)**	**PEDOT/PSS (*Baytron*® P)**
Thickness (nm)	150	150
Conductivity (mho cm^{-1})	52	59
Adhesion (ASTM D 3359-97)	5B [a]	0B [b]
Pencil Hardness (ASTM D 3363-00)	>6H	HB

[a]. According to ASTM D 3359-97, 5B means that the edges of the cuts are completely smooth; none of the squares of the lattice is detached. [b]. According to the same standard, 0B means that the coating has flaked along the edges of cuts in large ribbons and whole squares have detached. The area affected is more than 35 to 65 % of the lattice. In this case it was 100%.

6. Figures

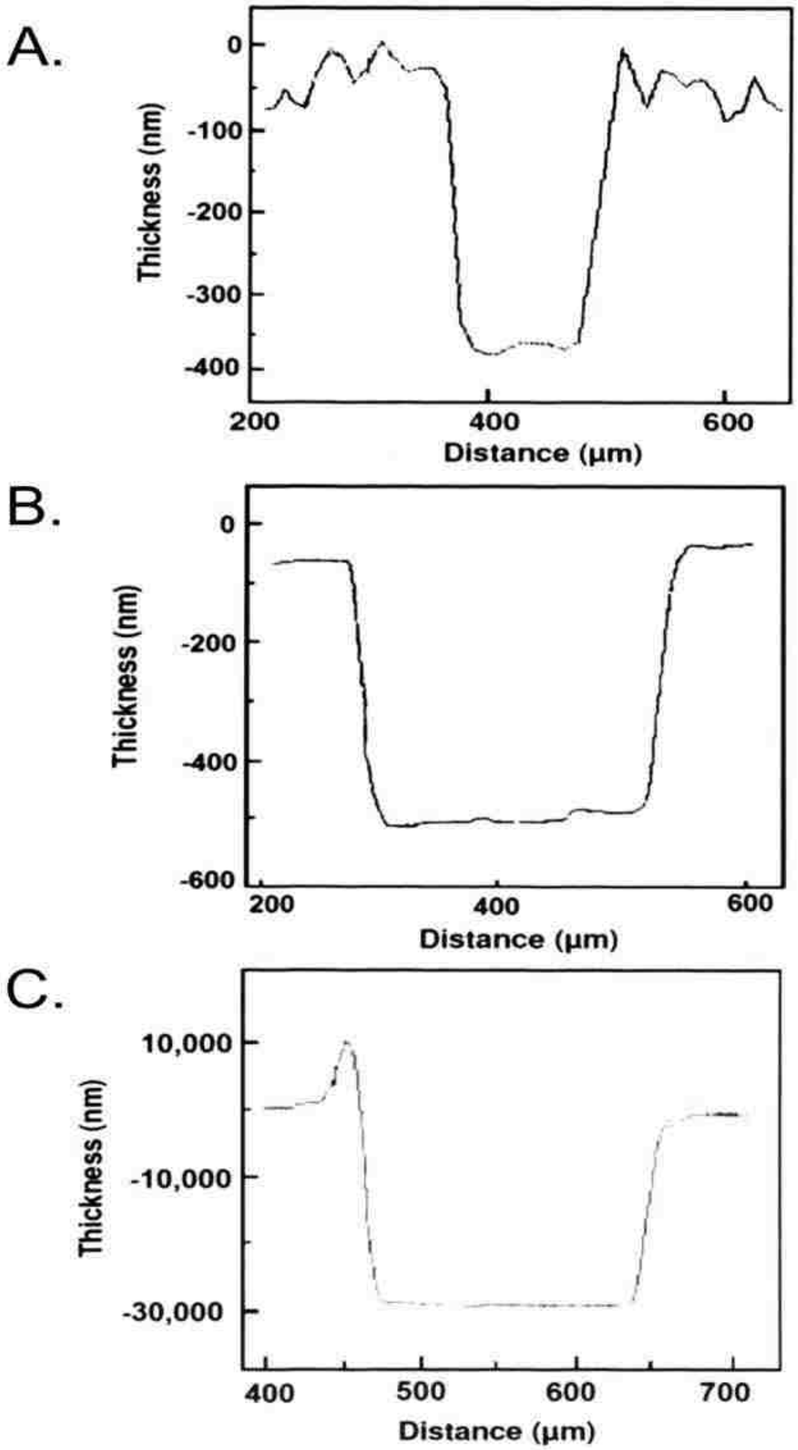

Figure 1. Profilometry of: (A) a ***Si-AIBN*** film spin-coated on a glass surface; (B) a PMMA film formed by dipping a film as in (A) in a MMA solution (toluene); and, (C) a PMMA film formed by spin-coating a film as in (A) with a PMMA pre-polymer (see Experimental).

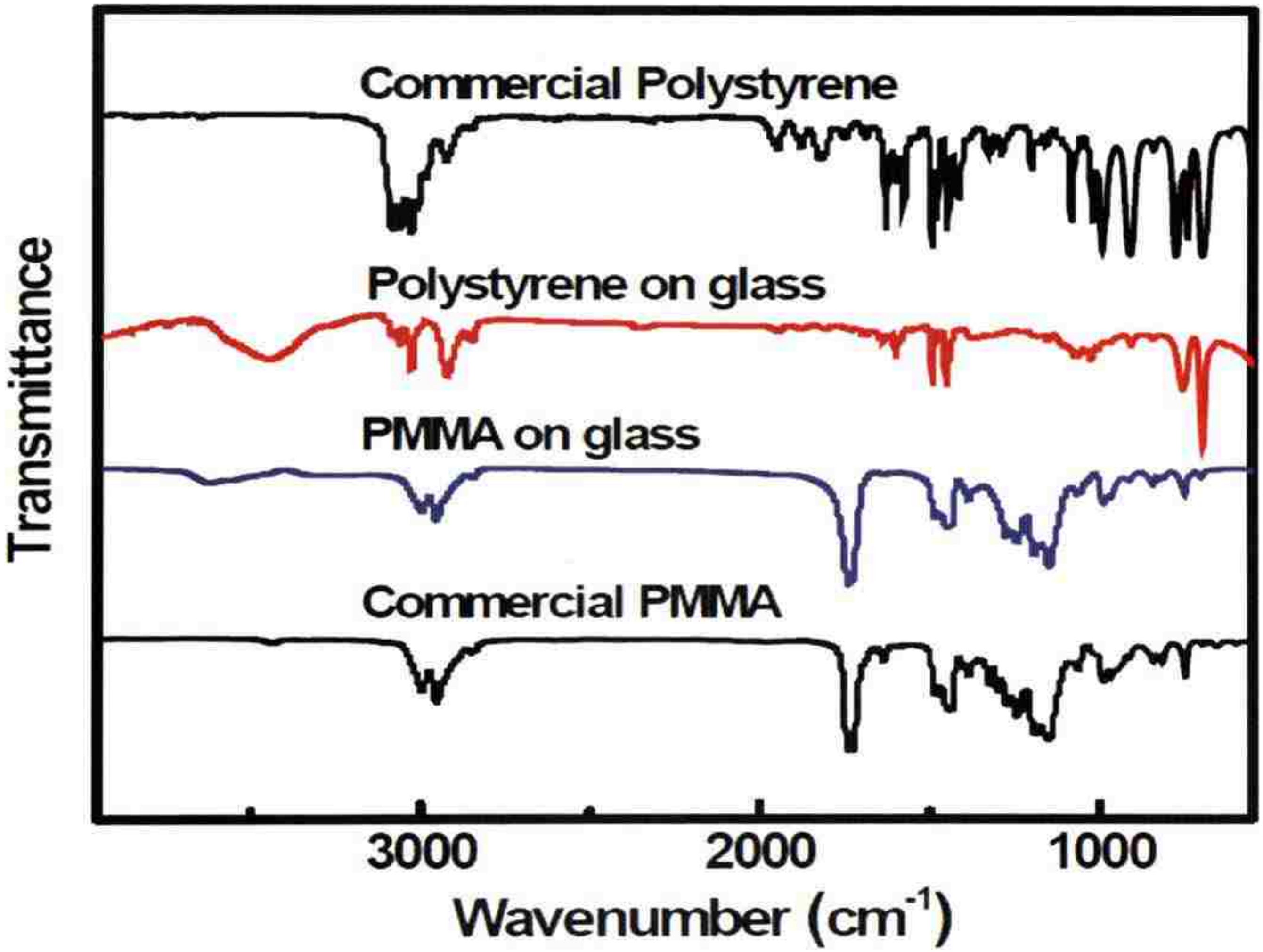

Figure 2. FTIR spectra of PMMA and polystyrene scrapped off films as in Figure 1B.

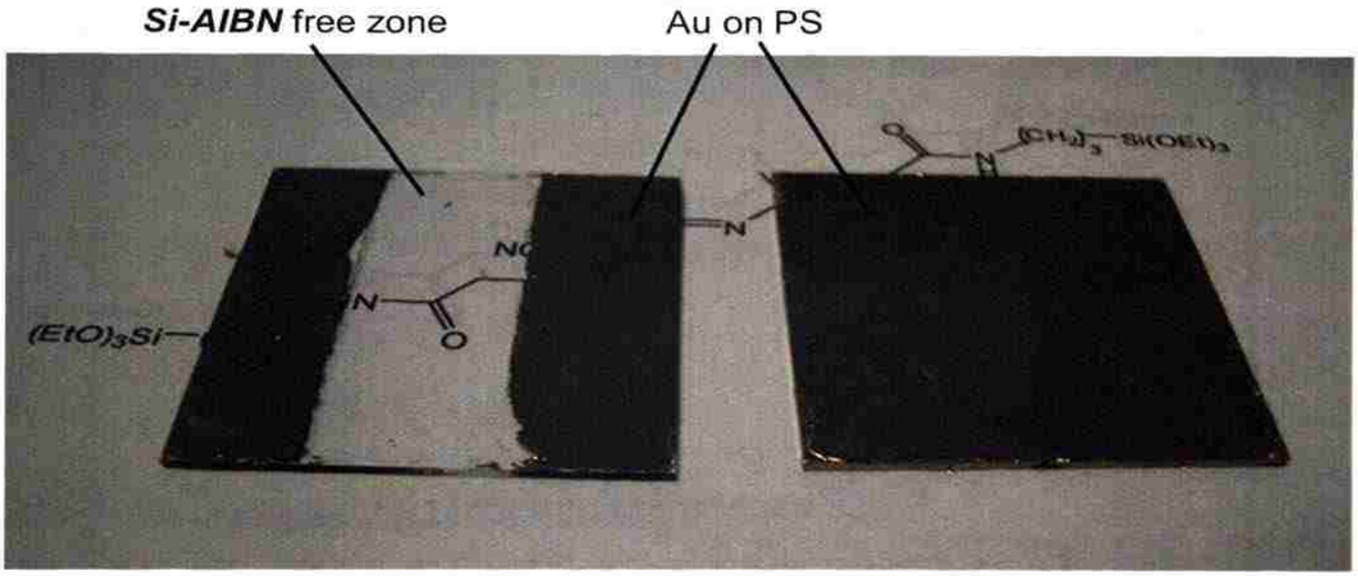

Figure 3. Au sputtered on polystyrene-coated glass slides after lift off by untrasonication in toluene. Left: The clear zone was not derivatized with ***Si-AIBN*** prior to polystyrene deposition from a prepolymer (see Experimental); polystyrene and its Au-coating survive only over areas where polystyrene is covalently bonded to the substrate via ***Si-AIBN***. Right: a similar slide, processed in parallel to the one at left, with uniform initiator coating.

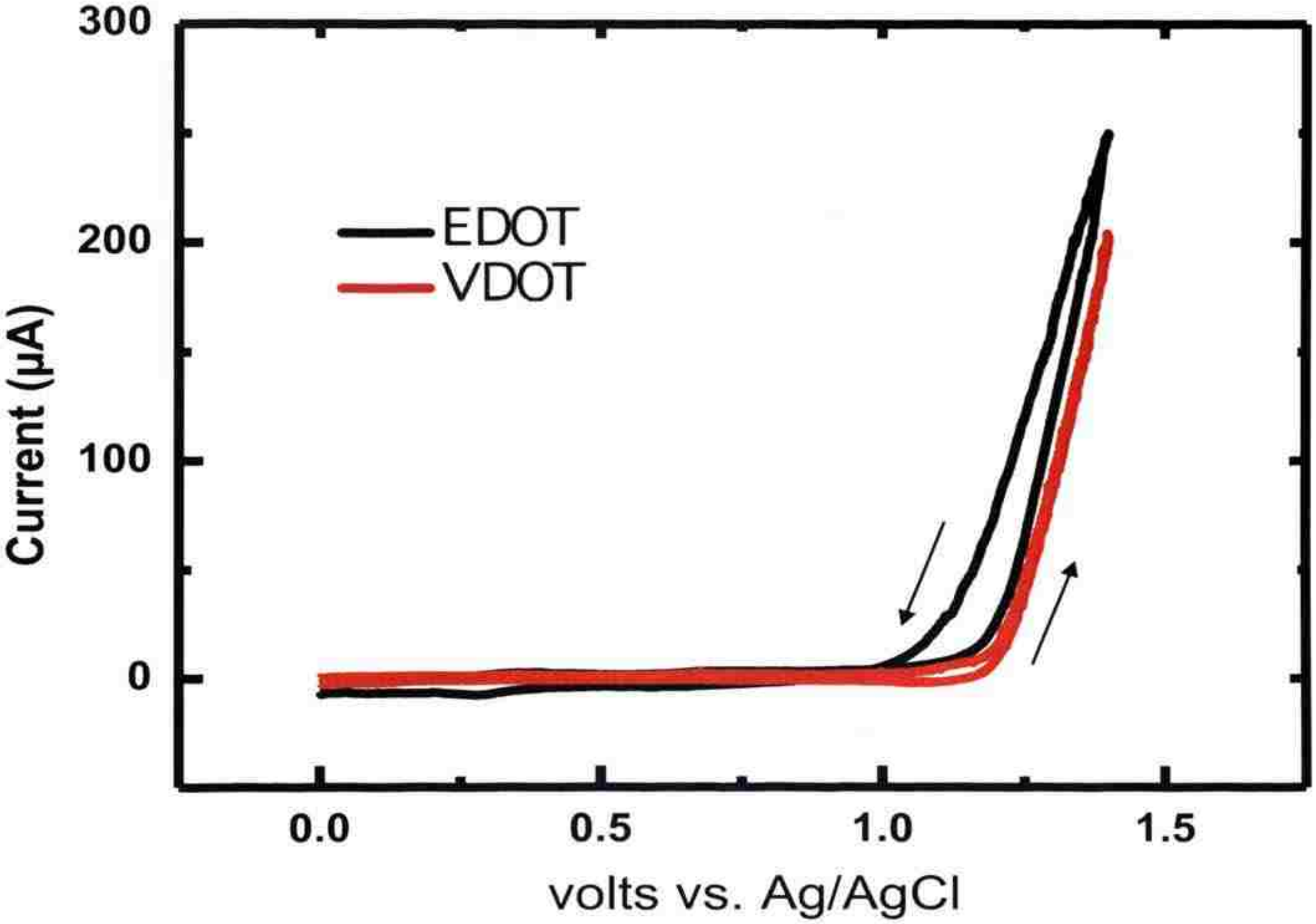

Figure 4. Cyclic voltammetry at 0.1 V s^{-1} with a Pt electrode (0.0314 cm^2) in Ar-degassed, 0.1 M solutions of VDOT and EDOT in acetonitrile containing 0.1M TBAP as supporting electrolyte.

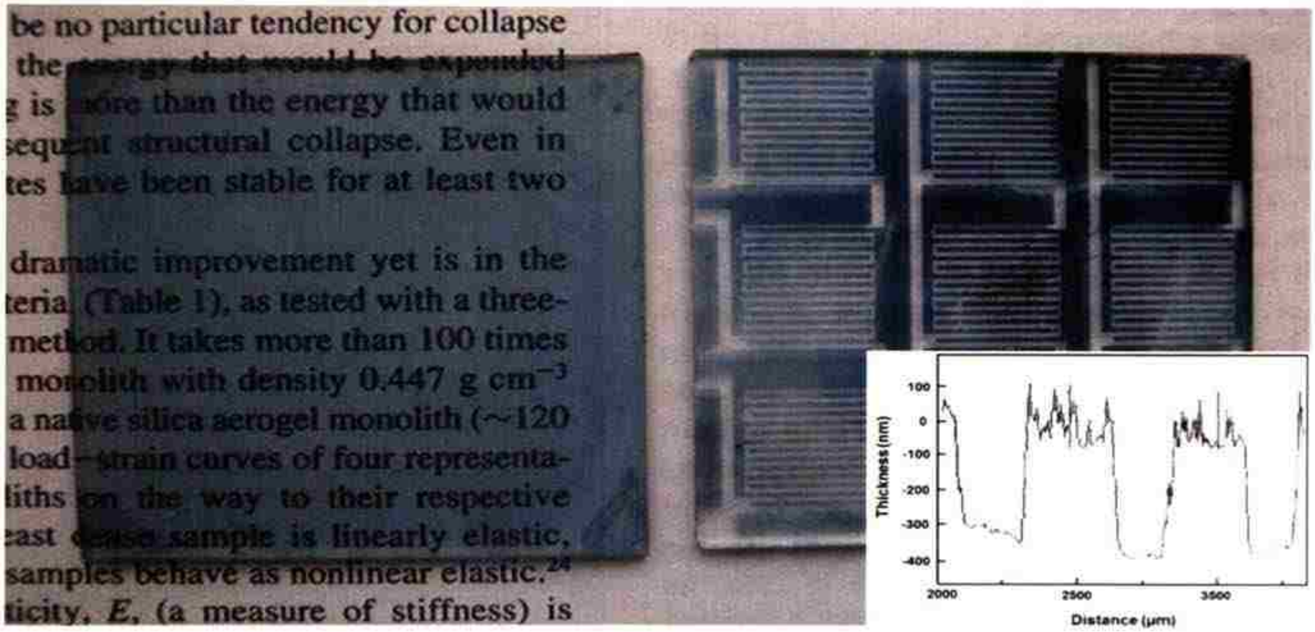

Figure 5. Optical photographs of BVOT-EDOT films on 2´´×2´´glass slides obtained by the process outlined in Scheme 3. Left, before; Right, after photolithographic patterning. (Inset: Dektak profilometry on the patterned substrate.)

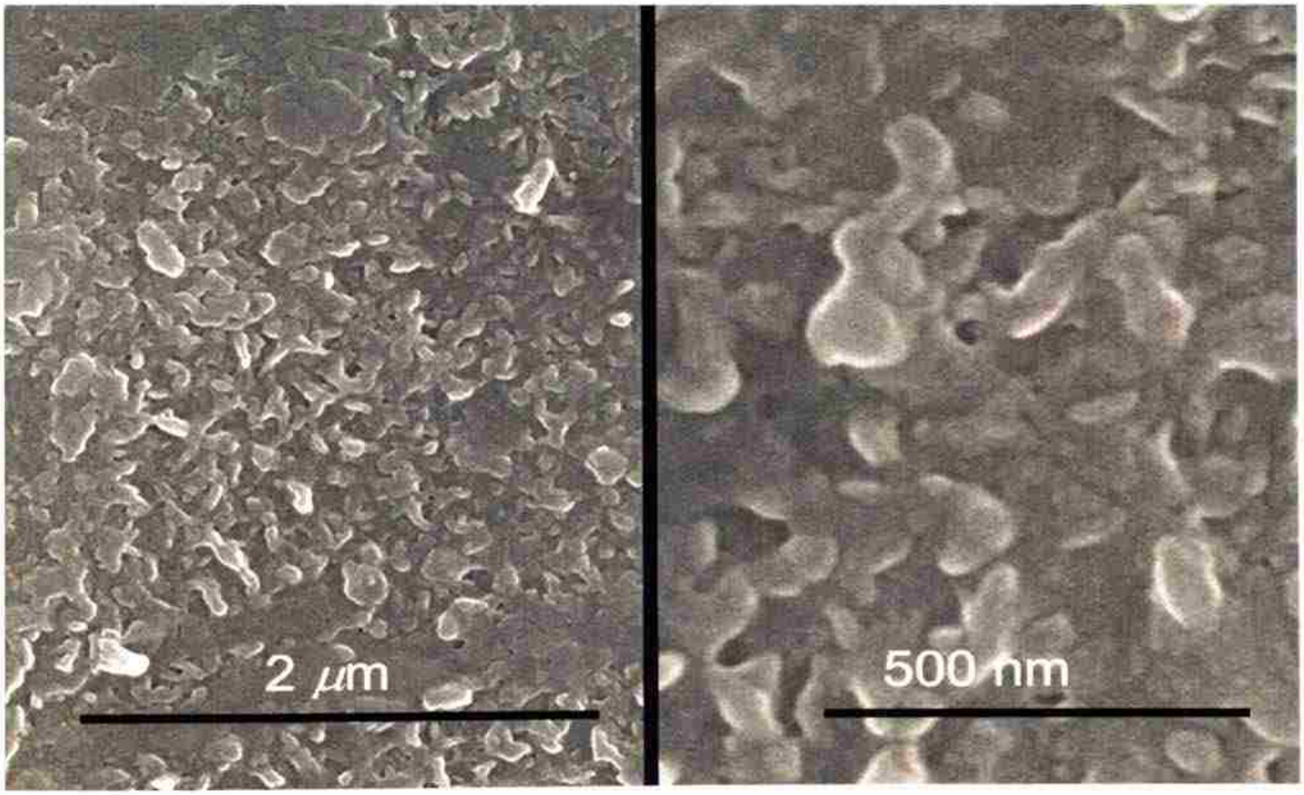

Figure 6. SEM at two different magnifications of a VDOT-EDOT film obtained by the process of Schemes 2 and 3.

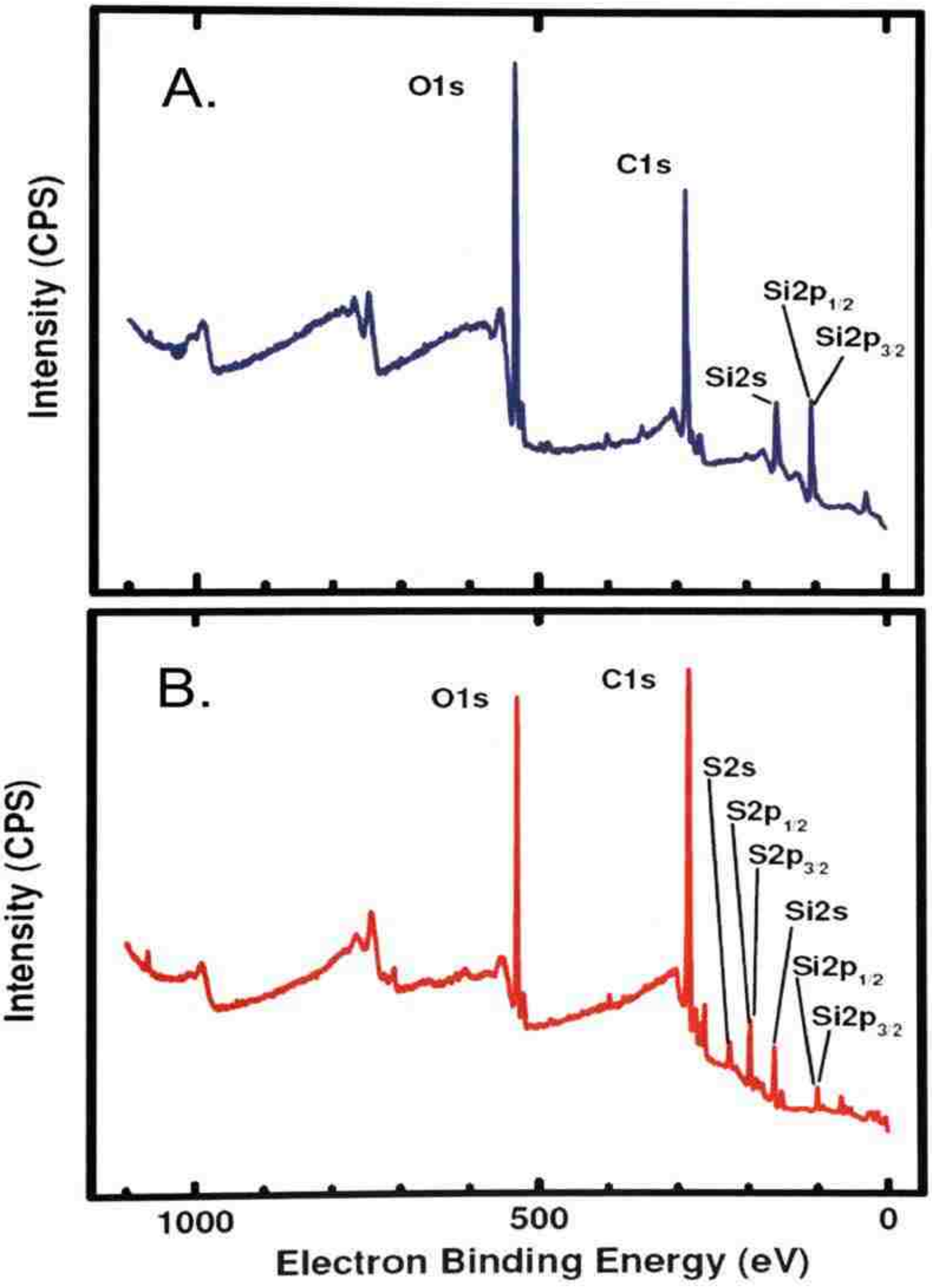

Figure 7. XPS analysis of ***Si-AIBN*** modified glass slides processed according to Scheme 3. (A) Control slide where VDOT was replaced by EDOT; (B) VDOT-EDOT film.

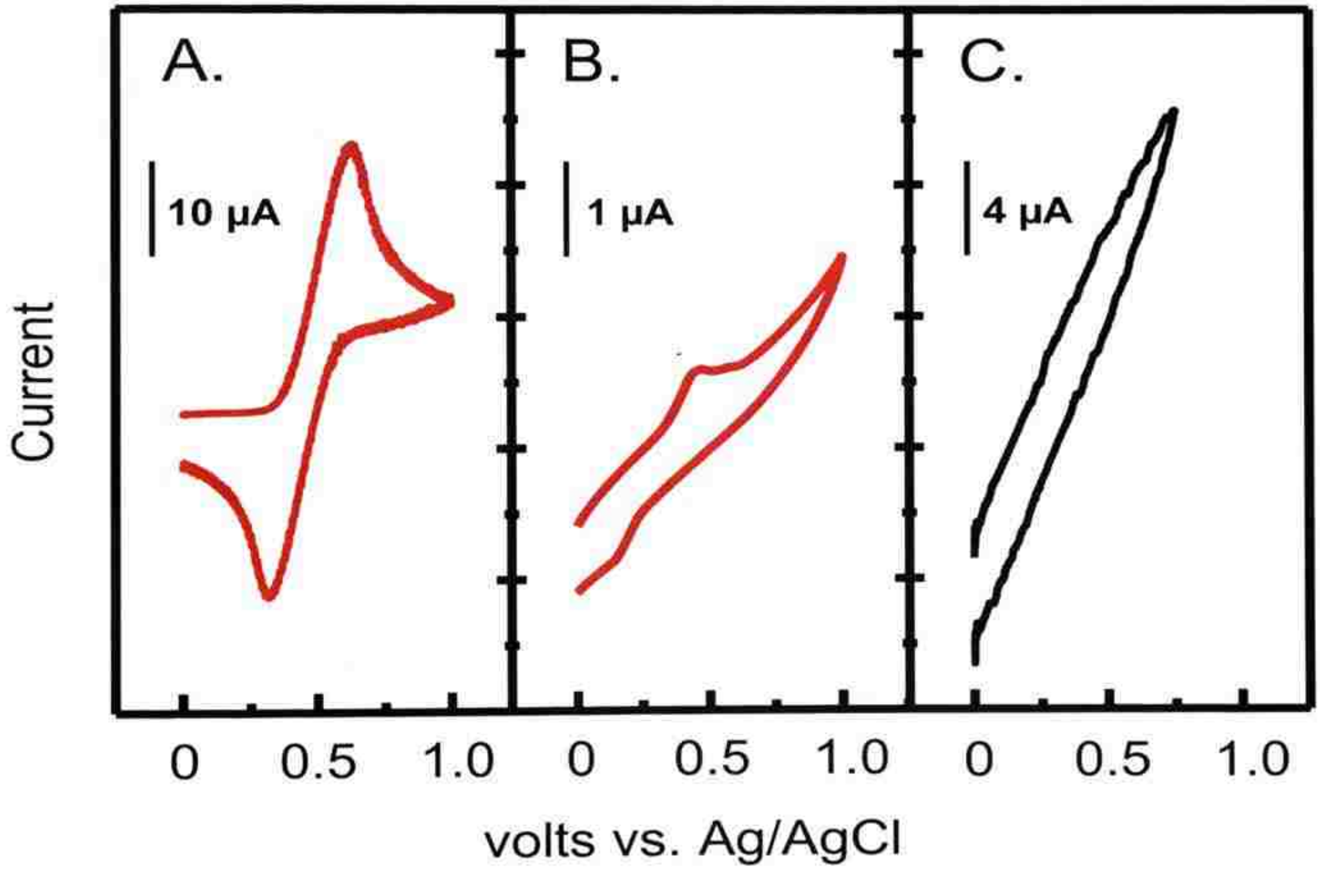

Figure 8. Electrochemistry at 0.1 V s^{-1} of ferrocene (3 mM) in an Ar-degassed CH_3CN/0.1 M TBAP solution, using: (A) a Pt-coated glass slide (~0.7 cm^2). (B) ***Si-AIBN*** modified, Pt-coated glass slide; (C) a VDOT-EDOT film on a ***Si-AIBN*** modified, Pt-coated glass slide.

II. Click Synthesis of Monolithic Silicon Carbide Aerogels from Polyacrylonitrile-Coated 3D Silica Networks

Nicholas Leventis*, Anand Sadekar, Naveen Chandrasekaran and
Chariklia Sotiriou-Leventis*

Department of Chemistry, Missouri University of Science and Technology,
(formerly University of Missouri-Rolla) Rolla, MO 65409, U.S.A.

Published in *Chemistry of Materials* **2010**, 22, 2790-2803.

SiC retains high mechanical strength and oxidation stability at over 1500 °C comprising a viable alternative to silica, alumina and carbon that have been in use as catalyst supports for over 60 years. Preparation of monolithic porous SiC is usually elaborate and porosities around 30% v/v are typically considered high. This report describes the synthesis of monolithic highly porous (70% v/v) SiC by carbothermal reduction (1200-1600 °C) of 3D sol-gel silica nanostructures (aerogels) conformally coated and crosslinked with polyacrylonitrile (PAN). Synthesis of PAN-crosslinked silica aerogels is carried out in one pot by simple mixing of the monomers, while conversion to SiC is carried out in a tube reactor by programmed heating. Intermediates after aromatization (225 °C in air) and carbonization (800 °C under Ar) were isolated and characterized for their chemical composition and materials properties. Data are interpreted mechanistically and were used iteratively for process optimization. Solids ^{29}Si NMR validates use of skeletal densities (by He pycnometry) for the quantification of the conversion of silica to SiC. Consistently with the topology of the carbothermal process, data support that complete conversion of SiO_2 to SiC requires a higher than the stoichiometric C:SiO_2 ratio of 3. The morphology of the SiC network is invariant of the processing temperature between 1300 °C and 1600 °C, hence it is advantageous to carry

out the carbothemal process at higher temperatures where reactions run faster. Samples consist of pure polycrystalline β-SiC (skeletal density: 3.20 g cm^{-3}) with surface areas in the range reported previously for biomorphic SiC (~20 m^2 g^{-1}). Albeit the invariance of the micromorphology, the crystallite size of SiC increases with the processing temperature (from 7.1 nm at 1300 °C to 16.5 nm at 1600 °C). Samples processed at 1200 °C are amorphous (by XRD), even though they consist of ~75% mol/mol SiC. This comprises the first report of using a polymer crosslinked aerogel for the synthesis of another porous material.

1. Introduction

Silicon carbide (SiC), a bioinrert large band-gap semiconductor, combines hardness (9 to 9.5 in the Mohs scale), high thermal conductivity (120 W m^{-1} K^{-1}), low thermal expansion coefficient (4×10^{-6} °C^{-1}), good thermal shock resistance, high mechanical strength / oxidation resistance at high temperatures (>1500°) and is a viable candidate for replacing silica, alumina, and carbon as supports for catalysts.[1,2]

Monolithic porous SiC can be prepared by sintering powders,[3,4] which are synthesized economically by carbothermal reduction of silica with carbon according to the old (1891) Acheson process (eq 1).[5] However, because of the high covalent character

$$SiO_2 + 3\,C \longrightarrow SiC + 2\,CO \qquad (1)$$

and strength of the sp^3- sp^3 C-Si bonds,[6] SiC itself is basically a non-sinterable material,[7] thereby sintering is carried out reactively, usually with sintering aids (e.g., alumina, carbon). Oxidation bonding, whereas SiC compacts are heated at 1100-1500 °C in air, can be considered as a simple version of reactive sintering; porosities of up to 30% have been achieved by including sacrificial (oxidizable) graphite in the compacts.[8]

Alternatively, porous SiC is obtained by shape-memory-synthesis (SMS) whereas the product of eq 1 mimics the shape of the carbon source.[2] As it will be discussed later, eq 1 is a complex process that starts with generation of SiO gas and CO at the SiO_2/C interface.[5] SiC is primarily the result of the gas-solid reaction between SiO(g) and C(s).[9] Thus, SMS of porous SiC was carried out initially with SiO(g) generated independently (e.g., by reacting Si and SiO_2) and porous carbon from various sources.[2] Since natural materials are renewable and relatively inexpensive, SMS-conversion of biomorphic carbon (charcoal) to SiC that retains the hierarchical porous structure of the parent wood has been investigated extensively.[10] More economic alternatives include infiltration of charcoal with silica sol,[11] and ultimately infiltration of wood directly with sodium silicate, thus eliminating even the pyrolysis step of converting wood to charcoal as that takes place *in situ* along the way of setting off the carbothermal process of eq 1.[12] Typical surface areas for biomorphic SiC are about 14 m^2g^{-1}. The methodology of using charcoal as a structure directing agent has also been extended to artificial porous graphitic substrates.[13] The major drawback of using silica sols is the requirement of multi-infiltrations in order to bring the $C:SiO_2$ ratio at the stoichiometry of eq 1.

Carbon- or carbon-precursor doped silica aerogels and xerogels have been employed as SiC precursors, not so much from a SMS perspective, but rather because of their high surface area that would increase the contact between the two solid-state reactants of eq 1.[14] In most instances, however, the resulting SiC is more whiskery than particulate. Whiskers are formed via a gas-phase reaction (eq 2) between the SiO(g) and

$$SiO(g) + 3\,CO(g) \longrightarrow SiC(s) + 2\,CO_2(g) \qquad (2)$$

Table 1. Formulations for one-pot synthesis of PAN-crosslinked silica aerogels

Formulation	**TMOS** **mL (mol)**	**Si-AIBN** **mL (mol)** [a]	**CH_3OH** **mL**	**H_2O** **mL**	**AN** **mL (mol)**
F-10-00	3.465 (0.0234)	11.5 (0.0130)	9.00	1.5	0.00 (0.0000)
F-10-30	3.465 (0.0234)	11.5 (0.0013)	6.30	1.5	2.70 (0.0407)
F-10-45	3.465 (0.0234)	11.5 (0.0013)	4.95	1.5	4.05 (0.0611)
F-10-60	3.465 (0.0234)	11.5 (0.0013)	3.60	1.5	5.40 (0.0814)
F-20-00	3.068 (0.0207)	23.0 (0.0026)	9.00	1.5	0.00 (0.0000)
F-20-30	3.068 (0.0207)	23.0 (0.0026)	6.30	1.5	2.70 (0.0407)
F-20-45	3.068 (0.0207)	23.0 (0.0026)	4.95	1.5	4.05 (0.0611)
F-20-60	3.068 (0.0207)	23.0 (0.0026)	3.60	1.5	5.40 (0.0814)
F-30-00	2.68 (0.0181)	34.5 (0.0039)	9.00	1.5	0.00 (0.0000)
F-30-30	2.68 (0.0181)	34.5 (0.0039)	6.30	1.5	2.70 (0.0407)
F-30-45	2.68 (0.0181)	34.5 (0.0039)	4.95	1.5	4.05 (0.0611)
F-30-60	2.68 (0.0181)	34.5 (0.0039)	3.60	1.5	5.40 (0.0814)

[a] Volume of a stock solution of ***Si-AIBN*** (0.1122 M) in THF.

Preparation of silicon carbide aerogels from PAN-crosslinked aerogels. PAN-crosslinked aerogels were initially aromatized by heating in air at 225 °C for 36 h. The color changed from white to brown. Subsequently, they were transferred to an MTI GSL1600X-80 tube furnace and they were heated further under flowing Ar (70 mL min^{-1}): The temperature of

3. Results

3.1 General. Scheme 1 summarizes the overall process for the synthesis and conversion of PAN-coated silica aerogels to porous monolithic SiC. That process starts with the one-pot synthesis of PAN-coated silica wet-gels that are dried to PAN-crosslinked silica aerogels with SCF CO_2. The PAN coating is aromatized at 225 °C in air, and subsequently samples are placed in a tube furnace and are heated stepwise under flowing Ar to a range of terminal temperatures from 1200 °C to 1600 °C. Unreacted carbon is removed at 600 °C in air. Although the entire process can be carried out continuously, several runs were interrupted at various intermediate stages and samples were analyzed in order to identify the controlling parameters and optimize the synthetic conditions for complete conversion of SiO_2 to monolithic SiC. Specifically, samples were also analyzed after aromatization at 225 °C, after carbonization at 800 °C, and before removal of unreacted carbon. Results are summarized in Tables 2-4. Alternatively, the entire process is shortened by eliminating the SCF CO_2 drying step and it was found (Table 5) that the porous SiC samples were identical to those received by the lengthier process.

3.2 Synthesis of PAN-crosslinked aerogels. Mesoporous monolithic silica was coated (crosslinked) with PAN in one pot through surface initiated free-radical polymerization (SIP) of the monomer (AN) according to eq 3. ***Si-AIBN***, a bidentate free-radical initiator,

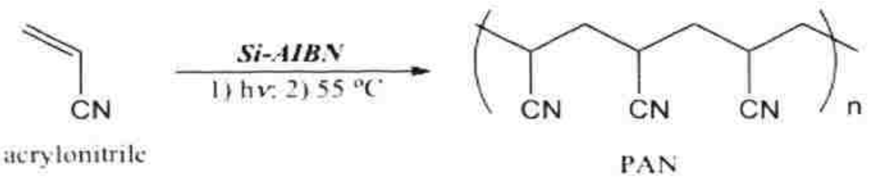

(3)

was incorporated in the silica structure. The complete characterization data for the native and PAN-crosslinked samples are summarized in Table 2.

Scheme 1. Flowchart for the Synthesis and Characterization of SiC Aerogels

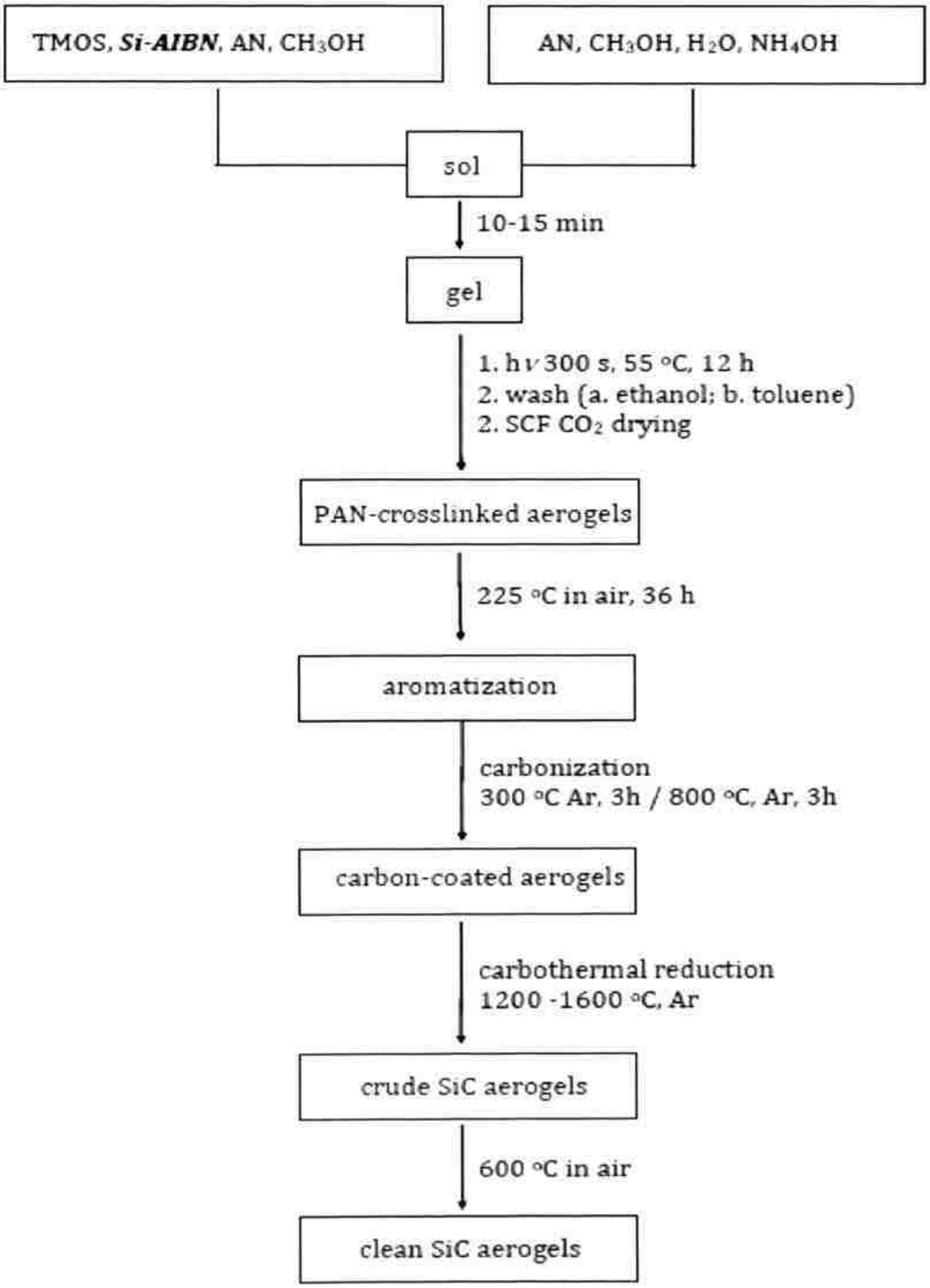

Table 2. Selected properties of PAN-crosslinked silica aerogels

sample	diameter (cm) [a]	percent shrinkage [b]	bulk density, ρ_b (g cm^{-3})	skeletal density, ρ_s (g cm^{-3}) [c]	porosity, Π(% void space)	BET surface area, σ (m^2 g^{-1})	average pore diameter (nm) [d]	particle radius, r (nm) [e]
F-10-00	0.925±0.003	5.0	0.177±0.004	1.887±0.006	90	681	8.5 [10.0]	2.2
F-10-30	0.923±0.001	7.7	0.329±0.011	1.498±0.003	78	322	14.1 [14.5]	6.2
F-10-45	0.938±0.003	6.2	0.426±0.004	1.462±0.003	71	206	13.2 [20.1]	10.0
F-10-60	0.945±0.007	5.5	0.475±0.007	1.478±0.002	68	228	15.6 [17.6]	8.9
F-20-00	0.920±0.005	8.0	0.190±0.002	1.798±0.004	89	647	14.28 [9.9]	2.2
F-20-30	0.936±0.004	6.4	0.360±0.005	1.435±0.009	75	275	15.0 [15.6]	7.6
F-20-45	0.948±0.003	5.2	0.414±0.004	1.458±0.010	72	157	23.7 [26.7]	13.1
F-20-60	0.947±0.004	5.3	0.467±0.004	1.423±0.007	67	144	13.9 [26.6]	14.6
F-30-00	0.922±0.003	7.8	0.198±0.003	1.705±0.002	88	643	9.5 [9.4]	2.7
F-30-30	0.925±0.002	7.5	0.378±0.003	1.428±0.009	74	195	14.3 [21.5]	10.8
F-30-45	0.931±0.002	6.9	0.470±0.002	1.448±0.007	68	147	15.6 [26.6]	14.1
F-30-60	0.950±0.001	5.0	0.473±0.003	1.423±0.089	67	151	32.4 [25.1]	13.9

[a]. Average of 5 samples. [b]. Relative to the molds (1 cm diameter). [c]. One sample, average of 50 measurements. [d] By the $4\times V_{Total}/\sigma$ method. For the first number, V_{Total} was calculated by the single-point adsorption method; for the number in brackets V_{Total} was calculated via V_{Total} = $(1/\rho_b)$-$(1/\rho_s)$. [e]. Calculated via $r = 3/\rho_s\sigma$.

The porosity, Π, as % v/v of empty space, has been decreased from ~90% in the native samples to ~70% in the crosslinked samples, consistent with the particle size increase (calculated via radius $r = 3/\rho_s\sigma$, Table 2) brought about by the conformal polymer coating.

3.3 Aromatization of PAN-crosslinked aerogels. Conversion of PAN to carbon requires prior aromatization, which is typically induced oxidatively by heating the polymer between 270 and 300 °C in air (eq 4).[24,26,27] Indeed, direct heating of PAN-crosslinked aerogels at 800 °C in argon causes decomposition of the polymer and complete loss of the organic matter. Heating PAN-crosslinked samples in air shows a sharp exotherm at 253 °C (by DSC; Figure 3). Aromatization (followed by ^{13}C NMR, Figure 4) takes place at both sides of the endotherm, albeit more slowly at the low temperature end (225 °C versus 300 °C, refer to Figure 4). However, processing PAN-crosslinked silica aerogel monoliths at 300 °C tends to break them into small pieces, presumably due to stresses on the silica framework created by the structural rearrangement of the polymer during its aromatization. On the other hand, a combination of conditions expected to produce shorter polymer chains (higher ***Si-AIBN*** concentrations: F-20 and F-30 formulations) with lower aromatization temperatures seem to yield monoliths with 100% success rate. Microscopically, those samples look quite similar to their parent PAN-crosslinked

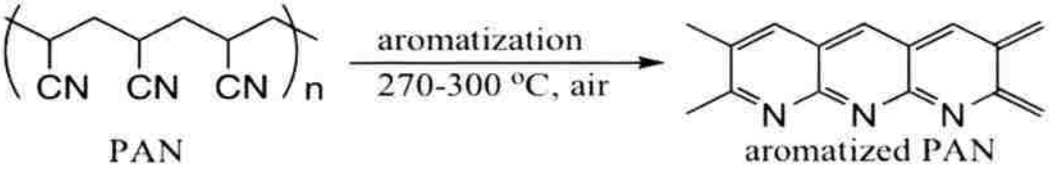

(4)

aerogels (Figure 1B). Therefore, for further processing we opted to heat samples for longer time periods (36 h) at 225 °C (Scheme 1). The incomplete aromatization of PAN under those conditions (see spectrum in Figure 4 labeled "225 °C in air") necessitated determination of the C:SiO_2 mol ratio produced after carbonization as a function of the initial formulation of the PAN-crosslinked samples.

3.4 Carbonization of aromatized PAN-crosslinked aerogels. Aromatized PAN-crosslinked aerogels are converted to SiC by heating in the 1200-1600 °C range under Ar. As confirmed by ^{13}C NMR (Figure 4), at around 800 °C aromatized PAN is converted to carbon (eq 5).[24,26] Aromatized samples heated at just 800 °C allow correlation of the initial synthetic conditions to the C:SiO_2 mol ratio. The complete analysis of the carbonized samples is summarized in Table 3. Carbonization causes additional shrinkage (12-13 %) relative to the parent PAN-crosslinked aerogel precursors, but samples retain their shape and micro-morphology (by SEM, Figure 1C). N_2 adsorption isotherms (Figure 2B) show signs of macroporosity (lower total volume of N_2 adsorbed, lack of saturation, increase in the volume adsorbed mainly above 90% of relative pressure), and pore diameters calculated via the $V_{\mathrm{Total}}/4\sigma$ method using V_{Total} obtained by the single point

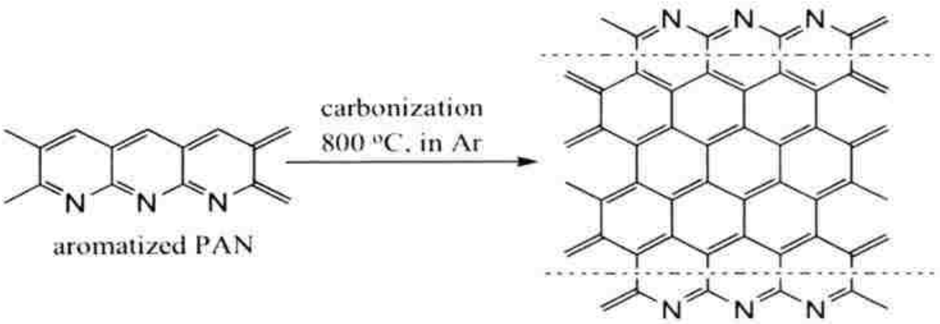

(5)

Table 3. Characterization of PAN-crosslinked silica aerogels after pyrolysis at 800 °C.

sample	diameter (cm)	percent shrinkage [a]	bulk density, ρ_b (g cm^{-3})	skeletal density, ρ_s (g cm^{-3})	porosity, Π (% void space)	BET surface area, σ (m^2 g^{-1})	average pore diameter (nm) [b]	particle radius, r (nm) [c]	C:SiO$_2$ (mol/mol)
F-10-30	0.823	13	0.290	2.187±0.024	86	124	24.2 [60.8]	11.0	2.55
F-10-45	0.832	12	0.333	2.118±0.003	84	93	13.8 [76.1]	15.1	4.65
F-10-60	0.845	11	0.357	2.149±0.006	83	79	16.5 [90.5]	17.6	8.85
F-20-30	0.849	13	0.276	2.134±0.042	87	96	13.5 [76.9]	14.5	4.36
F-20-45	0.834	12	0.365	2.178±0.011	83	94	12.8 [76.7]	14.6	7.08
F-20-60	0.834	12	0.410	2.140±0.008	80	74	18.0 [93.2]	18.9	7.66
F-30-30	0.843	13	0.321	2.178±0.011	85	99	17.1 [74.9]	13.9	4.36
F-30-45	0.822	13	0.396	2.156±0.009	81	79	14.2 [88.1]	17.4	6.85
F-30-60	0.840	12	0.495	2.140±0.007	77	69	18.4 [90.0]	20.3	9.49

[a]. Relative to the PAN-crosslinked aerogels. [b]. By the $4\times V_{\text{Total}}/\sigma$ method. For the first number, V_{Total} was calculated by the single-point adsorption method; for the number in brackets V_{Total} was calculated via $V_{\text{Total}} = (1/\rho_b)-(1/\rho_s)$. [c]. Calculated via $r = 3/\rho_s\sigma$.

Table 4. Characterization of SiC aerogels prepared under different conditions

sample °C(hours) (nm) [d]	diameter (cm)	shrinkage (%) [a]	bulk density, ρ_b (g cm^{-3})	skeletal density, ρ_s (g cm^{-3})	porosity, Π(% void space)	BET surface area, σ (m^2 g^{-1})	avera pore diameter (nm) [b]	radius, r (nm) [c]	Crystallite size
F-20-30 (C:SiO$_2$ = 4.36 mol/mol)									
1200(36)	0.487	48	0.623	2.968±0.024	81	221	14.6 [23.0]	4.6	[e]
1200(72)	0.555	41	0.533	2.944±0.017	78	198	15.6 [31.0]	5.1	[e]
1300(36)	0.536	43	0.591	3.014±0.028	79	108	20.9 [51.4]	9.4	
	7.5±0.9								
1300(72)	0.540	42	0.526	3.078±0.010	76	42	21.3 [150]	23.2	[f]
1400(36)	0.578	39	0.503	3.021±0.019	75	16	21.2 [415]	61.9	
	14.6±0.3								
1400(72)	0.565	40	0.515	3.118±0.013	74	18	15.4 [360]	53.5	[f]
F-20-45 (C:SiO$_2$ = 7.08 mol/mol)									
1200(36)	0.578	30	0.410	2.919±0.006	71	394	17.6 [21.3]	2.6	[e]
1200(72)	0.567	40	0.401	2.928±0.032	71	381	16.1 [22.6]	2.7	[e]
1200(110)	0.563	40	0.447	2.917±0.099	71	370	10.8 [20.5]	2.8	[e]
1200(140)	0.583	38	0.441	2.930±0.124	69	385	9.4 [20.0]	2.7	[e]
1300(36)	0.589	38	0.473	3.088±0.014	71	53	22.7 [135]	18.3	[f]
1300(72)	0.612	35	0.446	3.170±0.028	72	22	18.1 [350]	43.0	7.1±0.8
1400(72)	0.598	37	0.481	3.153±0.054	72	20	12.5 [353]	47.6	14.9±0.9
1500(72)	0.590	38	0.430	3.190±0.033	70	16	16.9 [502]	58.8	16.6±0.8
1600(72)	0.579	39	0.482	3.200±0.043	75	13	21.7 [542]	72.1	16.5±1.3

[a] Shrinkage relative to the diameter of the PAN-crosslinked aerogels. [b] By the $4\times V_{Total}/\sigma$ method. For the first number, V_{Total} was calculated by the single-point adsorption method; for the number in brackets V_{Total} was calculated via $V_{Total} = (1/\rho_b)-(1/\rho_s)$. [c] Calculated via $r = 3/\rho_s\sigma$. [d] By XRD using the Scherrer equation; averages from the values obtained from the (111), (220) and (311) reflections. [e] Amorphous. [f] Not determined.

Table 4. Characterization of SiC aerogels prepared under different conditions

sample °C(hours) (nm) [d]	diameter (cm)	shrinkage (%) [a]	bulk density, ρ_b (g cm^{-3})	skeletal density, ρ_s (g cm^{-3})	porosity, Π(% void space)	BET surface area, σ (m^2 g^{-1})	avera pore diameter (nm) [b]	radius, r (nm) [c]	Crystallite size
F-20-30 ($C:SiO_2$ = 4.36 mol/mol)									
1200(36)	0.487	48	0.623	2.968±0.024	81	221	14.6 [23.0]	4.6	[e]
1200(72)	0.555	41	0.533	2.944±0.017	78	198	15.6 [31.0]	5.1	[e]
1300(36)	0.536 7.5±0.9	43	0.591	3.014±0.028	79	108	20.9 [51.4]	9.4	
1300(72)	0.540	42	0.526	3.078±0.010	76	42	21.3 [150]	23.2	[f]
1400(36)	0.578 14.6±0.3	39	0.503	3.021±0.019	75	16	21.2 [415]	61.9	
1400(72)	0.565	40	0.515	3.118±0.013	74	18	15.4 [360]	53.5	[f]
F-20-45 ($C:SiO_2$ = 7.08 mol/mol)									
1200(36)	0.578	30	0.410	2.919±0.006	71	394	17.6 [21.3]	2.6	[e]
1200(72)	0.567	40	0.401	2.928±0.032	71	381	16.1 [22.6]	2.7	[e]
1200(110)	0.563	40	0.447	2.917±0.099	71	370	10.8 [20.5]	2.8	[e]
1200(140)	0.583	38	0.441	2.930±0.124	69	385	9.4 [20.0]	2.7	[e]
1300(36)	0.589	38	0.473	3.088±0.014	71	53	22.7 [135]	18.3	[f]
1300(72)	0.612	35	0.446	3.170±0.028	72	22	18.1 [350]	43.0	7.1±0.8
1400(72)	0.598	37	0.481	3.153±0.054	72	20	12.5 [353]	47.6	14.9±0.9
1500(72)	0.590	38	0.430	3.190±0.033	70	16	16.9 [502]	58.8	16.6±0.8
1600(72)	0.579	39	0.482	3.200±0.043	75	13	21.7 [542]	72.1	16.5±1.3

[a]. Shrinkage relative to the diameter of the PAN-crosslinked aerogels. [b]. By the $4\times V_{Total}/\sigma$ method. For the first number, V_{Total} was calculated by the single-point adsorption method; for the number in brackets V_{Total} was calculated via $V_{Total} = (1/\rho_b)-(1/\rho_s)$. [c]. Calculated via $r = 3/\rho_s\sigma$. [d]. By XRD using the Scherrer equation; averages from the values obtained from the (111), (220) and (311) reflections. [e]. Amorphous. [f]. Not determined.

Table 5. Conversion efficiency of SiO_2 in PAN-crosslinked F-20-45 samples into SiC

processing at ^{o}C [a]	sample (g)	weight of SiO_2 (g) [b]	expected SiC (g)	"crude" [c] material (g)	calculated weight of pure SiC (g) [d]	SiC yield (% w/w)
1300/600	1.1987	0.3836	0.2578	0.2581	0.2544	98.7
1400/600	1.1677	0.3737	0.2511	0.2570	0.2358	93.9
1500/600	1.1498	0.3679	0.2473	0.2511	0.2500	101.1
1600/600	1.1504	0.3681	0.2474	0.2384	0.2384	96.4

[a]. Processing time at the two temperatures: 72 h / 5 h, as described in the Experimental Section. [b]. Based on 32% w/w silica. [c]. "Crude" means uncorrected for the amount of SiO_2 contained. [d]. Calculated by considering the SiC/SiO_2 mol/mol ratio in the samples as dictated by the skeletal density data (Table 4).

Spatial information for the location of the carbothermal reduction is obtained by SEM before and after oxidative removal of unreacted carbon. Before treatment at 600 °C in air, F-20-45 samples heated anywhere between 1300 °C and 1600 °C look superficially similar to their carbonized precursors recovered at 800 °C (compare the left column of Figure 8 to Figure 1C). Upon closer examination of Figure 8 though, larger particles (pointed at by circles and arrows) are discernible under the top layer. After treatment at 600 °C in air the debris is removed, confirming that it consists of unreacted carbon. All samples having been heated carbothermally for 72 h between 1300 °C and 1600 °C look identical to one another (Figure 8, right column). No whiskery material synthesis took place in the pores. All samples are macroporous (confirmed by N_2 adsorption – see Figure 2C) with average pore diameters between 135 and 540 nm (Table 4). By XRD (Figure 6) SiC particles are polycrystalline and the crystallite size (via the Scherrer equation) increases with the processing temperature from 7.1 nm in samples prepared at 1300 °C to 16.5 nm for samples processes at 1600 °C. (It is noted though that those

72 h at 1200-1600 °C is 76-93 mol percent, which is of course higher than what is expected from the model (75%), but lower than the SiC content in F-20-45 samples ($C:SiO_2=7.1$) where it reaches 100%. Thus, diffusion of CO through the C layer should be restricted but not completely prevented. Accordingly, a higher than the stoichiometric $C:SiO_2$ ratio of "3" is required for complete conversion of SiO_2 to SiC.

Scheme 2. Carbothermal processes at the interface of silica and carbon

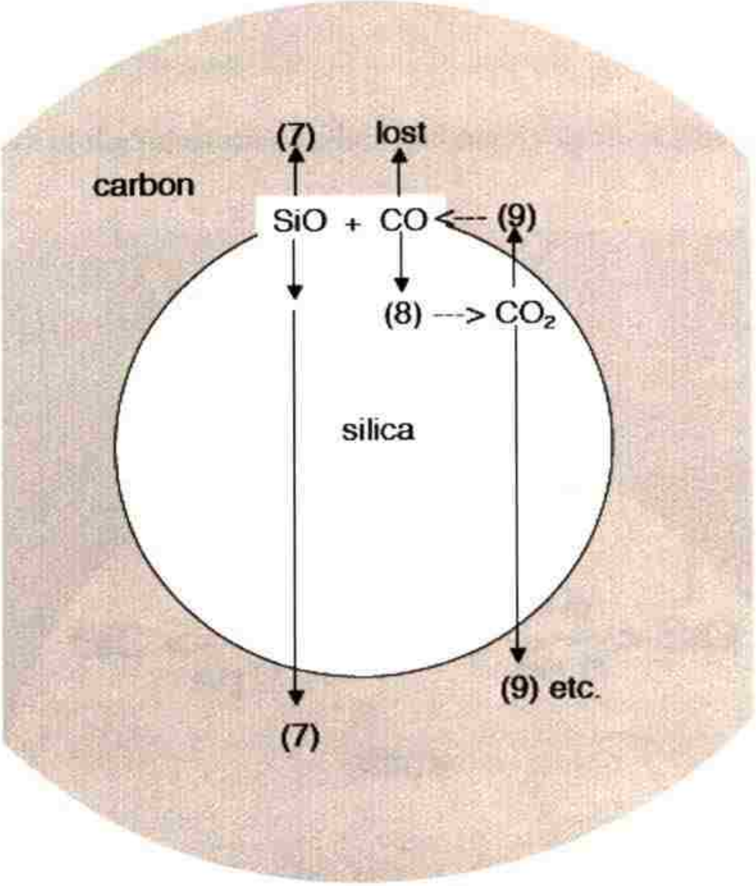

Upon closer examination, since reaction 6, which sets off the entire process, takes place at the points of contact between SiO_2 and C, once those points have been consumed, reaction 6 and all subsequent processes should stop.[31] However, as data from the F-20-45 samples show formation of SiC can continue till complete conversion SiO_2 to SiC. Continuation of the carbothermal process is attributed to the solid-solid reaction of eq 10 at the points of contact of SiC with SiO_2:[17,34,35,36]

$$SiC(s) + 2\,SiO_2(s) \longrightarrow 3\,SiO(g) + CO(g) \qquad (10)$$

Eq 10 generates SiO(g) and it is known that it causes loss of SiC during prolonged contact with SiO_2 at high temperatures.[17] Eq 10 injects 3 mols of SiO and 1 mol of CO in the yet unreached SiO_2 layer (Scheme 3). One mol of SiO may react with 3 mols of CO

Scheme 3. Processes at the interface of silica and newly formed silicon carbide

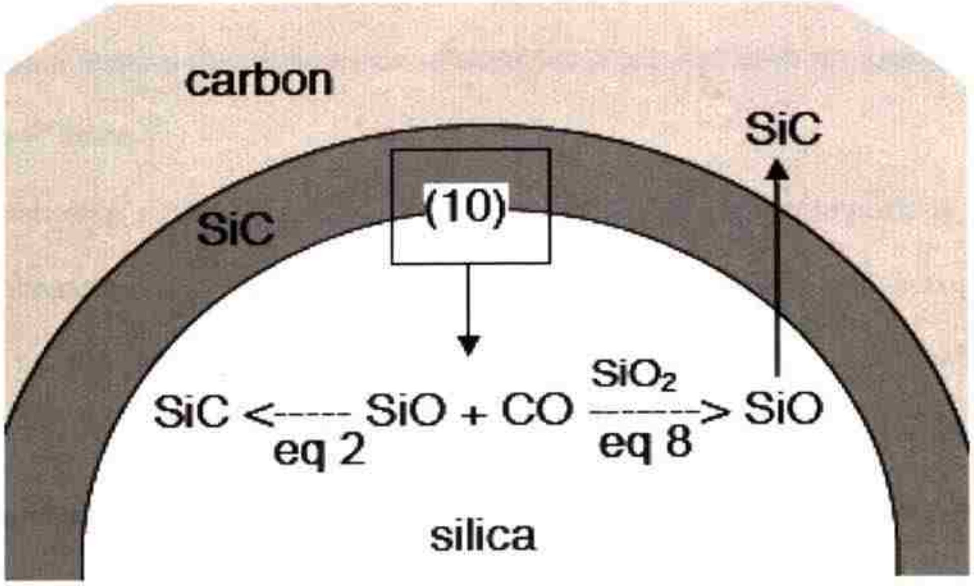

(eq 2) yielding SiC nanocrystals, while the remaining SiO has no other option but to diffuse through SiC and react with C as it emerges into the outer C layer yielding SiC according to eq 7. Alternatively, CO injected into the SiO_2 layer may react with SiO_2 according to eq 8 producing more SiO. Diffusion of SiO through SiC should be slow,

Table 6. Characterization of SiC aerogels processed from PAN-crosslinked aerogels without SCF CO_2 drying. [a]

sample °C (h)	diameter (cm)	shrinkage (%) [b]	bulk density, ρ_b (g cm^{-3})	skeletal density, ρ_s (g cm^{-3})	porosity, Π (% void space)	BET surface area, σ (m^2 g^{-1})	average pore diameter (nm) [c]	particle radius, [d] r (nm)	crystallite size [e] (nm)
F-20-45 ($C:SiO_2$ = 7.08 mol:mol)									
1500 (72)	0.550	42	0.587	3.178±0.018	82	18	19.7 [308]	52.4	14.8±1.2

[a] Data for samples processed carbothermally at the temperature and time-period indicated, followed by oxidative removal of unreacted carbon at 600 °C in air for 5 h. [b] Shrinkage relative to the diameter of the PAN-crosslinked aerogels. [c] By the $4\times V_{Total}/\sigma$ method. For the first number, V_{Total} was calculated by the single-point adsorption method; for the number in brackets V_{Total} was calculated via $V_{Total} = (1/\rho_b)-(1/\rho_s)$. [d] Calculated via $r = 3/\rho_s\sigma$. [e] By XRD using the Scherrer equation; averages from the values obtained from the (111), (220) and (311) reflections.

7. Figures

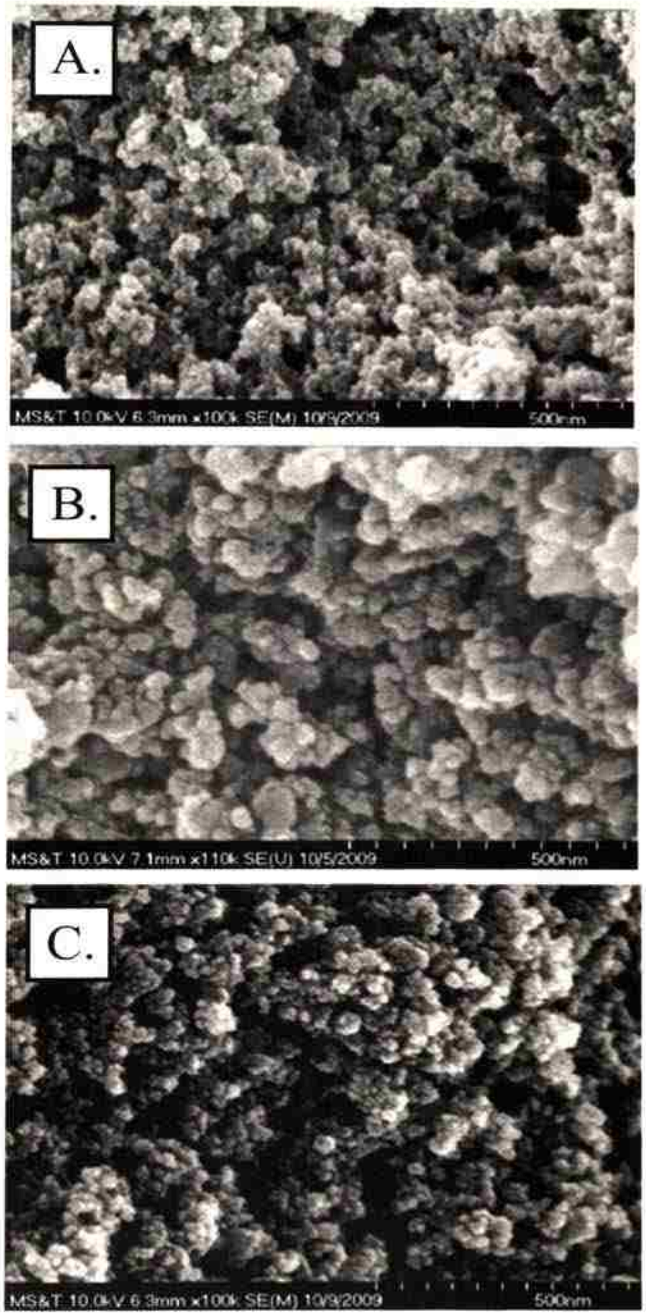

Figure 1. Scanning Electron Micrographs (SEM) of PAN-crosslinked F-20-45 samples: (A) as prepared; (B) after heating at 225 °C in air for 36 h (aromatization) and, (C) after additional heating first at 300 °C for 3 h and at 800 °C under argon for 3 h (carbonization).

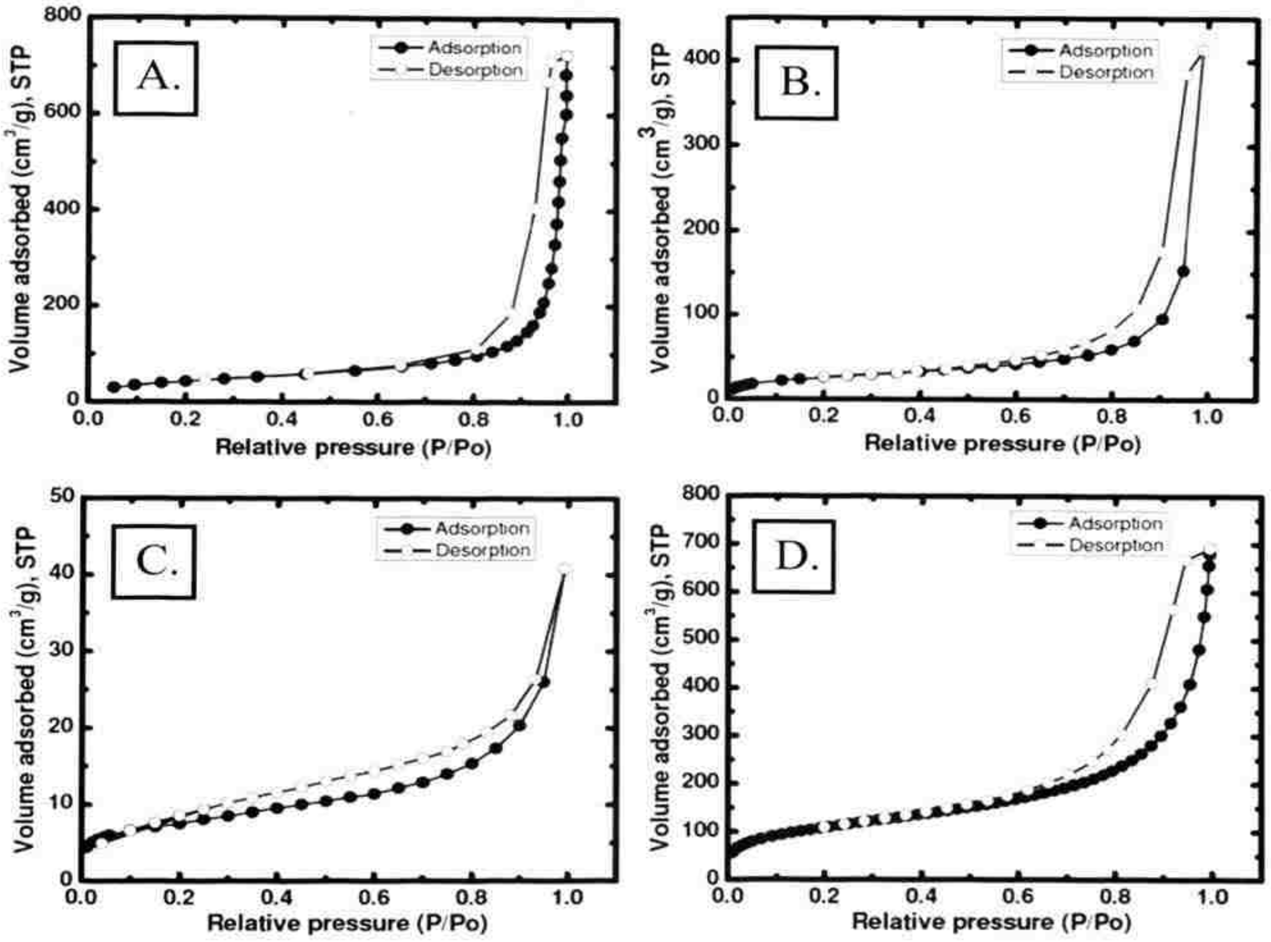

Figure 2. Nitrogen sorption isotherms of F-20-45 samples: (A) as prepared; (B) after aromatization and carbonization (heating at 225 °C in air, followed by heating at 800 °C under Ar); (C) after carbothermal treatment at 1200 °C for 72 h under Ar, followed by oxidative cleaning at 600 °C in air; and, (D) after carbothermal treatment at 1600 °C for 72 h under Ar, followed by oxidative cleaning at 600 °C in air

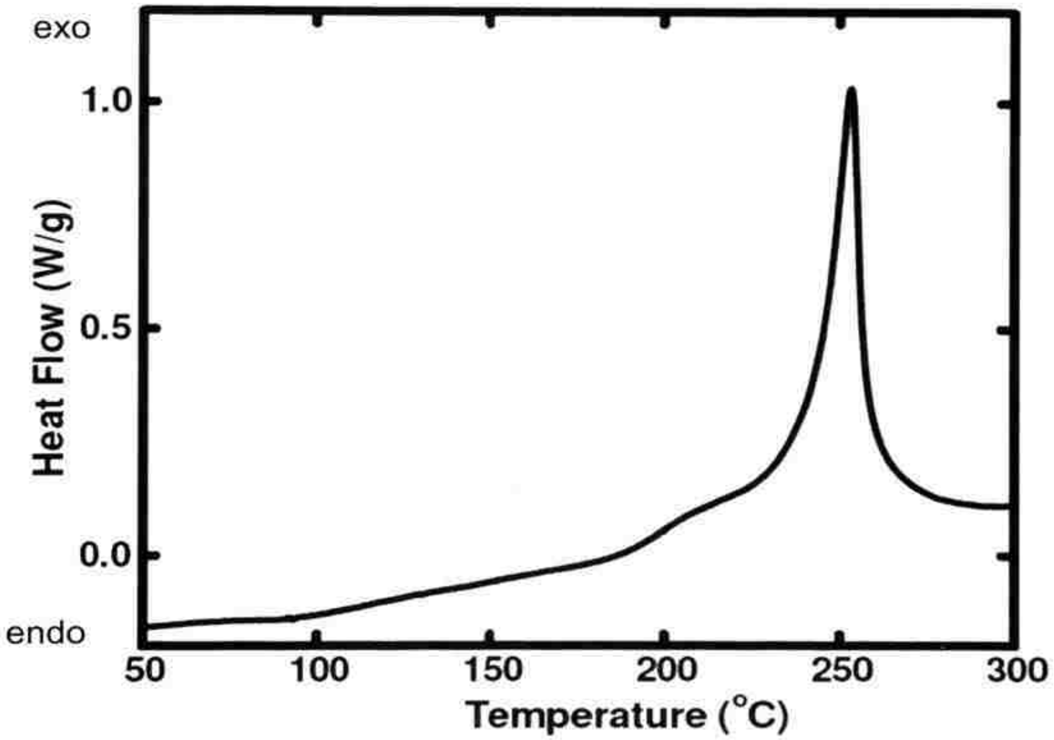

Figure 3. Differential scanning calorimetry (DSC) in air of a F-10-60 aerogel. (Heating rate: 10 °C min^{-1}.)

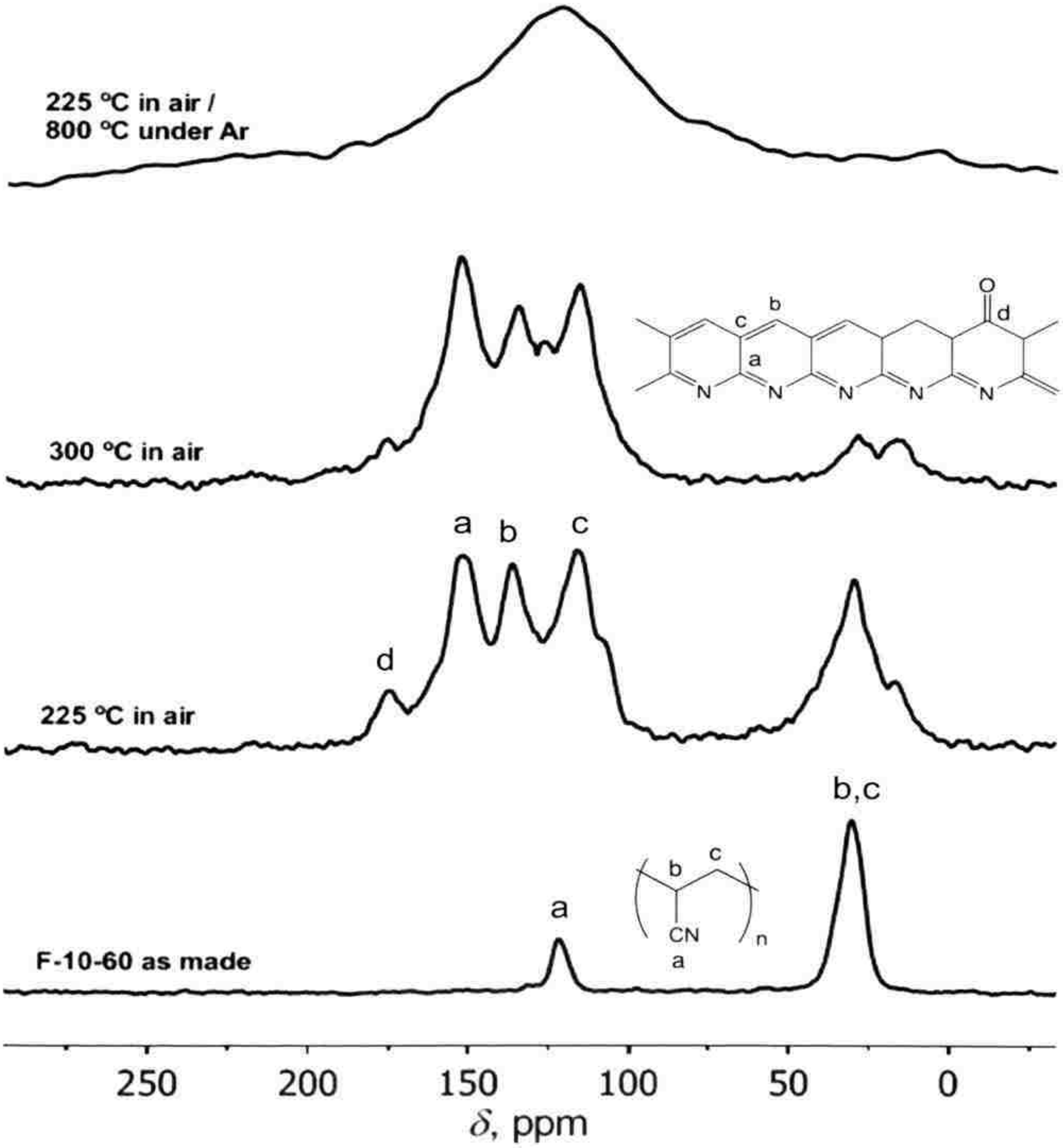

Figure 4. Solids CPMAS ^{13}C NMR data of F-10-60 aerogels processed under the conditions indicated. Peak assignment according to reference 27, confirmed by simulations.

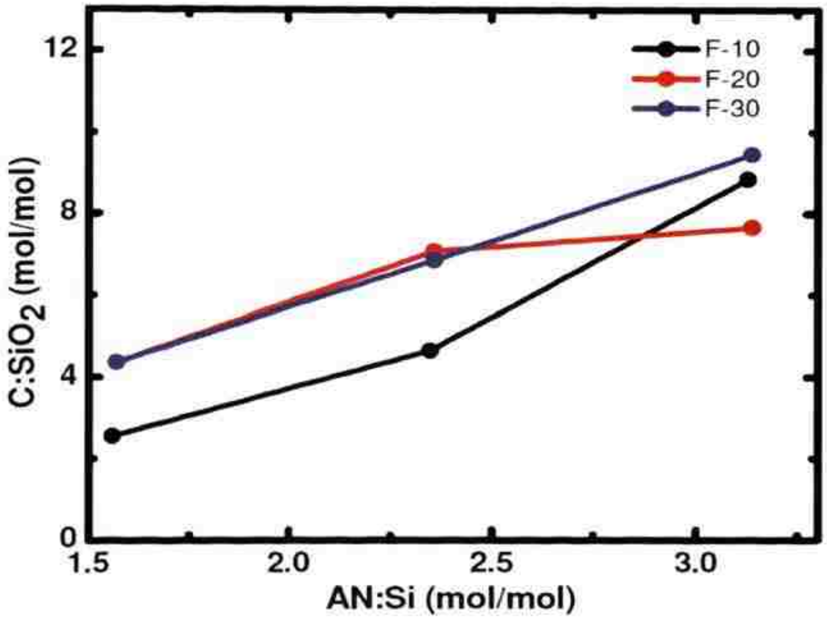

Figure 5. Correlation of C:SiO$_2$ mol ratio after aromatization (225 °C) and carbonization (800 °C) with the initial AN/total Si (TMOS+2 ***Si-AIBN***) mol ratio in the sols of the formulations listed in Table 1.

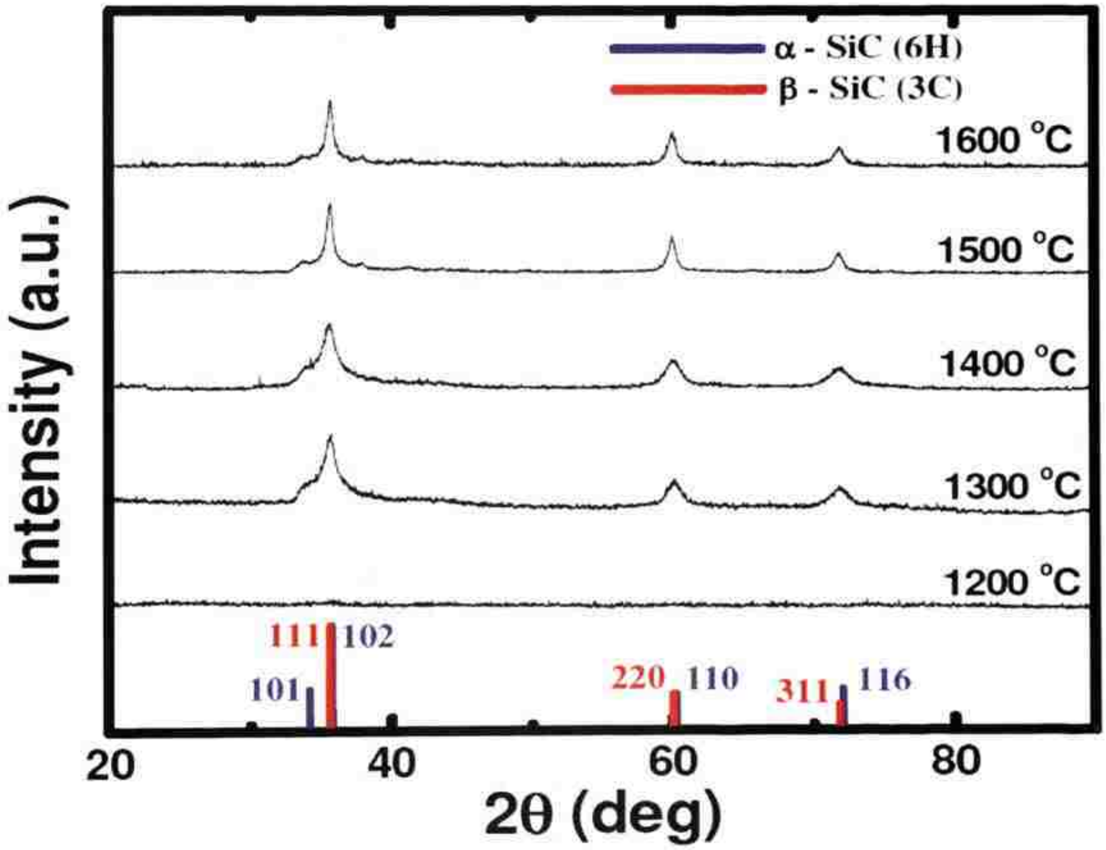

Figure 6. XRD data for F-20-45 samples after carbothermal treatment under flowing Ar for 72 h at the temperatures indicated, followed by oxidative removal of unreacted carbon at 600 °C in air.

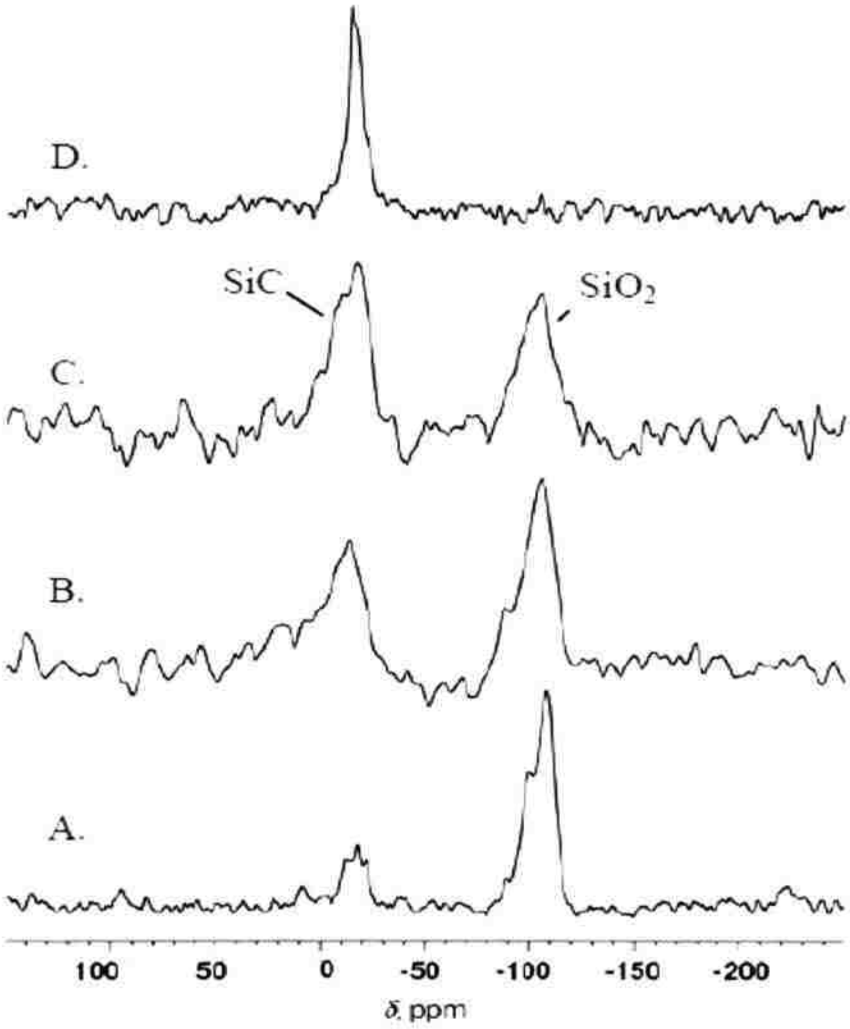

Figure 7. Solids ^{29}Si NMR of: (A) a 1:1 mol/mol mixture of commercial SiC and silica (calibration sample used for integration of B and C); (B) a F-20-30 sample treated carbothermally at 1200 °C for 36 h followed by treatment at 600 °C in air; (C) a F-20-30 sample treated carbothermally at 1300 °C for 36 h, followed by treatment at 600 °C in air; and, (D) a F-20-45 sample treated carbothermally at 1600 °C followed by treatment at 600 °C in air.

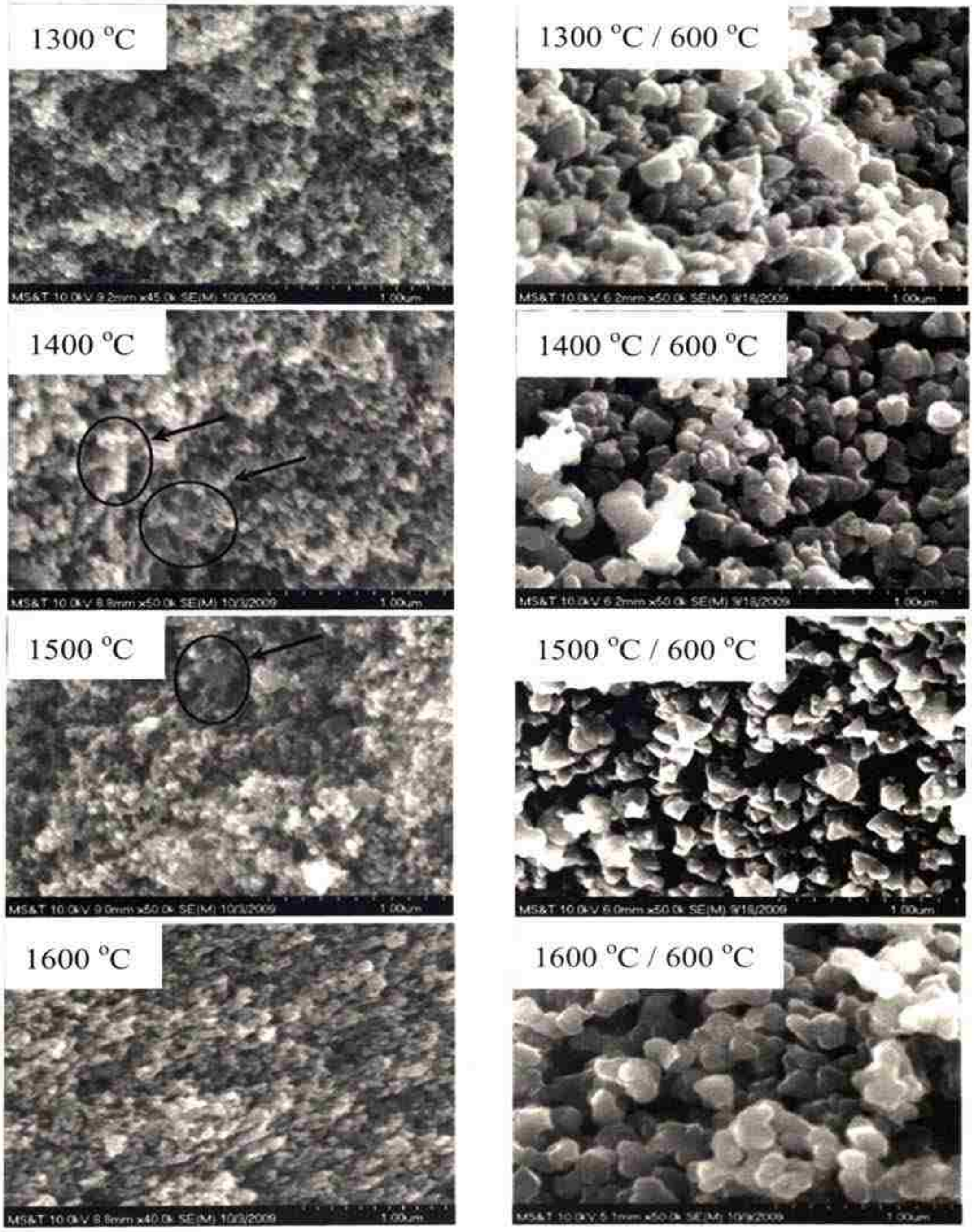

Figure 8. SEM of F-20-45 samples treated carbothermally for 72 h at the temperatures shown. Left column: samples before oxidative cleaning at 600 °C in air. SiC particles (pointed at by arrows and circles) are discernible under the "debris" on top. Right column: after removal of unreacted carbon, confirming that the debris on top was unreacted carbon. (All full-scale bars at 1 μm.)

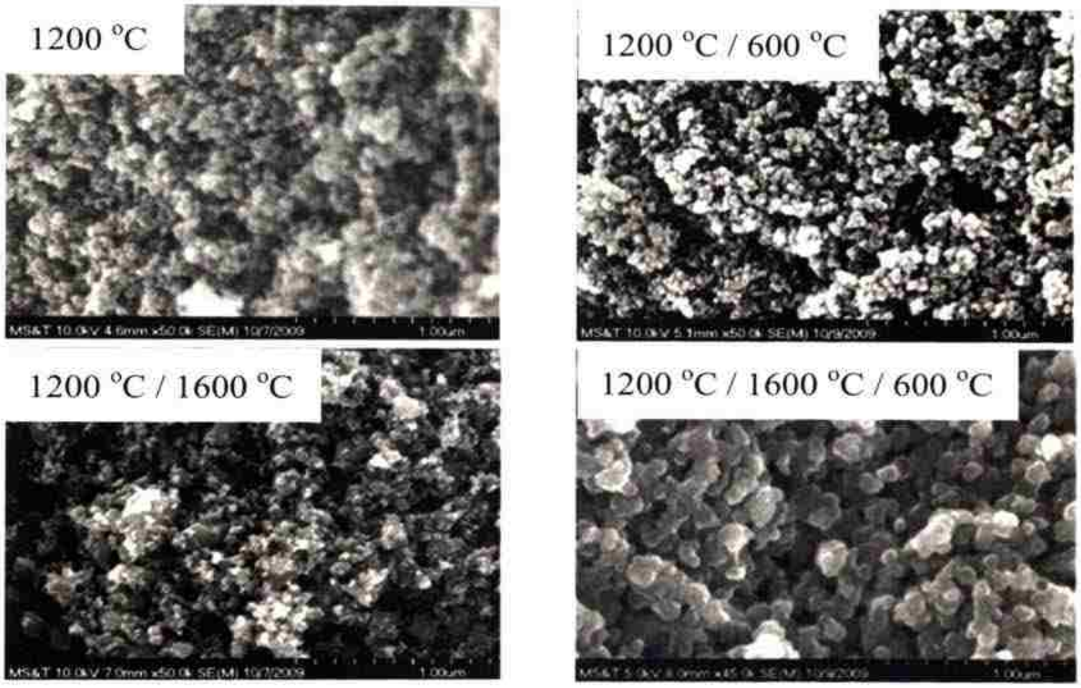

Figure 9. SEM of F-20-45 samples treated carbothermally at 1200 °C and also at 200 °C and subsequently at 1600 °C. Left column: samples before oxidative cleaning of unreacted carbon at 600 °C in air. Right column: after removal of unreacted carbon. Considering the data together with Figure 8, macroporosity and large particles are created by processes taking place between 1200 °C and 1300 °C. (All full-scale bars at 1 μm.)

Figure 10. Photographs of a F-20-45 PAN-crosslinked silica aerogel (left), and of the resulting SiC aerogel (right) after (a) aromatization (225 °C in air); (b) carbothermal reduction (1400 °C under flowing Ar); and (c) oxidative removal of unreacted carbon (600 °C in air).

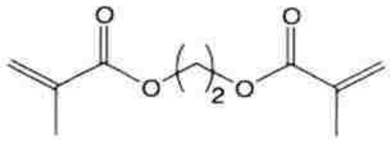

EGDMA

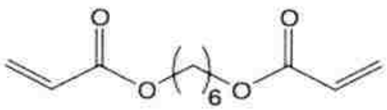

HDDA

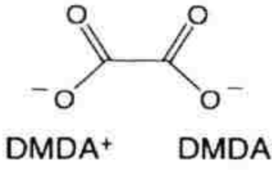

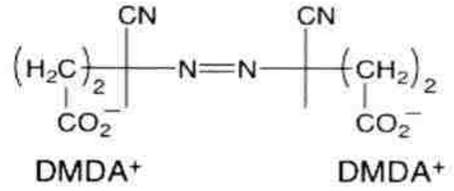

DMDA$^+$:

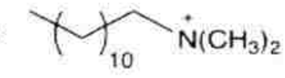

surf-1 ***surf-AIBN***

macroporous chromatographic stationary phases.[16] Also, during solution polymerization (in toluene), crosslinking decreases the solubility of the developing polymeric strands and causes phase-separation of radical-terminated colloidal nanoparticles that get linked covalently among themselves into non-collapsible porous 3D networks. That process is transferred into water by using emulsion polymerization methods,[17] whereas surfactant micelles play the role of reaction nano-vessels. Polymer growing in micelles comprises particles that get crosslinked to a network similar to the one obtained by solution polymerization. In most cases, stable emulsions were obtained with combinations of non-ionic Triton® X-100 and cationic surfactant ***surf-1***. The free-radical process was initiated with a dicarboxylate derivative of 2,2′-azobisisobutyrolitrile (AIBN) introduced as a surfactant itself (***surf-AIBN***).

Wet-gels from either the solution (toluene), or the emulsion (water) polymerization route include macropores that withstand the surface tension forces of the evaporating solvents, therefore are dried into aerogels under ambient pressure. After carbonization at 800 °C, C-aerogels from either solution or emulsion polymerization are strictly identical. Differences are traced only to the crosslinkers (EGDMA versus HDDA). Upon further pyrolysis in the 2200-2300 °C range, C-aerogels remain

Table 1. Emulsion water-based (W-) PAN aerogels

sample	AN (mL) [mol]	X-linker [d] (mL) [mol]	total AN+ X-linker (mL)	surfactants				water from surfactants (mL)	additional water (mL)	total water (mL)	total volume (mL)
				surf-AIBN (mL)	*surf-1* (mL)	Triton® X-100 (g)	SDS (g)				
W-E-50-40 [a]	20.0 [0.304]	20.0 [0.089]	40.0	10	45	10	0	39	21	60	126.0
W-E-50-50 [b]	25.0 [0.380]	25.0 [0.112]	50.0	10	0	25	0	9	41	50	126.0
W-E-75-40 [a]	30.0 [0.456]	10.0 [0.045]	40.0	10	45	10	0	39	21	60	126.0
W-E-75-50 [a]	37.5 [0.570]	12.5 [0.056]	50.0	10	45	10	0	39	11	50	126.0
W-H-50-40 [a]	20.0 [0.304]	20.0 [0.106]	40.0	10	45	10	0	39	21	60	126.0
W-H-50-50 [b]	25.0 [0.380]	25.0 [0.132]	50.0	10	0	10	15	9	41	50	105.0
W-H-75-40 [a]	30.0 [0.456]	10.0 [0.053]	40.0	10	45	10	0	39	21	60	126.0
W-H-75-50 [a]	37.5 [0.570]	12.5 [0.066]	50.0	10	45	10	0	39	11	50	126.0
W-H-75-50+ [b,c]	37.5 [0.570]	12.5 [0.066]	50.0	10	0	10	15	39	41	50	105.0

[a] Clear emulsion, stable indefinitely. [b] Quasi-stable (for a few hours) opaque-white (milky) emulsion. [c] Sample prepared using SDS as surfactant for direct comparison of the micelle size with SANS. [d] X-Linker: E: EGDMA; H: HDDA.

Table 2. Formulations of solvent- (**S-**) based PAN aerogels

sample	AN (mL) [mol]	X-linker (mL) [mol]	total AN + X-linker (mL)	volume of toluene (mL)	total solution volume (mL)	AIBN (g)
S-E-25-30	1.5 [0.023]	4.5 [0.020]	6	14	20	0.075
S-E-25-40	2.0 [0.030]	6.0 [0.027]	8	12	20	0.100
S-E-25-50	2.5 [0.038]	7.5 [0.033]	10	10	20	0.125
S-E-50-30	3.0 [0.046]	3.0 [0.013]	6	14	20	0.075
S-E-50-40	4.0 [0.061]	4.0 [0.018]	8	12	20	0.100
S-E-50-50	5.0 [0.076]	5.0 [0.022]	10	10	20	0.125
S-E-75-30	4.5 [0.068]	1.5 [0.007]	6	14	20	0.075
S-E-75-40	6.0 [0.091]	2.0 [0.009]	8	12	20	0.100
S-E-75-50	7.5 [0.114]	2.5 [0.011]	10	10	20	0.125
S-H-25-30	1.5 [0.023]	4.5 [0.024]	6	14	20	0.075
S-H-25-40	2.0 [0.030]	6.0 [0.031]	8	12	20	0.100
S-H-25-50	2.5 [0.038]	7.5 [0.040]	10	10	20	0.125
S-H-50-30	3.0 [0.046]	3.0 [0.016]	6	14	20	0.075
S-H-50-40	4.0 [0.061]	4.0 [0.021]	8	12	20	0.100
S-H-50-50	5.0 [0.076]	5.0 [0.026]	10	10	20	0.125
S-H-75-30	4.5 [0.068]	1.5 [0.008]	6	14	20	0.075
S-H-75-40	6.0 [0.091]	2.0 [0.011]	8	12	20	0.100
S-H-75-50	7.5 [0.114]	2.5 [0.013]	10	10	20	0.125

Conversion of carbon aerogels to graphite aerogels. Carbon aerogel monoliths produced at 800 °C as above were placed in a hot-zone graphite furnace (Thermal Technologies Inc., Model:1000-3060-FP20) under a helium atmosphere. The temperature was raised from room temperature to 400 °C at the rate 40 °C min^{-1} and then to 2200 or 2300 °C at 10 °C min^{-1}. Samples were kept at that temperature for a period of 24 h. At the end, the power to the furnace switched off and it was allowed to cool to room temperature at its normal rate (overnight).

"latex" particles develop interparticle covalent bridges, and the structure will resist collapse upon drying.

Scheme 1. Bottom-up synthesis of polymeric aerogel monoliths

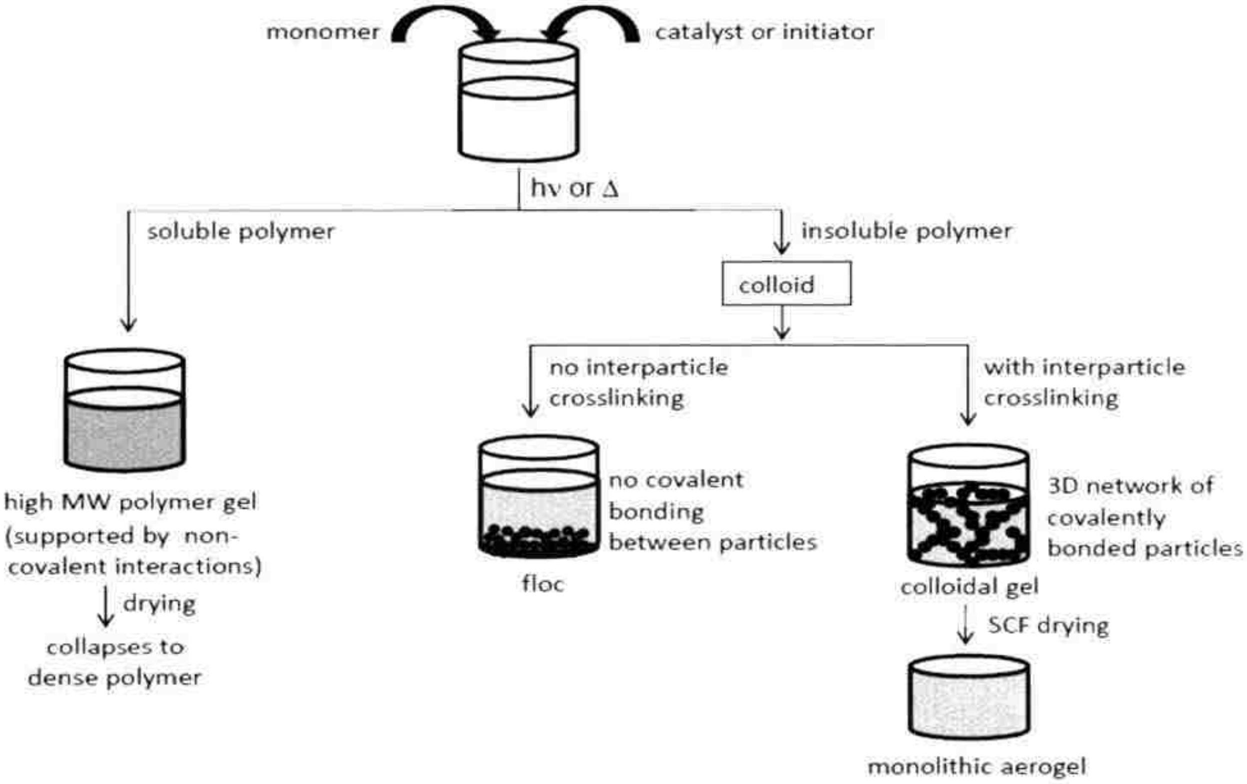

3.b Synthesis of PAN aerogels by solution and emulsion polymerization. PAN wet-gels were synthesized by solution or emulsion polymerization according to equation 1.

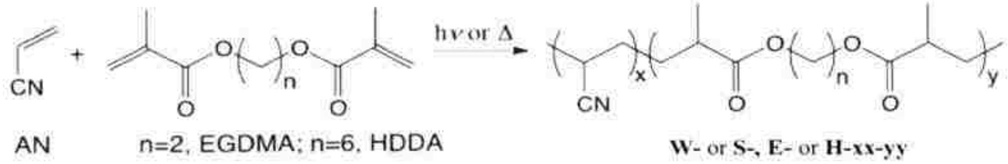

(1)

Surprisingly, although copolymerization of AN with EGDMA or HDDA is straightforward, relevant reports are scarce, and not related to carbons.[23] These sample

Scheme 2. Solution (**S-**) and emulsion (**W-**) polymerization routes to polyacrylonitrile (PAN) aerogels followed by carbonization and graphitization

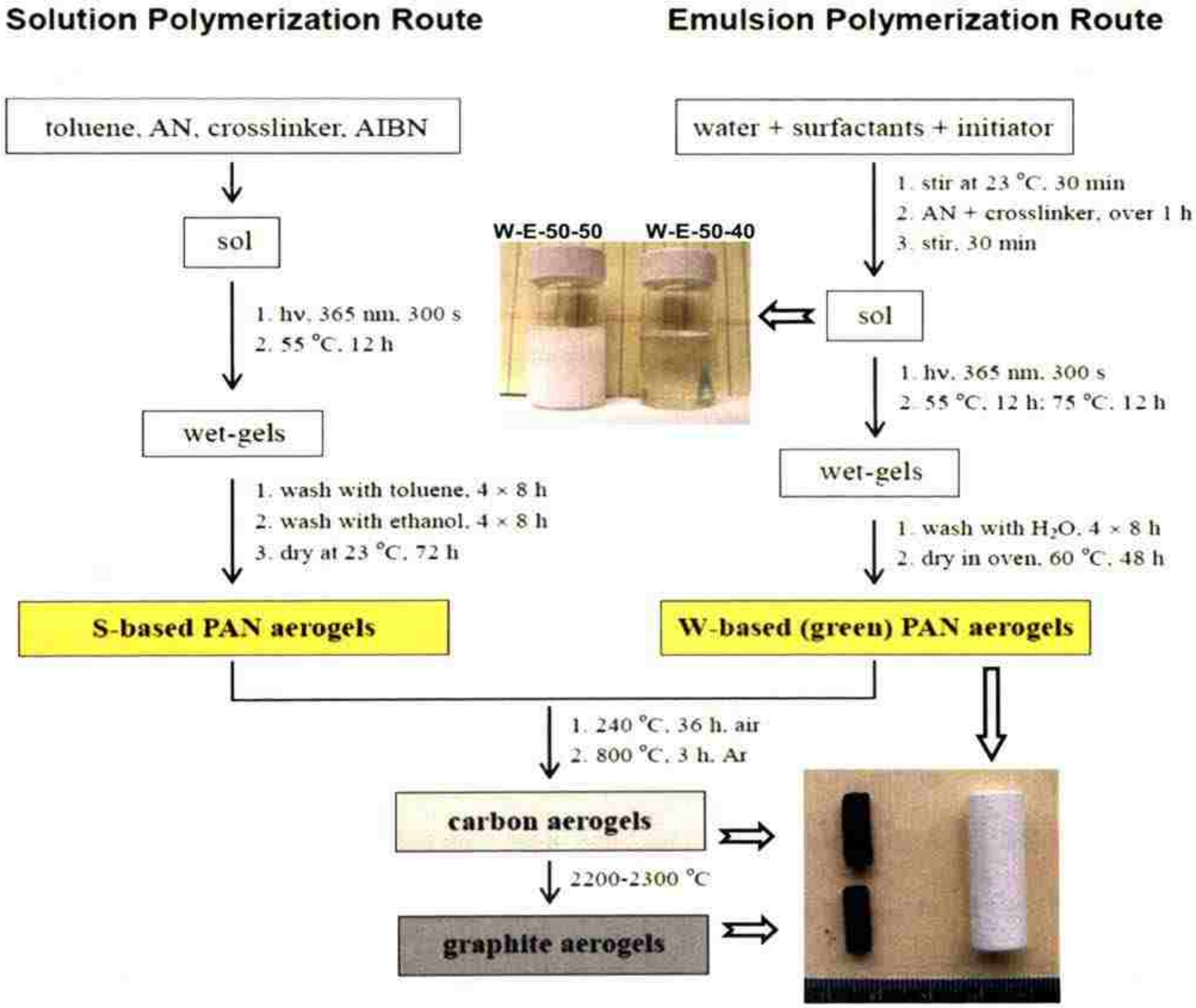

Scheme 2 summarizes the two synthetic routes and also includes carbonization and graphitization (see Sections 3.d.1 and 3.d.2). Gelation was induced photochemically at room temperature and wet-gels were aged at slightly elevated temperatures. (The aging step was not optimized.) Wet-gels were dried with SCF CO_2 as well as under ambient pressure, and they were found to have identical properties (see Table S.1 in Supporting Information). The following discussion refers to materials dried under ambient pressure.

Gelation in toluene proceeds according to Scheme 1, as planned. On the other hand, although surfactans have been employed numerous times in aerogel synthesis, mainly in order to reduce surface tension for efficient drying,[24] as templating agents for macroporous carbons[13] or ordered mesoporous silica,[25] and in reverse emulsions for the synthesis of carbon aerogel spheres,[26] to our knowledge, monolithic aerogel synthesis via classical emulsion polymerization in water has not been described before.

In formulating our emulsions, the primary goal was stability during photogelation. ("Stability" in the sense that emulsions would not separate into layers.) ***Surf-1*** was introduced for that purpose, and it was noted that most emulsions using ***surf-1*** were also clear and shelf-stable indefinitely. Exceptions were **W-E-50-50** and **W-H-50-50** that were neither clear nor photostable. Eventually, they became photostable when **surf-1** was replaced with either higher concentrations of Triton® X-100, or SDS, respectively (Table 1). Nevertheless, those emulsions were opaque-white (photograph in Scheme 2) and quasi-stable, meaning that they separate into layers upon standing for a few hours. Also, for control purposes (see below) we introduced an extra sample, **W-H-75-50***, even though the original **W-H-75-50** was already photochemically stable and clear. **W-H-75-50*** was made with SDS instead of **surf-1**, and it was quasi-stable/milky (Table 1). Optical clarity signifies smaller light-scatterers, while a milky appearance indicates larger droplets, which, in agreement with the temporary stability of those emulsions, are prone to form separate layers upon standing.

Table 3. SANS data for selected emulsions and the corresponding aerogels

sample	emulsion (25 °C)		aerogel		
	R_s (nm)	D (nm)	High-Q slope	R_G (nm)	R (nm) [a]
W-E-75-50	3.03±0.05	-	3.45±0.02	44.4±1.2 [b]	57.7 [b]
W-H-50-40	2.88±0.06	3.52±0.06	4.00±0.05	43.0±1.1 [b]	55.8 [b]
W-H-75-50	3.39±0.04	4.55±0.05	4.00±0.05	45.4±1.4 [b]	59.0 [b]
W-H-75-50*	2.88±0.08	3.1±0.1	4.00±0.04	42.6±1.1 [b]	55.3 [b]
S-H-75-50			3.64±0.02	26.4±1.4	34.0

[a]. Radius, R, calculated via R_G=0.77×R. [b]. Possible multiple scattering.

Typical SANS data are represented in Figure 2 by the clear-stable emulsion **W-H-75-50**, its quasi-stable milky counterpart **W-H-75-50*** and the corresponding aerogels. Figure 2 also includes the SANS data for the **S-H-75-50** aerogel, prepared by solution polymerization in toluene. Data for all samples tested are summarized in Table 3. Emulsion data were obtained at three different temperatures. With the exception of the **W-E-75-50** emulsion, clearly defined peaks are observed in all other emulsion data, indicative of liquid-like order. Based upon their breath, it is concluded that the peaks define characteristic length scales of the emulsion rather than Bragg scattering. The peak positions are not affected by the temperature up to 40-45 °C. Afterwards, the scattering profile of all clear emulsions (e.g., **W-H-75-50** of Figure 2) changes shape, with the peak position shifting to higher Q-values, and a low-Q power-law region, which might be attributed either to onset of polymerization and formation of aggregates (secondary

Table 4. Selected properties of emulsion (water)- based PAN aerogels

sample	[monomers] in sol (M)	linear shrinkage (%) [a,b]	bulk density, ρ_b (g cm^{-3}) [a]	skeletal density, ρ_s (g cm^{-3}) [c]	porosity, Π (%void space)	BET surface area, σ (m^2 g^{-1})	average pore diameter (nm) [d]	BJH plot maxima (nm) [half width (nm)] [e]	particle radius, r (nm) [f]
W-E-50-40	3.11	12	0.403±0.014	1.289±0.005	68	27	20 [253]	29.5 [8.2]	86.1
W-E-50-40-A [g]	3.11	10	0.433±0.018	1.234±0.011	64	7	95 [857]	101.3 [88.2]	347.3
W-E-50-50	3.90	4	0.534±0.014	1.184±0.002	54	35	18 [117]	41.6 [24.4]	72.4
W-E-75-40	3.98	14	0.387±0.011	1.266±0.004	69	25	23 [287]	36.9 [28.3]	94.8
W-E-75-50	4.97	10	0.512±0.027	1.174±0.001	56	39	14 [113]	36.3 [12.7]	65.5
W-H-50-40	3.25	10	0.432±0.037	1.215±0.002	64	27	24 [221]	27.5 [15.9]	91.4
W-H-50-40-A [g]	3.25	9	0.442±0.044	1.258±0.008	65	9	76 [652]	96.6 [81.6]	265.0
W-H-50-50	4.88	9	0.515±0.011	1.175±0.001	56	40	27 [109]	41.6 [42.1]	63.7
W-H-75-40	4.04	12	0.385±0.012	1.232±0.001	69	26	21 [275]	36.3 [34.9]	93.7
W-H-75-50	5.05	11	0.522±0.011	1.174±0.001	55	34	18 [125]	37.1 [25.1]	75.2
W-H-75-50+ [b]	6.06	10	0.544±0.031	1.201±0.002	56	31	21 [130]	44.0 [37.8]	80.5

[a]. Average of 5 samples. [b]. Relative to the molds (1.00 cm diameter). [c]. One sample, average of 50 measurements [d]. By the 4 · V_{Total} σ method. For the first number, V_{Total} was calculated by the single-point adsorption method; for the number in brackets, V_{Total} was calculated via $V_{\text{Total}} = (1\ \rho_b)\text{-}(1\ \rho_s)$. [e]. From the desorption branch of the isotherms. First numbers are the peak maxima; numbers in brackets are the full widths at half maxima. [f]. Calculated via $r = 3\ \rho_s\sigma$. [g]. Samples made using AIBN as initiator (enforcing suspension polymerization). [h]. See footnotes b and c, Table 1.

Table 5. Selected properties of solvent (toluene)- based PAN aerogels

sample	[monomers] in sol (M)	linear shrinkage (%) [a,b]	bulk density, ρ_b (g cm^{-3}) [a]	skeletal density, ρ_s (g cm^{-3}) [c]	porosity, Π (% void space)	BET surface area, σ (m^2 g^{-1})	average pore diameter (nm) [d]	particle radius, r (nm) [e]
S-E-00-50 [f]	2.23	14	0.583±0.038	1.277±0.009	54	33	33.1 [113]	71.2
S-E-50-40	4.10	3	0.509 ±0.008	1.273±0.002	60	135	17.2 [34.9]	17.4
S-E-50-50	4.90	2	0.594 ±0.004	1.290±0.001	53	121	18.1 [30.0]	19.2
S-E-75-40	5.00	1	0.492 ±0.009	1.258±0.004	69	145	16.6 [34.1]	16.4
S-E-75-50	6.25	1	0.597 ±0.001	1.263±0.001	59	157	14.1 [22.5]	15.1
S-H-00-50 [f]	2.65	14	0.562±0.044	1.267±0.010	56	37	39.4 [107]	64
S-H-50-40	4.10	8	0.487 ±0.027	1.273±0.001	61	42	19.2 [121]	56.1
S-H-50-50	5.10	10	0.605 ±0.010	1.219±0.007	47	34	25.1 [97.9]	72.4
S-H-75-40	5.10	5	0.452±0.038	1.197±0.002	62	56	19.8 [98.4]	44.7
S-H-75-50	6.35	7	0.567±0.049	1.233±0.003	54	52	17.3 [73.3]	46.8

[a]. Average of 5 samples. [b]. Relative to the molds (1.00 cm diameter). [c]. One sample, average of 50 measurements [d]. By the $4 \cdot V_{\mathrm{Total}}\ \sigma$ method. For the first number, V_{Total} was calculated by the single-point adsorption method; for the number in brackets, V_{Total} was calculated via $V_{\mathrm{Total}} = (1\ \rho_b)\text{-}(1\ \rho_s)$. [e]. Calculated via $r = 3\ \rho_s\sigma$. [f]. Samples made with the crosslinkers only (EGDMA or HDDA).

Table 6. CHN elemental analysis data for selected **W-** and **S-**, **E-** and **H-**samples along the aromatization, carbonization and graphitization processes.[a]

sample – temperature [b]	C (%, w/w)	H (%, w/w)	N (%, w/w)	O (% w/w) [c]
EGDMA- (E-) crosslinked PAN aerogels				
W-E-50-50	62.7±0.3	4.9±0.8	13.7±1.0	18.7
S-E-50-50	62.5±0.8	4.9±0.5	10.8±0.8	21.8
W-E-50-50 (theoretical)	63.7	6.5	11.5	18.3
W-E-50-50 (aromatized)	45.8±0.1	2.7±0.4	5.1±0.4	46.4
S-E-50-50 (aromatized)	43.7±1.8	3.1±0.2	5.5±0.6	47.7
C-W-E-50-50-800	79.3± 0.8	0.0±0.0	12.6±0.4	8.1
C-S-E-50-50-800	77.3±1.2	0.0±0.0	14.4±0.7	8.3
C-W-E-50-50-1600	97.7±0.3	0.0±0.0	$0.1_3\pm0.0_1$	2.2
C-W-E-50-50-2200	99.4±0.4	0.0±0.0	$0.1_2\pm0.0_2$	0.5
C-W-E-50-50-2300	99.7±0.2	0.0±0.0	$0.0_9\pm0.0_1$	0.3
HDDA- (H-) crosslinked PAN aerogels				
W-H-50-50	64.3±0.9	5.3±0.6	12.3±0.7	18.1
S-H-50-50	67.3±1.1	8.2±0.9	13.1±0.5	11.4
W-H-50-50 (theoretical)	65.7	6.9	11.5	15.9
W-H-50-50 (aromatized)	46.9±0.8	2.6±0.5	4.0±0.5	46.5
S-H-50-50 (aromatized)	44.5±1.5	3.7±0.4	5.3±0.3	46.5
C-W-H-50-50-800	75.6± 0.6	0.0±0.0	14.2±0.3	10.2
C-S-H-50-50-800	73.8±0.2	0.0±0.0	15.4±0.9	10.8
C-W-H-50-50-1600	97.6±0.2	0.0±0.0	$0.1\pm0.0_1$	2.3
C-W-H-50-50-2200	99.7±0.3	0.0±0.0	$0.1\pm0.0_1$	0.2
C-W-H-50-50-2300	99.7±0.2	0.0±0.0	$0.0_4\pm0.0_1$	0.3

[a]. All samples were run thrice. [b]. Treatment temperatures have been added to the sample names. [c]. calculated by the difference of CHN from 100%.

Table 7. Mechanical properties under quasi-static compression of PAN aerogels

sample	bulk density ρ_b, (g cm^{-3})	strain rate (s^{-1})	Young's modulus (*E*, MPa)	speed of sound (m s^{-1})^a	ultimate compressive strength (MPa)	ultimate strain (%)	specific energy absorption (J g^{-1})
Emulsion based (W-) aerogels							
W-E-50-40	0.403±0.014	0.005	2.1	73.7	0.52±0.05	23±3	0.146±0.012
W-E-50-50	0.534±0.014	0.005	9.4	152.0	1.36±0.05	14±1	0.237±0.008
W-E-75-40	0.387±0.011	0.005	4.1	106.3	0.91±0.10	20±2	0.171±0.019
W-E-75-50	0.512±0.027	0.005	22	238.4	1.25±0.05	9±1	0.142±0.027
W-H-50-40	0.432±0.037	0.005	4.8	111.3	0.53±0.04	37±3	0.265±0.038
W-H-50-50	0.515±0.011	0.005	3.6	94.6	0.81±0.18	22±2	0.204±0.043
W-H-75-40	0.385±0.012	0.005	2.4	81.4	0.19±0.03	20±2	0.038±0.007
W-H-75-50	0.522±0.0113	0.005	29.7	273.8	1.93±0.02	7±0.1	0.278±0.019
Solvent based (S-) aerogels ^{b}							
S-E-50-40	0.509 ±0.008	0.01	134±3	258	21±2	63±3	3.8 ± 1.2
S-E-50-50	0.594 ±0.004	0.01	246±14	644	68±13	67±2	18.0 ± 2.3
S-E-75-40	0.492 ±0.009	0.01	17±2	186	7±3	61±2	1.2 ± 0.4
S-E-75-50	0.597 ±0.001	0.01	175±22	588	95±7	64±3	11.9 ± 3.8
S-H-50-40	0.487 ±0.027	0.01	102±9	458	11±3	58±4	11.5 ± 3.1
S-H-50-50	0.605 ±0.010	0.01	191±17	562	110±13	52±4	17.1 ± 1.8

[a] Calculated by speed of sound = $(E/\rho_b)^{0.5}$. [b] Samples S-**H**-75-40 and S-**H**-75-50 from Tables 2 and 5 were too weak and were not tested

Figure 4 shows the microstructures and the N_2-sorption isotherms of two representative **W**-aerogel samples, one from a clear and one from a milky emulsion (**W-E-50-40** and **W-E-50-50**, respectively), as well as the data from the corresponding **S**-aerogel (**S-E-50-40**), and also from a typical **H**-sample (**S-H-50-50**). By SEM all samples appear similar. At higher magnification they all consist of 30-80 globules (indicated by circles) that could be considered as clusters of smaller particles. Despite that appearance, however, both SANS (Table 3), and particle radius calculations from skeletal density and BET surface areas (Tables 4 and 5) indicate that those globules are indeed the smallest building blocks of the material (primary particles). In certain cases, their "bumpy" appearance amounts to surface fractality, as indicated by the range of the high-*Q* power

the role of the cross-linkers, EGDMA or HDDA, if any, in the properties of the terminal materials.

3.d.1 Aromatization of PAN aerogels. Modulated Differential Scanning Calorimetry (MDSC, Figure 5) under N_2 shows only minor, unidentified, heat exchanges up to 300° C. In air, however, all samples show a sharp exotherm above 250° C, associated with equation 3.[37]

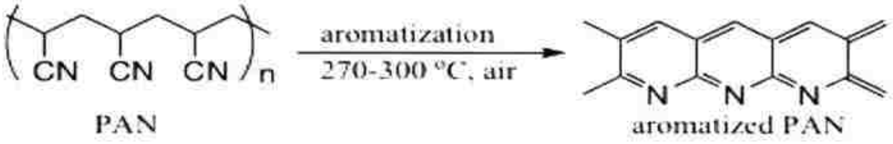

(3)

Aromatized samples are brown, and by SEM they appear much more compact than their parent PAN aerogels (Figure 6). Presumably, that propensity for contraction causes samples to break into pieces if heated directly after the exotherm of Figure 5 e.g., at 300 °C. Thus, in order to give samples time to accommodate the structural reorganization imposed by equation 3 and remain monolithic, aromatization was conducted at 240 °C, i.e., at the foot of the reaction exotherm. Post-aromatization elemental analysis (Table 6) shows a significant increase in the O content, suggesting a considerable departure from the idealized product of equation 3. Indeed, albeit surviving features from the starting polymers, the ^{13}C NMR of both **E**- and **H**-aerogels show resonances assigned (by simulation) to fused pyridines and to additional carbonyls (Figure 7).[37] Finally, it is important for the following discussion to note that the original **E**-aerogels appear to have a higher crystalline order (by XRD, included in Figure 6), than their **H**-counterparts. Although broad, two peaks in the general region of the (100), and the (110) diffractions[38] of the original PAN aerogels are also clearly present in the aromatized sample. It is unclear though whether those diffractions are due to remaining monomer or to the product of equation 3.

3.d.2 Carbonization of aromatized PAN aerogels and materials properties. Carbonization of aromatized PAN aerogels takes place according to equation 4, and was conducted under Ar at 800 °C.[15,38] ^{13}C NMR spectra (Figure 7) lose all features associated with the aromatized products, and elemental analyses (Table 6) shows complete loss of H, but also relatively high percentages of N and O. The C:N ratio corresponds to a stack of just 3-4 fused rings in the idealized structure of equation 4, although the presence of 8-10% w/w of O suggests again a significant amount of defects.

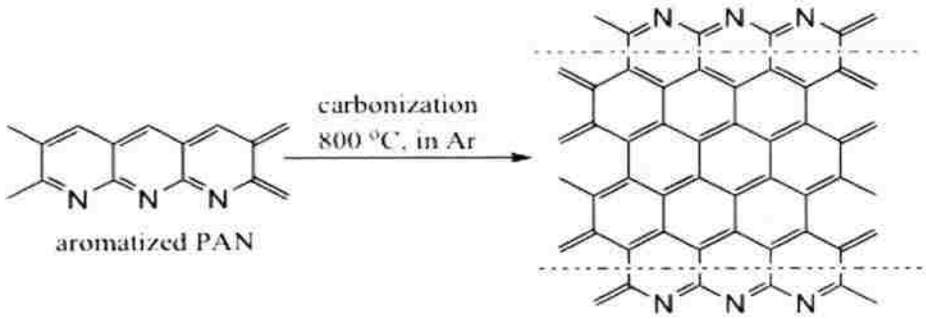

(4)

Table 8. Materials properties of 800 °C carbon aerogels from emulsion- and solution- polymerization based PAN aerogels

sample	% yield of carbon (w/w) [theoretical] [a]	% shrinkage [b]	bulk density, ρ_b (g cm^{-3}) [c]	skeletal density, ρ_s (g cm^{-3}) [d]	porosity, Π (% void space)	BET surface area, σ (m^2 g^{-1})	average pore diameter (nm) [e]	BJH plot maxima (nm) [half width (nm)] [f]	particle radius, r (nm) [g]	electrical conductivity (mho cm^{-1})
Carbons by 800 °C pyrolysis of emulsion based (W-) PAN aerogels										
C-W-E-50-40	37±3 [30.5]	32	0.573±0.011	1.844±0.002	61	300	18.2 [16.0]	45.7 [30.7]	5.42	0.022±0.008
C-W-E-50-50	36±2 [30.5]	38	0.713±0.013	1.834±0.001	68	145	19.1 [23.6]	63.1 [39.3]	11.2	0.035±0.010
C-W-E-75-40	54±3 [48.9]	43	0.749±0.009	1.920±0.003	67	249	15.1 [13.1]	43.6 [17.4]	6.2	0.027±0.008
C-W-E-75-50	51±4 [48.9]	43	0.991±0.017	1.802±0.001	49	137	13.0 [13.3]	24.5 [8.3]	12.1	0.053±0.010
C-W-H-50-40	34±2 [31.4]	34	0.582±0.008	1.728±0.001	41	43	33.3 [106]	29.5 [20.8]	40.3	0.620±0.064
C-W-H-50-50	38±4 [31.4]	42	0.632±0.009	1.781±0.001	57	39	35.8 [105]	35.4 [26.5]	43.1	0.683±0.088
C-W-H-75-40	53±5 [49.6]	33	0.713±0.011	1.818±0.002	68	42	31.2 [81.2]	29.5 [16.5]	53.2	0.554±0.098
C-W-H-75-50	51±5 [49.6]	35	0.921±0.018	1.718±0.003	58	41	28.8 [49.1]	8.9 [4.0]	42.5	0.888±0.113
Carbons by 800 °C pyrolysis of solvent (toluene) based (S-) PAN aerogels										
C-S-E-50-40	33±3 [30.5]	35	0.541±0.007	1.893±0.033	73	204	23.2 [25.9]	31.6 [22.6]	7.4	0.033±0.012
C-S-E-50-50	37±5 [30.5]	33	0.614±0.009	1.858±0.007	67	183	19.4 [23.8]	36.2 [28.8]	8.8	0.043±0.011
C-S-E-75-40	52±4 [48.9]	32	0.698±0.015	1.887±0.009	65	193	14.2 [18.7]	28.2 [19.9]	7.8	0.037±0.009
C-S-E-75-50	49±2 [48.9]	31	0.815±0.008	1.817±0.012	57	178	9.4 [15.2]	18.1 [16.2]	8.8	0.049±0.006
C-S-H-50-40	40±2 [31.4]	57	0.805±0.018	1.825±0.037	58	62	28.7 [44.8]	35.5 [27.7]	25.1	0.821±0.190
C-S-H-50-50	36±4 [31.4]	56	0.945±0.013	1.819±0.047	51	46	18.8 [44.2]	25.1 [18.8]	34.0	0.733±0.089
C-S-H-75-40	57±3 [49.6]	54	1.042±0.019	1.893±0.023	45	50	16.3 [34.5]	37.5 [26.6]	31.7	0.666±0.132
C-S-H-75-50	54±1 [49.6]	53	1.187±0.021	1.901±0.017	41	44	18.7 [28.8]	37.2 [24.2]	34.1	1.031±0.221

[a] Calculated based on the % w/w of AN in total monomers (AN+crosslinker) and a 70% carbonization yield for AN. [b] Relative to the original molds used to make the PAN aerogels (1.00 cm diameter). [c] Average of 5 samples. [d] One sample, average of 50 measurements. [e] By the $4 \times V_{Total}/\sigma$ method. For the first number, V_{Total} was calculated by the single-point adsorption method; for the number in brackets, V_{Total} was calculated via $V_{Total} = (1/\rho_b)-(1/\rho_s)$. [f] From the desorption branch of the isotherm. First numbers are the peak maxima; numbers in brackets are the width at half maxima. [g] Calculated via $r = 3/\rho_s\sigma$.

Table 9. Evolution of the materials properties of representative carbon aerogels by pyrolysis at different temperatures

sample	% weight loss	% shrinkage[a]	bulk density, ρ_b (g cm^{-3})	skeletal density, ρ_s (g cm^{-3}) [b]	% porosity, Π	BET surface area, σ (m^2 g^{-1}) [c]	average pore diameter (nm) [d]	particle radius, r (nm) [e]	electrical conductivity (mho cm^{-1})
C-W-E-50-50-800	[f]	[f]	0.71	1.834±0.001	61	145 [23]	19 [24]	11	0.035±0.010
C-W-E-50-50-1600	15	3.0	0.70	1.500±0.032	53	143 [44]	6 [5.3]	14	0.076±0.006
C-W-E-50-50-2200	23	6.0	0.72	1.401±0.035	49	8 [1]	17 [338]	267	2.387±0.220
C-W-E-50-50-2300	25	6.8	0.73	1.592±0.007	54	10 [N/A]	9 [297]	188	4.555±0.508
C-W-H-50-50-800	[f]	[f]	0.63	1.781±0.001	64	39 [7]	35 [105]	43	0.683±0.088
C-W-H-50-50-1600	15	4.0	0.63	1.429±0.038	56	58 [9]	7 [61]	36	1.703±0.206
C-W-H-50-50-2200	20	5.0	0.63	1.539±0.011	59	9 [N/A]	24 [417]	217	6.232±0.700
C-W-H-50-50-2300	20	8.7	0.64	1.646±0.022	61	10 [N/A]	14 [382]	182	6.694±1.182

[a]. Relative to the 800 °C aerogel. [b]. One sample, average of 50 measurements. [c]. Numbers in brackets represent micropore surface areas.
[d]. By the $4 \times V_{Total}/\sigma$ method. For the first number, V_{Total} was calculated by the single-point adsorption method; for the number in brackets, V_{Total} was calculated via $V_{Total} = (1/\rho_b)-(1/\rho_s)$. [e]. Calculated via $r = 3/\rho_s\sigma$.
[f]. N/A: those samples are the bases for the respective calculations.

(normal graphite structure) and a 2D peak at around 2700 cm^{-1} (second overtone of the D peak).[54] As the treatment temperature increases, the G peak increases in intensity and develops a shoulder at around 1620 cm^{-1}, referred to as D′ peak and attributed to microcrystalline graphite.[55] The ratio of the integral intensities of the D and G Raman peaks, I_D/I_G, is a typical parameter used to quantify the degree of disorder in carbons.[56] As shown in Table 10, as the treatment temperature increases the I_D/I_G ratio decreases, in agreement with increasing order. Eventually, at 2300 °C the Raman spectrum of PAN aerogels using EGDMA as crosslinker closely matches the Raman spectrum of commercial graphite (see Experimental). L_a values calculated via eq. 5 are cited in Table 10.

Table 10. XRD and Raman data for aerogels treated at the indicated temperatures

Sample temperature (°C)	**2 θ (deg.)**	**d_{002} (nm)**	**L_c by XRD (Å)**	**I_D/I_G**	**L_a by Raman (nm)**
Graphite	26.44	0.337	208.1	0.198	194.4
Carbon black				3.68	10.45
C-W-E-50-50 (EGDMA crosslinked PAN)					
800	24.67	0.3601	10.7	2.64	14.58
1600	24.98	0.3561	14.9	2.15	17.89
2200	25.10	0.3442	42.5	1.77	21.74
2300	25.25	0.3424	38.1	1.15	33.46
C-W-H-50-50 (HDDA crosslinked PAN)					
800	24.95	0.3566	11.4	2.78	13.84
1600	24.8	0.3585	13.6	1.63	23.60
2200	25.85	0.3443	29.8	1.58	24.36
2300	25.95	0.3438	43.2	1.45	26.54

Overall, XRD and Raman data considered together suggest annealing of carbon into long (large L_a) and thin (smaller L_c) ribbon-like graphitic structures, in agreement with HRTEM. The process takes place efficiently above 2200 °C. As far as the graphite

Figure Captions

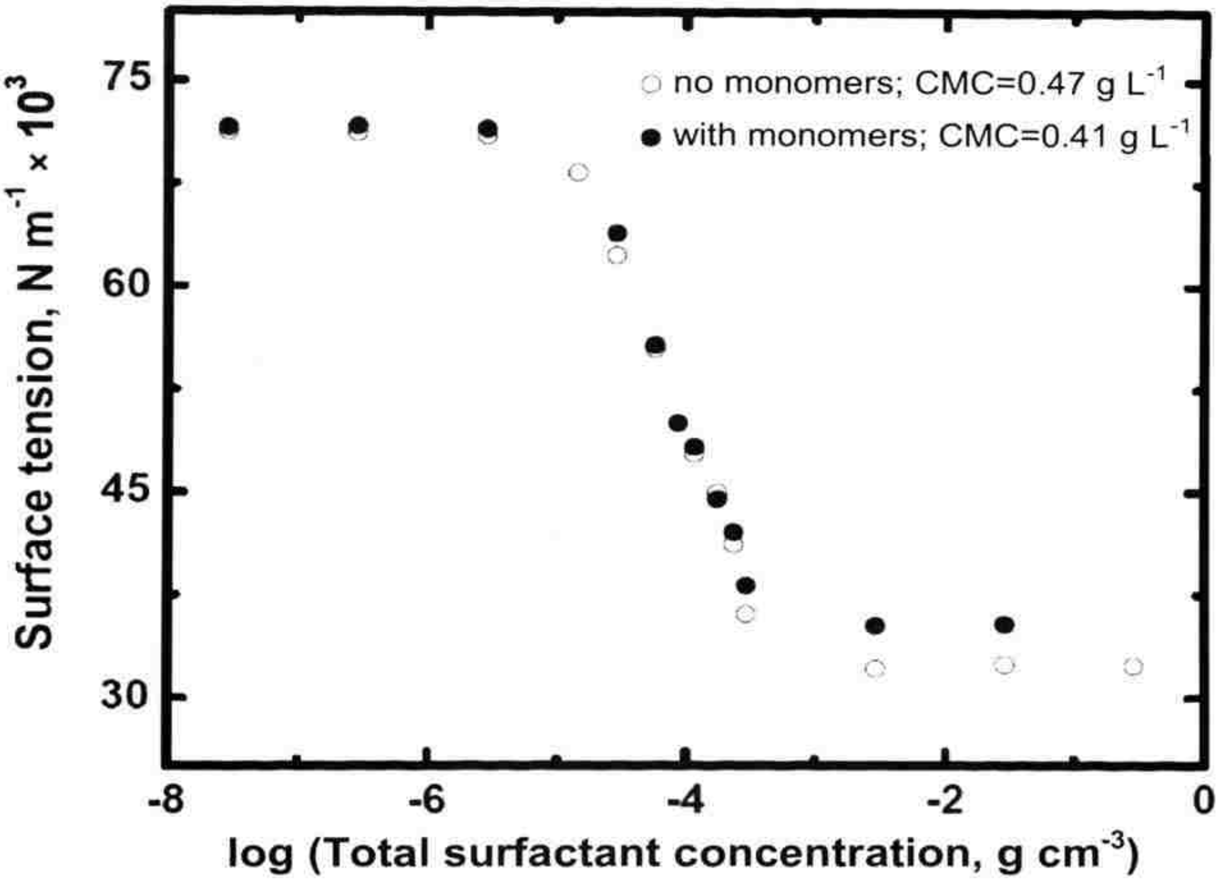

Figure 1. Surface tension versus surfactant concentration with and without monomers. Error bars within the symbols. Initial composition at right corresponds to the **W-H-50-40** sample. Only one CMC point is identified and remains about the same in both cases.

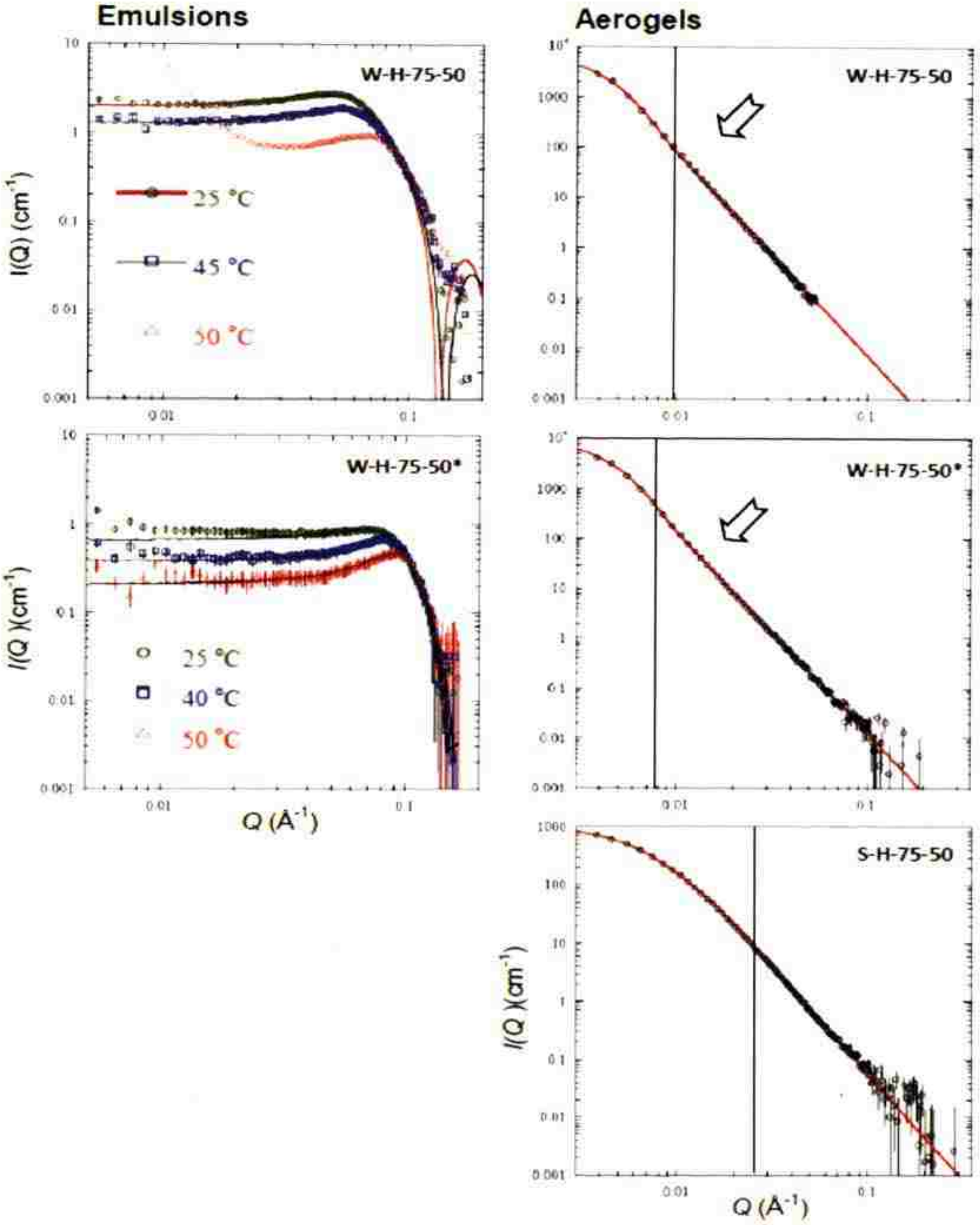

Figure 2. SANS data of representative emulsions and the corresponding aerogels. **W-H-75-50**: clear/stable emulsion, **W-H-75-50***: milky/quasi-stable emulsion. **S-H-75-50** sample prepared from solution polymerization in toluene. Data for emulsions have been obtained at three different temperatures and have been fitted assuming liquid-like order of spherical micelles. Vertical lines in the scattering profiles of the aerogel samples separate the high-*Q* power-law region from the Guinier knee (see text). Arrows indicate the minor deflections that suggest multiple scattering (see text).

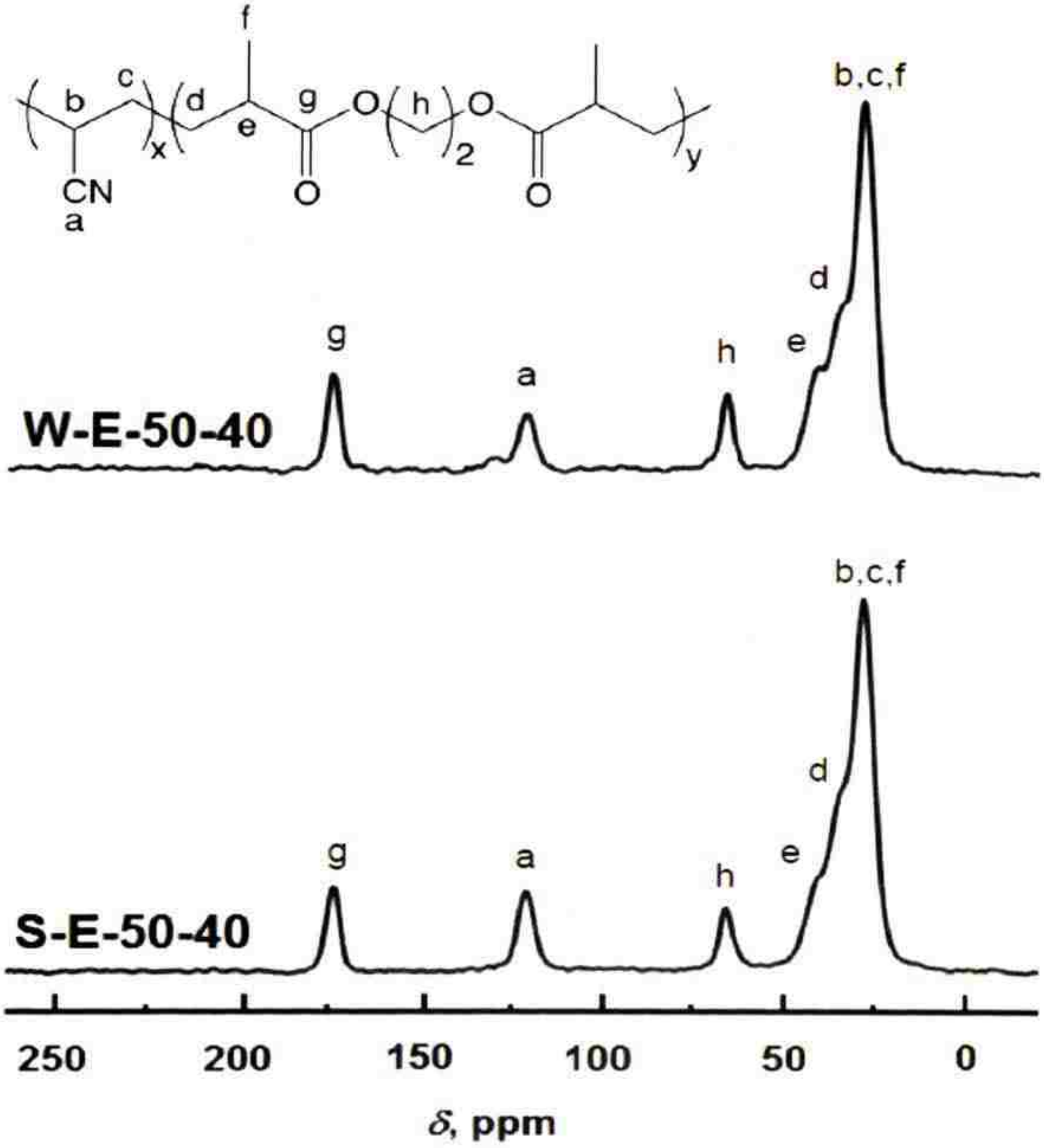

Figure 3. Solids ^{13}C CPMAS NMR data of two PAN aerogels, one made by emulsion polymerization in water (**W-**) and a similar one made in toluene (**S-**). The polymer structure is a simplification for the purpose of resonance assignment.

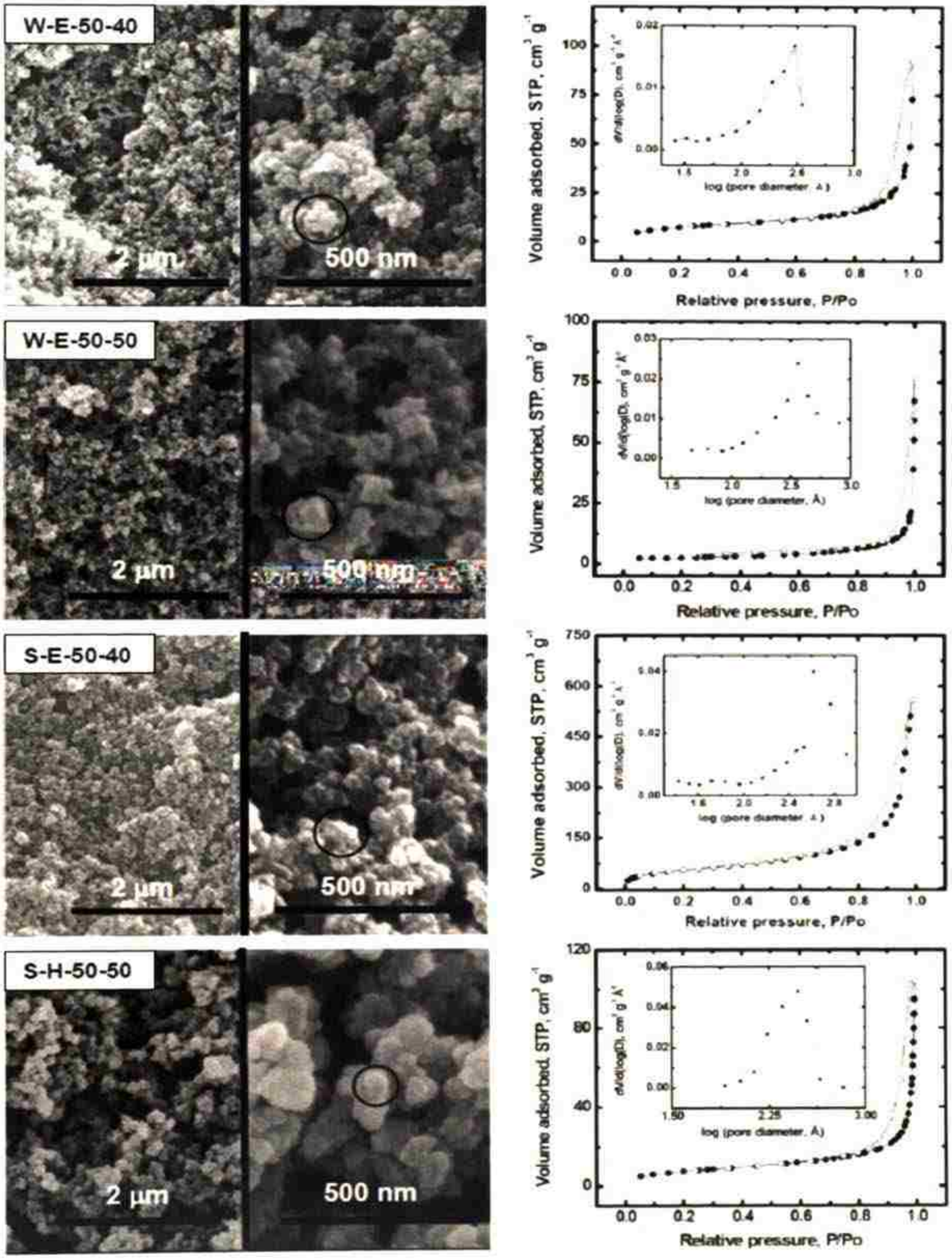

Figure 4. SEM and N_2-sorption data of representative emulsion (**W-**) and solution (**S-**) based PAN aerogels. Insets show the BJH plots derived from the desorption branch of the isotherms.

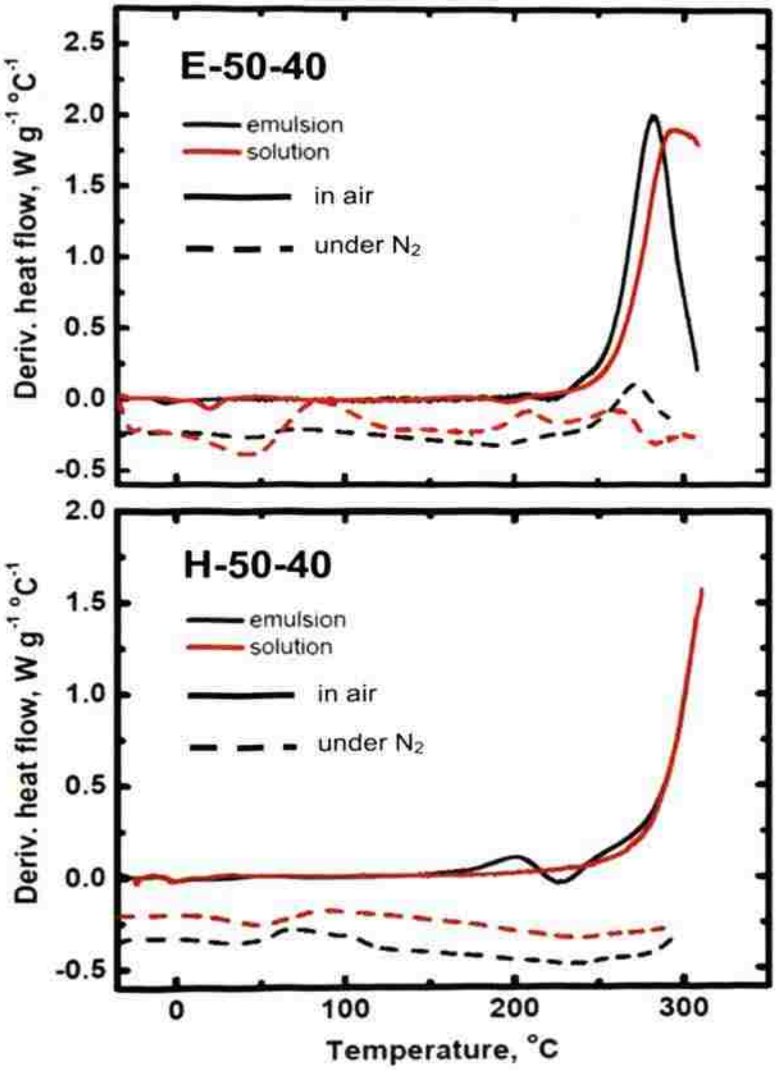

Figure 5. Representative Modulated Scanning Calorimetry (MDSC) data of the samples and conditions shown.

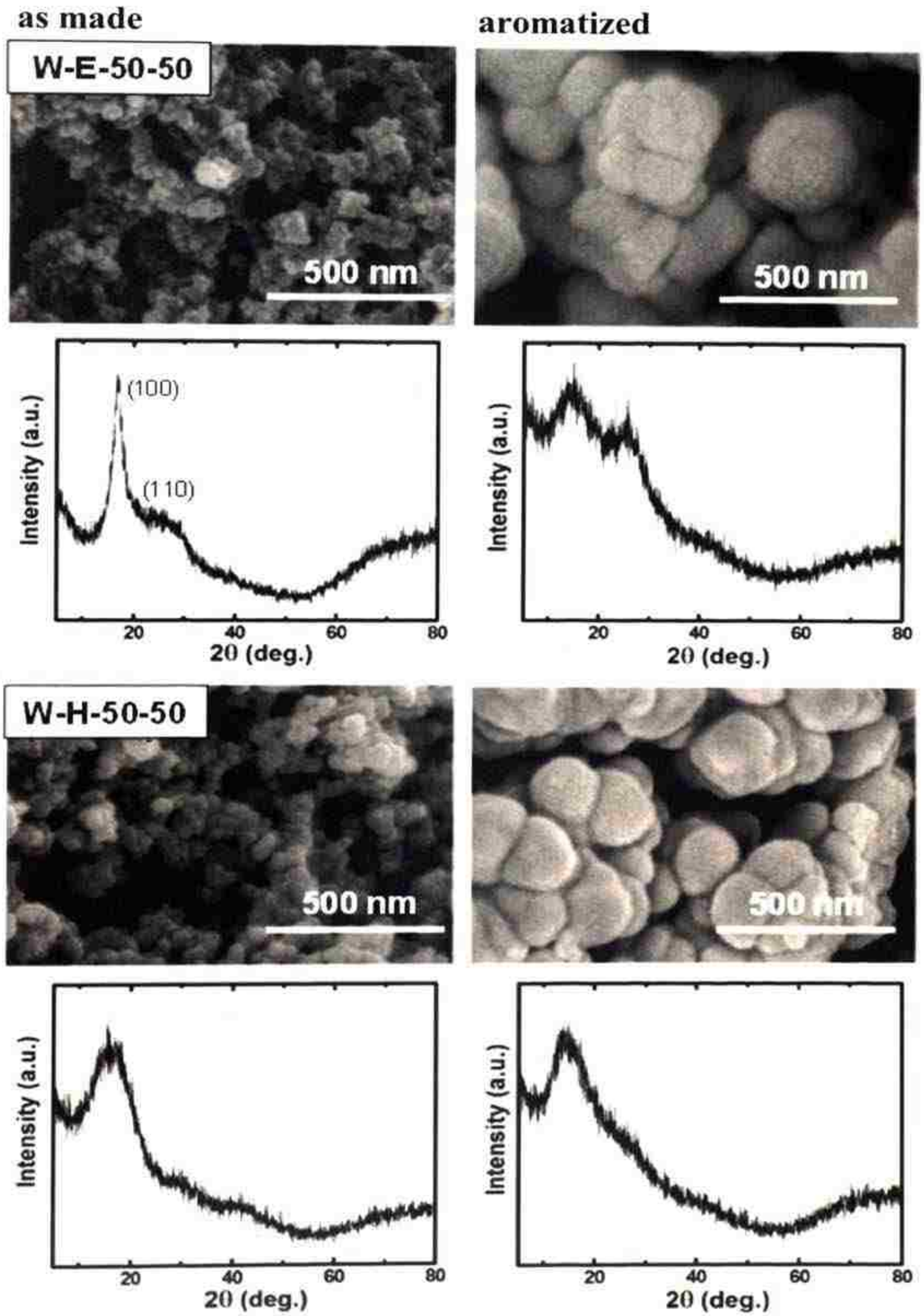

Figure 6. SEM and XRD of two representative samples before and after aromatization. SEM emphasizes the compactness imposed by the contraction expected by equation 3. XRD peak assignments according to reference 38.

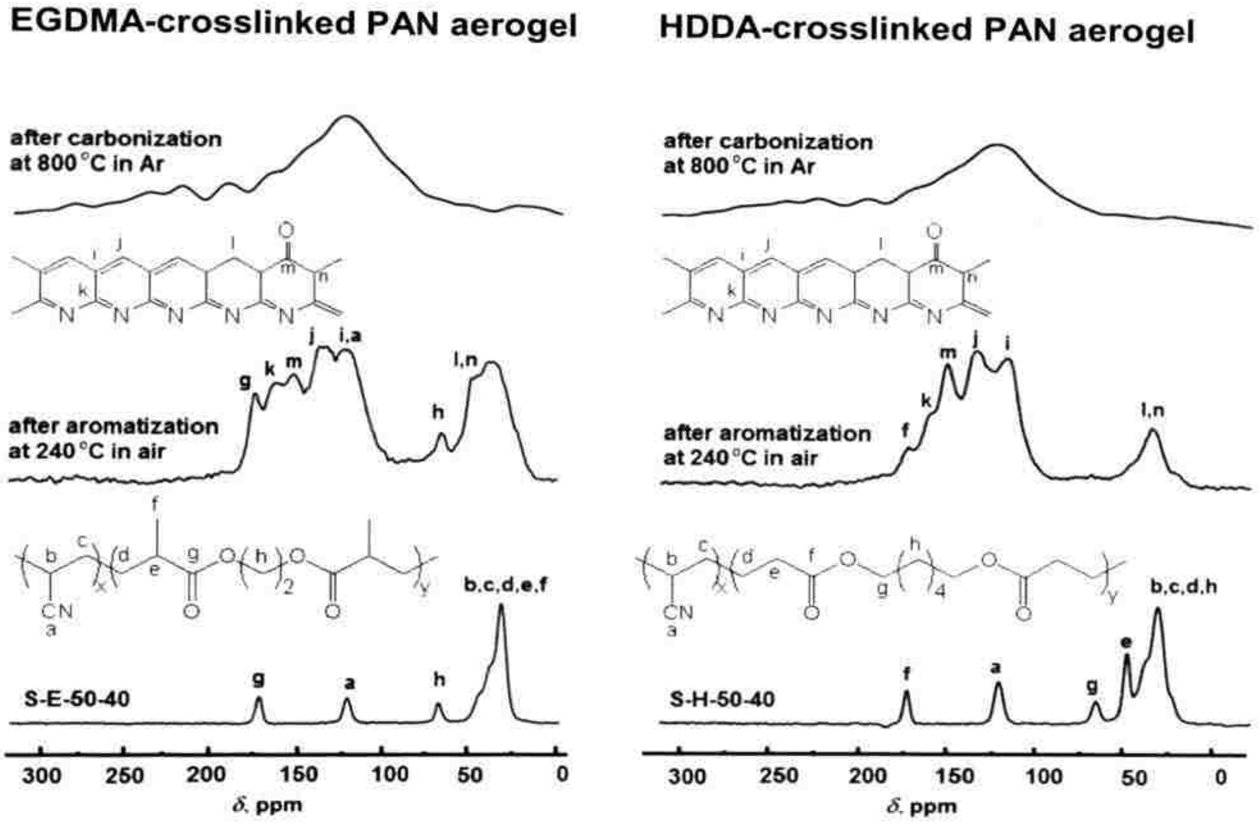

Figure 7. Solids ^{13}C NMR data of two representative PAN aerogel samples showing the changes that accompany aromatization and carbonization after treatment at the temperatures and conditions indicated.

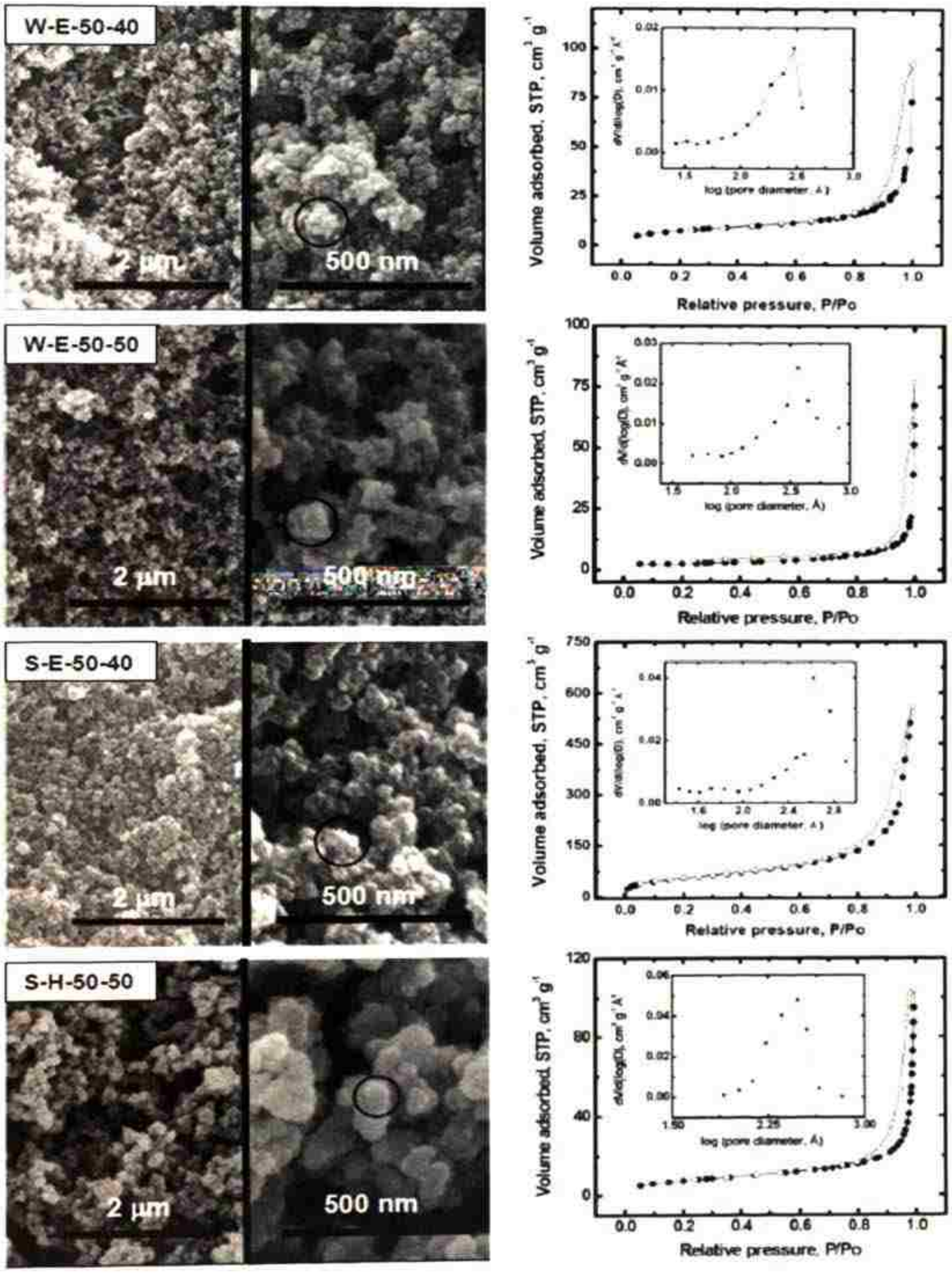

Figure 8. SEM and N_2-sorption data of a representative EGDMA-crosslined PAN aerogel along treatment at progressively higher temperatures. (For the corresponding data with a representative HDDA-crosslinked sample see Figure S.2 in supporting information.)

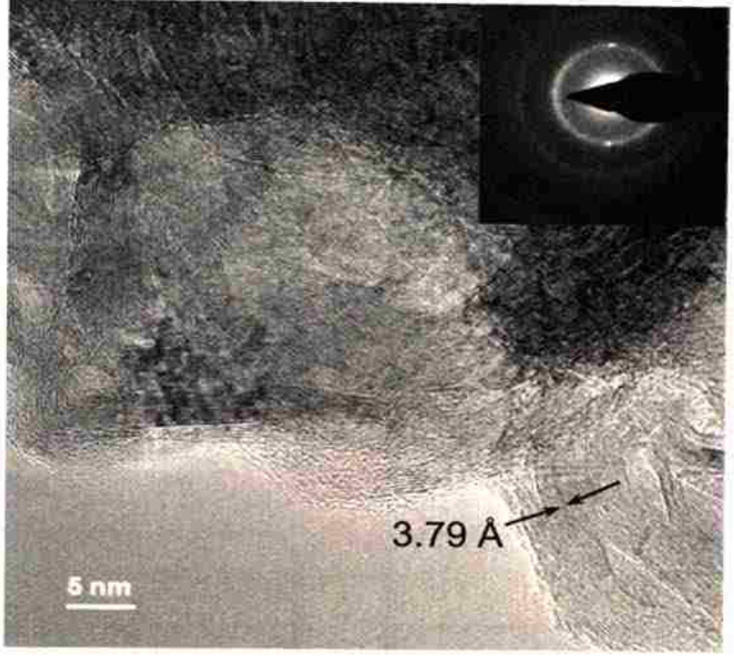

C-W-EGDMA-50-50 at 2300 °C

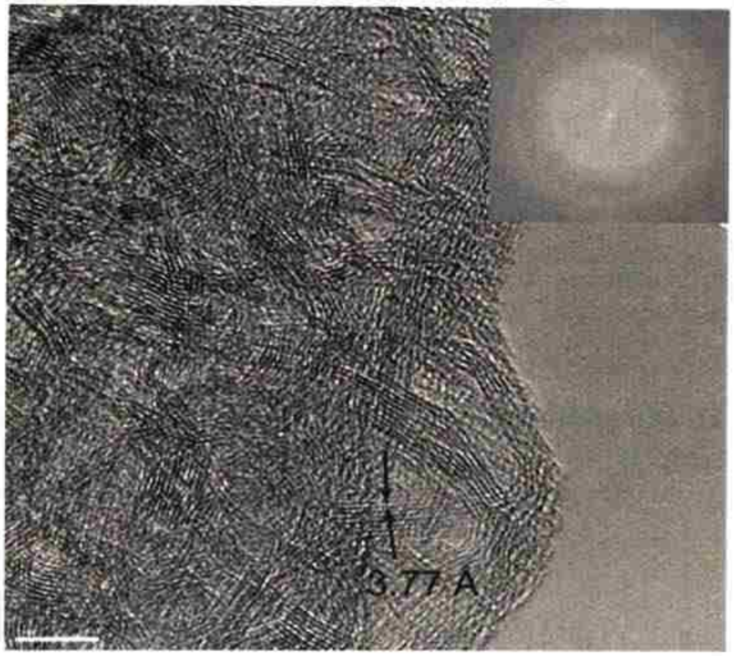

C-W-HDDA-50-50 at 2300 °C

Figure 9. HRTEM of two emulsion-based samples made with EGDMA or HDDA crosslinkers after final graphitization treatment at 2300 °C. (HRTEM data after pyrolysis at 800 °C, 1600 °C and 2200 °C are included in Figure S.3 in Supporting Information.) Insets: Left, actual electron diffraction pattern; right, diffraction pattern by Fourier Transform of the image.

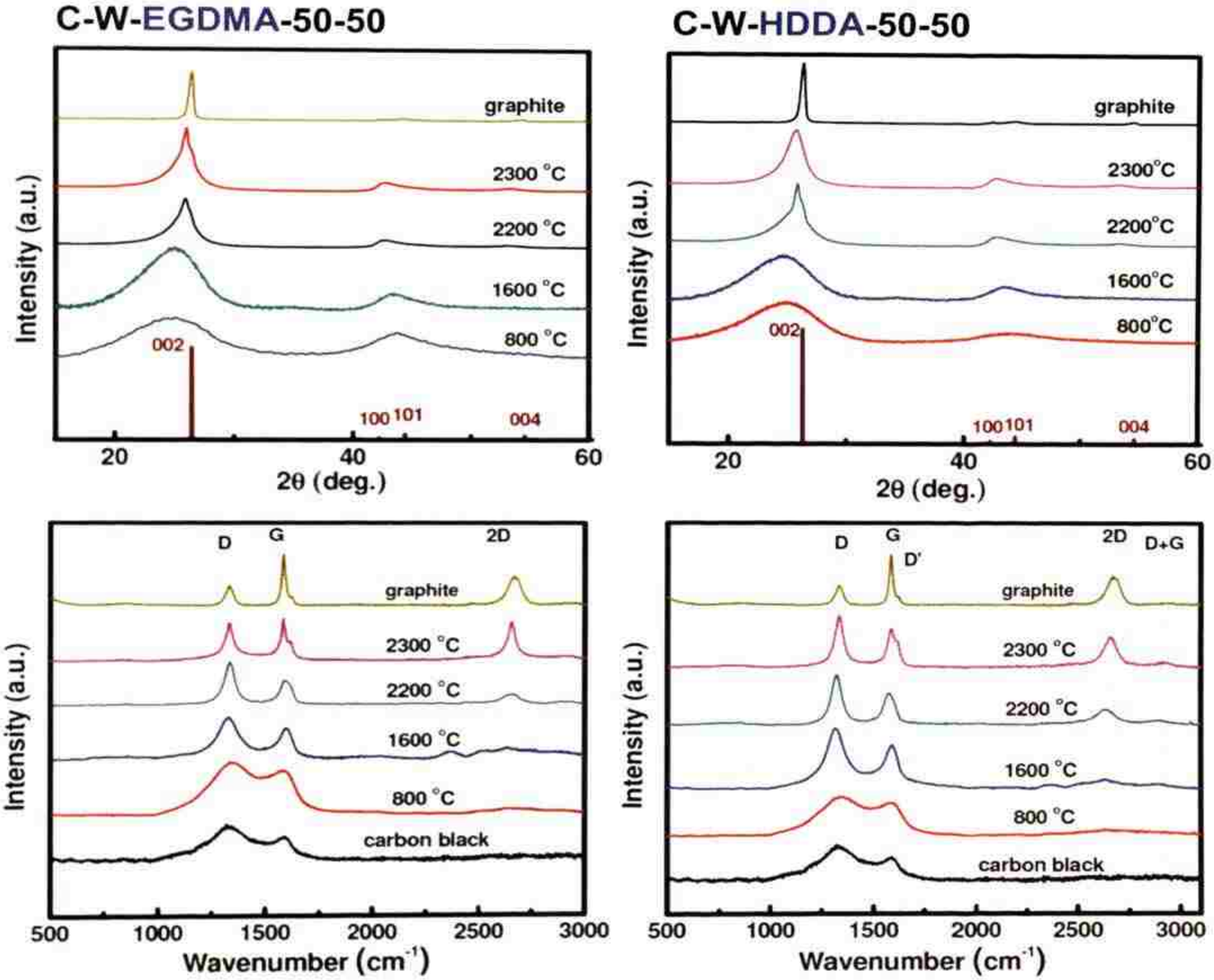

Figure 10. XRD and Raman data of two emulsion-based samples made with EGDMA or HDDA as crosslinkers after pyrolysis at the temperatures shown. (Data for commercial graphite and carbon black have been included for comparison

Table S.1 Selected properties of emulsion- (water-) based PAN aerogels (data in blue concern supercritically dried samples)

sample	diameter (cm) [a]	percent shrinkage [b]	bulk density, ρ_b (g cm^{-3})	skeletal density, ρ_s (g cm^{-3}) [c]	porosity, Π (% void space)	BET surface area, σ (m^2 g^{-1})	average pore diameter[d] (nm)	average pore diameter[e] (nm) [half width (nm)]	particle radius[f], r (nm)
W-E-50-40	0.880±0.021	12	0.403±0.014	1.289±0.005	68	27	20 [39]	29.5 [8.2]	86.1
W-E-50-40	0.896±0.018	10	0.412±0.021	1.233±0.009	68	29	18 [42]	27.2 [10.1]	83.9
W-E-50-50	0.954±0.013	4	0.534±0.014	1.184±0.002	54	35	18 [27]	41.6 [24.4]	72.4
W-E-50-50	0.945±0.019	6	0.521±0.024	1.211±0.007	54	28	21 [37]	34.3 [18.8]	88.5
W-E-75-40	0.866±0.010	14	0.387±0.011	1.266±0.004	69	25	23 [29]	36.9 [28.3]	94.8
W-E-75-40	0.847±0.017	15	0.393±0.018	1.232±0.010	69	22	26 [33]	29.9 [21.9]	110.7
W-E-75-50	0.901±0.017	10	0.512±0.027	1.174±0.001	56	39	14 [31]	36.3 [12.7]	65.5
W-E-75-50	0.888±0.013	11	0.530±0.026	1.240±0.005	56	34	21 [39]	33.2 [25.2]	71.2
W-H-50-40	0.898±0.023	10	0.432±0.037	1.215±0.002	64	27	24 [39]	27.5 [15.9]	91.4
W-H-50-40	0.912±0.016	9	0.444±0.022	1.224±0.006	64	30	26 [42]	23 [12]	81.7
W-H-50-50	0.910±0.032	9	0.515±0.011	1.175±0.001	56	40	27 [31]	41.6 [42.1]	63.7
W-H-50-50	0.8810±0.026	12	0.526±0.016	1.215±0.003	56	34	32 [47]	31.2 [19.9]	72.6
W-H-75-40	0.878±0.018	12	0.385±0.012	1.232±0.001	69	26	21 [13]	36.3 [34.9]	93.7
W-H-75-40	0.883±0.025	12	0.378±0.021	1.194±0.004	69	29	25 [24]	39.0 [33.1]	86.6
W-H-75-50	0.883±0.019	11	0.522±0.011	1.174±0.001	55	34	18 [21]	37.1 [25.1]	75.2
W-H-75-50	0.881±0.022	13	0.536±0.029	1.189±0.004	55	33	24 [11]	40.1 [18.7]	76.5

[a]. Average of 5 samples. [b]. Relative to the molds (1.00 cm diameter). [c]. One sample, average of 50 measurements [d]. By the $4 \times V_{Total}/\sigma$ method. For the first number, V_{Total} was calculated by the single-point adsorption method; for the number in brackets, V_{Total} was calculated via $V_{Total} = (1/\rho_b)-(1/\rho_s)$. [e]. From the BJH desorption plot. First numbers are the peak maxima; numbers in brackets are the widths at half maxima. [f]. Calculated via $r = 3/\rho_s\sigma$.

Table S.2 Selected properties for all solvent- (toluene-) based PAN aerogels

sample	diameter (cm) [a]	linear shrinkage (%) [b]	bulk density, ρ_b (g cm^{-3}) [a]	skeletal density, ρ_s (g cm^{-3})[c]	porosity, Π (% void space)	BET surface area, σ (m^2 g^{-1})	average pore diameter (nm) [from report] [d]	particle radius, r (nm) [e]
S-E-00-50 [f]	0.861±0.024	14	0.583±0.038	1.277±0.009	54	33	33.1 [18.2]	71.2
S-E-25-30	0.932±0.007	7	0.354 ±0.009	1.252±0.001	73	159	14.2 [10.9]	15.1
S-E-25-40	0.983±0.007	2	0.473 ±0.027	1.272±0.002	65	126	17.5 [8.9]	18.7
S-E-25-50	0.991±0.006	1	0.584 ±0.012	1.198±0.001	51	197	14.9 [9.8]	12.7
S-E-50-30	0.95±0.011	5	0.346 ±0.011	1.281±0.006	74	180	14.3 [27.2]	13
S-E-50-40	0.970±0.008	3	0.509 ±0.008	1.273±0.002	60	135	17.2 [12.5]	17.4
S-E-50-50	0.985±0.004	2	0.594 ±0.004	1.290±0.001	53	121	18.1 [12.2]	19.2
S-E-75-30	0.983±0.007	2	0.348 ± 0.010	1.299±0.004	73	184	22.7 [13.3]	12.5
S-E-75-40	0.990±0.003	1	0.492 ±0.009	1.258±0.004	69	145	16.6 [16.2]	16.4
S-E-75-50	0.987±0.009	1	0.597 ±0.001	1.263±0.001	59	157	14.1 [13.1]	15.1
S-H-00-50 [f]	0.872±0.031	14	0.562±0.044	1.267±0.010	56	37	39.4 [22.2]	64
S-H-25-30	0.918±0.019	8	0.372 ±0.032	1.242±0.006	70	54	21.0 [17.4]	44.7
S-H-25-40	0.905±0.015	10	0.517 ±0.017	1.221±0.001	58	61	13.0 [23.2]	40.3
S-H-25-50	0.910±0.005	9	0.613 ±0.022	1.196±0.005	49	36	23.6 [20.3]	69.7
S-H-50-30	0.913±0.152	9	0.342 ±0.037	1.224±0.003	72	36	23.6 [11.8]	68.1
S-H-50-40	0.922±0.012	8	0.487 ±0.027	1.273±0.001	61	42	19.2 [11.1]	56.1
S-H-50-50	0.905±0.010	10	0.605 ±0.010	1.219±0.007	47	34	25.1 [17.2]	72.4
S-H-75-30	0.943±0.033	6	0.323±0.044	1.277±0.003	75	63	14.6 [12.2]	45.1
S-H-75-40	0.952±0.017	5	0.452±0.038	1.197±0.002	62	56	19.8 [17.2]	44.7
S-H-75-50	0.934±0.021	7	0.567±0.049	1.233±0.003	54	52	17.3 [22.2]	46.8

[a] Average of 5 samples. [b] Relative to the molds (1.00 cm diameter). [c] One sample, average of 50 measurements. [d] By the $4\times V_{Total}/\sigma$ method. For the first number, V_{Total} was calculated by the single-point adsorption method; for the number in brackets, V_{Total} was calculated via $V_{Total} = (1/\rho_b)-(1/\rho_s)$. [e] Calculated via $r = 3/\rho_s\sigma$. [f] Samples made with the crosslinkers only (EGDMA or HDDA).

Table S.3 Heat capacities of PAN aerogels

sample	bulk density, ρ_b, (g cm^{-3})	heat capacity, c_p, (J g^{-1}K^{-1})
W-E-50-40	0.403±0.014	1.135±0.037
W-E-50-50	0.534±0.014	1.163±0.038
W-E-75-40	0.387±0.011	1.116±0.036
W-E-75-50	0.512±0.027	1.159±0.041
W-H-50-40	0.432±0.037	1.330±0.043
W-H-50-50	0.515±0.011	1.349±0.044
W-H-75-40	0.385±0.012	1.339±0.043
W-H-75-50	0.522±0.0113	1.376±0.044
S-E-50-40	0.509 ±0.008	1.163±0.038
S-E-50-50	0.594 ±0.004	1.181±0.038
S-E-75-40	0.492 ±0.009	1.135±0.037
S-E-75-50	0.597 ±0.001	1.179±0.038
S-H-50-40	0.517 ±0.017	1.367±0.044
S-H-50-50	0.613 ±0.022	1.386±0.045
S-H-75-40	0.487 ±0.027	1.349±0.044
S-H-75-50	0.605 ±0.010	1.339±0.043

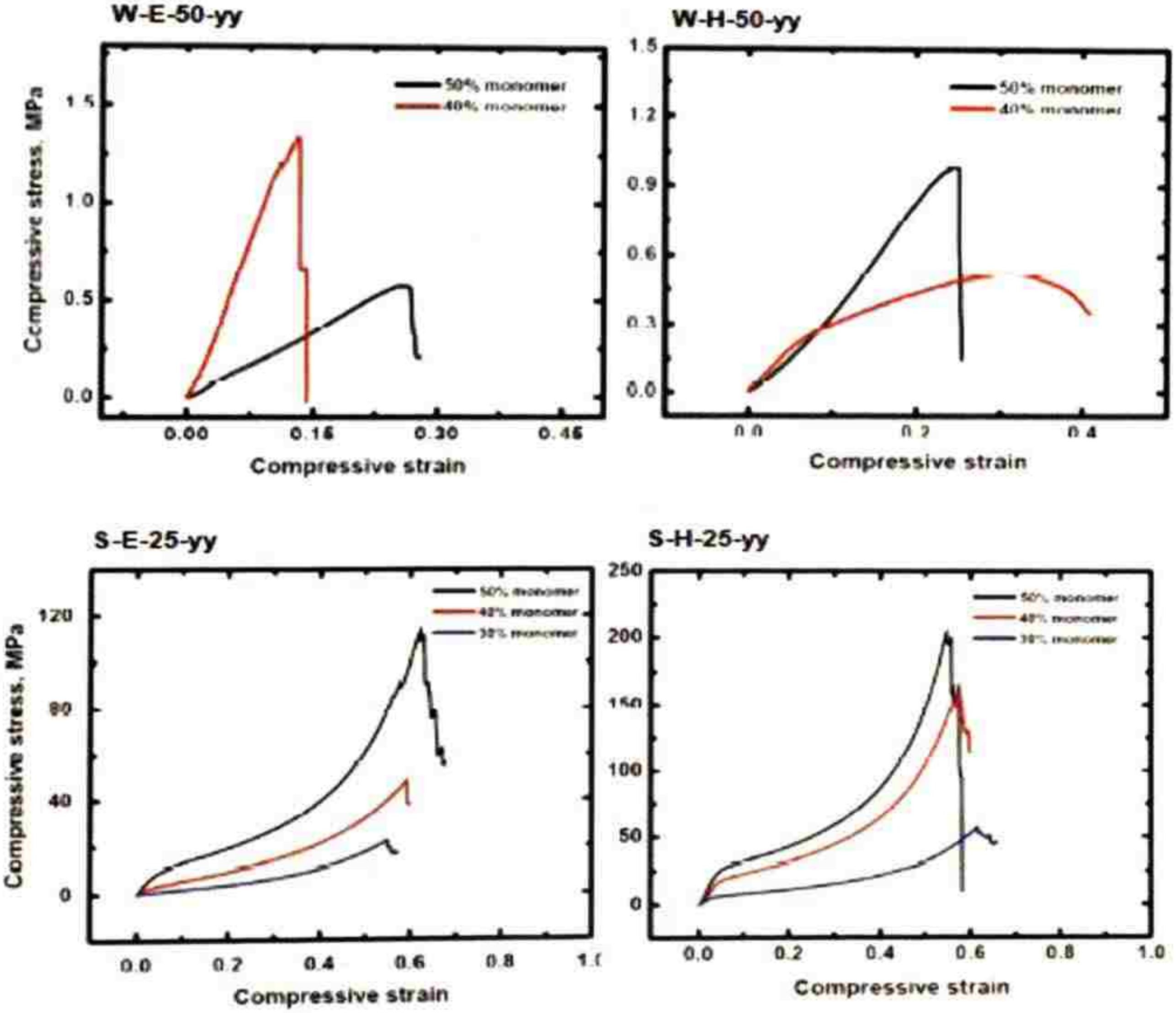

Figure S.1 Typical mechanical characterization data under quasi-static compression

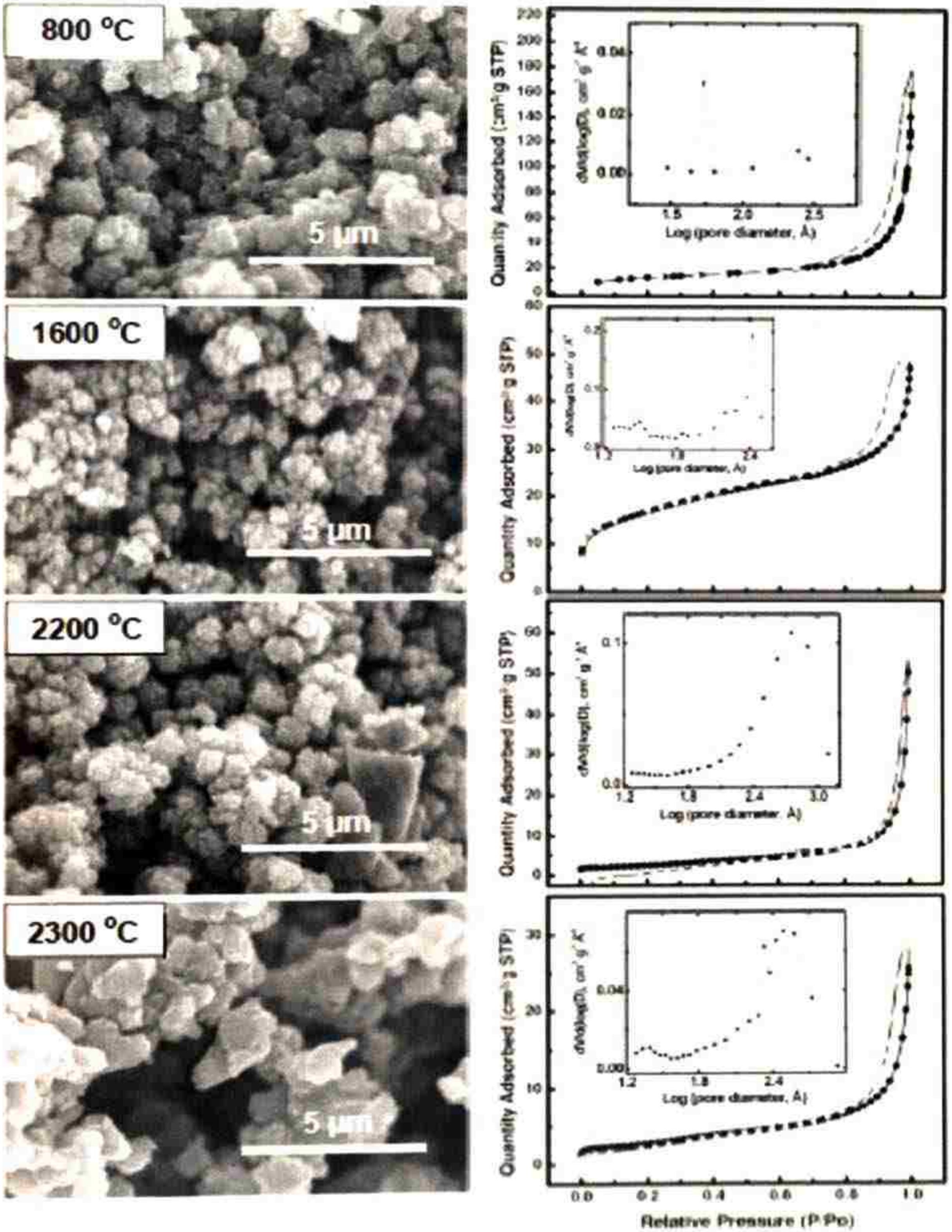

Figure S.2 SEM and N_2-soprtion data of a representative HDDA-crosslinked PAN aerogel as a function of temperature

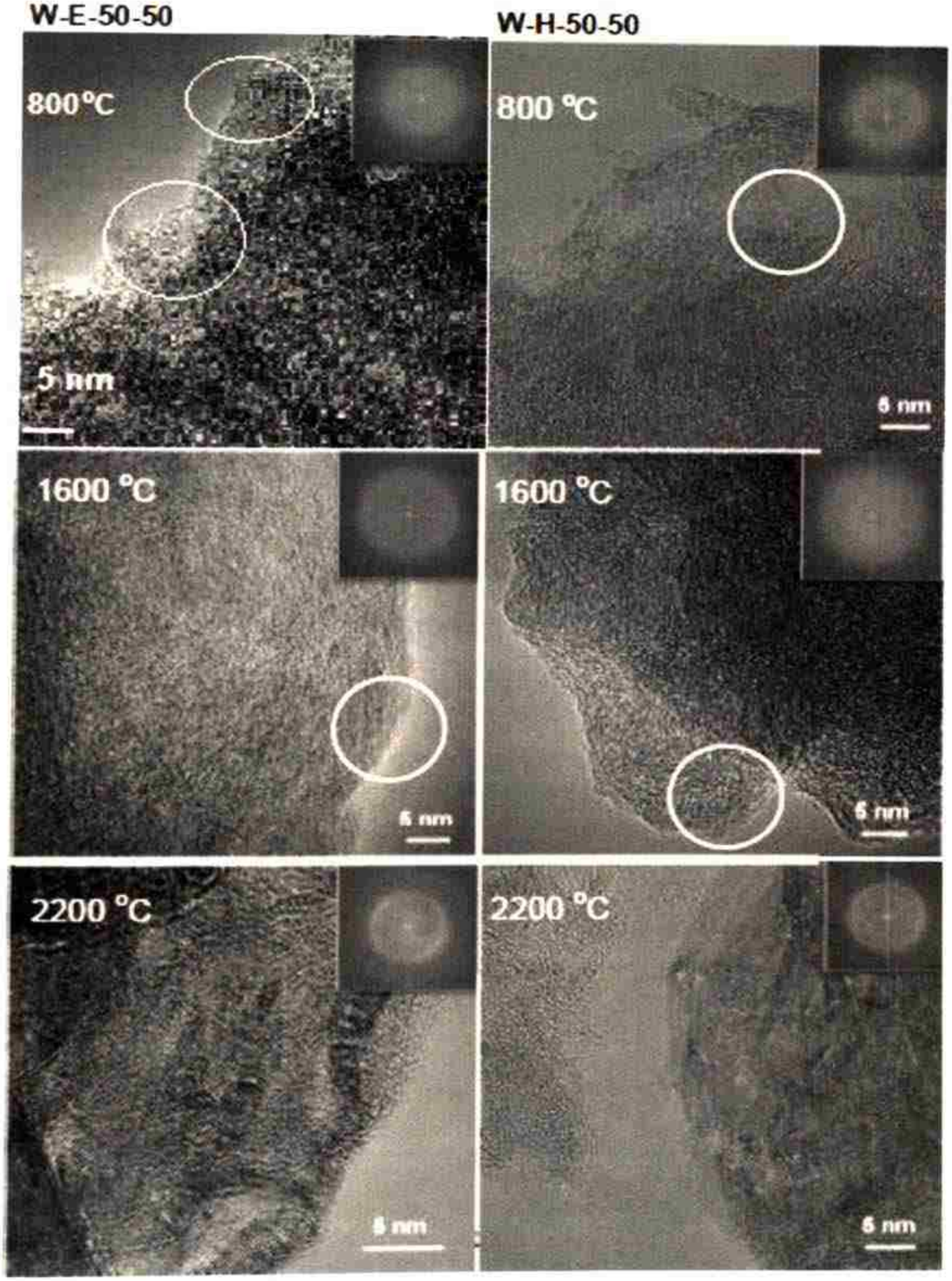

Figure S.3 HRTEM at 800 °C, 1600 °C and 2200 °C of EGDMA and HDDA crosslinked PAN aerogels

ρ_s=1.73±0.03 g cm^{-3}

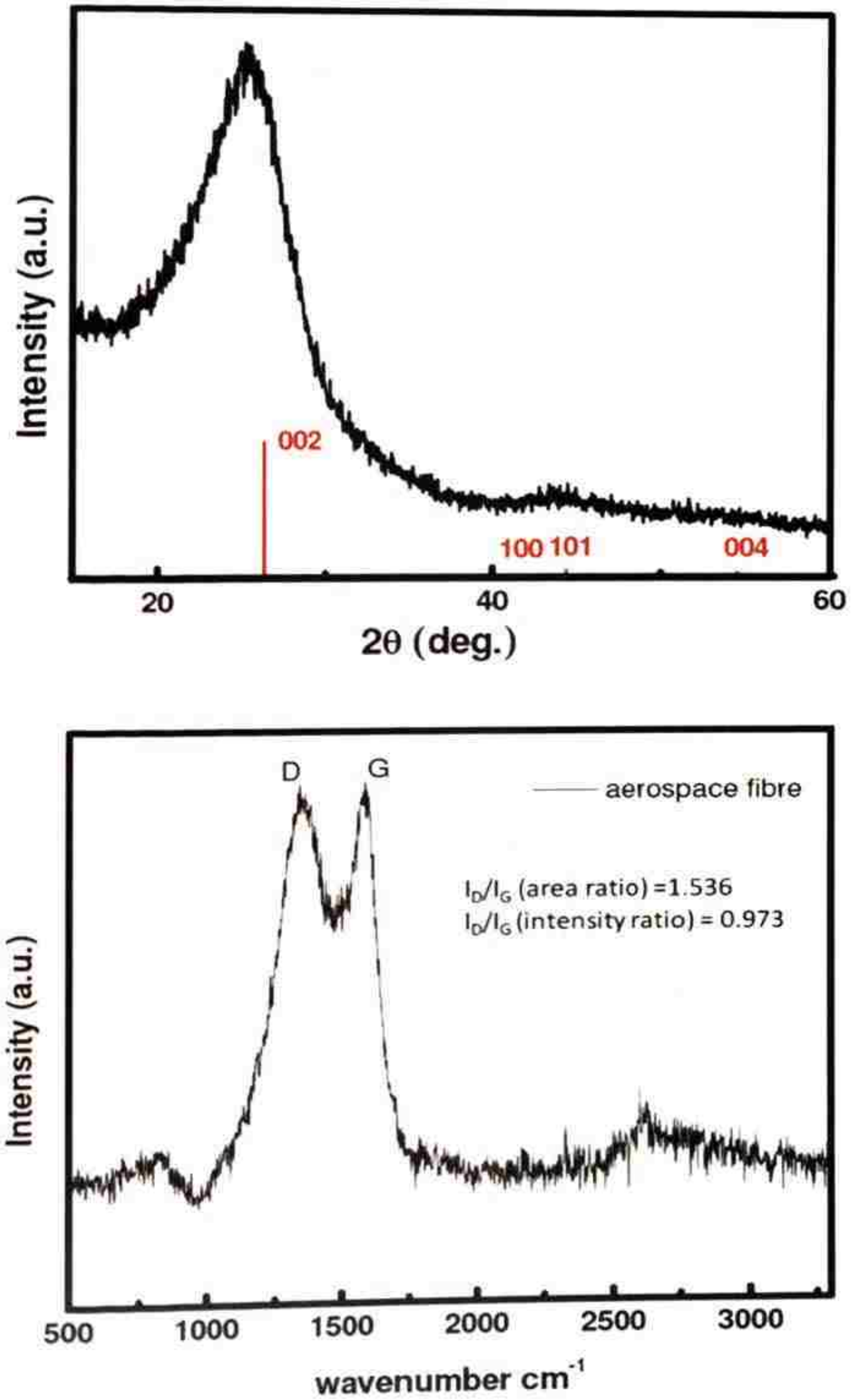

Figure S.4 XRD and Raman data of aerospace grade graphite fiber